

## Controlled mechanical systems with friction

**Citation for published version (APA):**

Hensen, R. H. A. (2002). *Controlled mechanical systems with friction*. [Phd Thesis 1 (Research TU/e / Graduation TU/e), Mechanical Engineering]. Technische Universiteit Eindhoven.  
<https://doi.org/10.6100/IR551394>

**DOI:**

[10.6100/IR551394](https://doi.org/10.6100/IR551394)

**Document status and date:**

Published: 01/01/2002

**Document Version:**

Publisher's PDF, also known as Version of Record (includes final page, issue and volume numbers)

**Please check the document version of this publication:**

- A submitted manuscript is the version of the article upon submission and before peer-review. There can be important differences between the submitted version and the official published version of record. People interested in the research are advised to contact the author for the final version of the publication, or visit the DOI to the publisher's website.
- The final author version and the galley proof are versions of the publication after peer review.
- The final published version features the final layout of the paper including the volume, issue and page numbers.

[Link to publication](#)

**General rights**

Copyright and moral rights for the publications made accessible in the public portal are retained by the authors and/or other copyright owners and it is a condition of accessing publications that users recognise and abide by the legal requirements associated with these rights.

- Users may download and print one copy of any publication from the public portal for the purpose of private study or research.
- You may not further distribute the material or use it for any profit-making activity or commercial gain
- You may freely distribute the URL identifying the publication in the public portal.

If the publication is distributed under the terms of Article 25fa of the Dutch Copyright Act, indicated by the "Taverne" license above, please follow below link for the End User Agreement:

[www.tue.nl/taverne](http://www.tue.nl/taverne)

**Take down policy**

If you believe that this document breaches copyright please contact us at:

[openaccess@tue.nl](mailto:openaccess@tue.nl)

providing details and we will investigate your claim.

# **Controlled Mechanical Systems with Friction**

CIP-DATA LIBRARY TECHNISCHE UNIVERSITEIT EINDHOVEN

Hensen, Ronnie H.A.

Controlled mechanical systems with friction / by Ronnie H.A. Hensen. - Eindhoven :  
Technische Universiteit Eindhoven, 2002.

Proefschrift. - ISBN 90-386-2693-2

NUGI 841

Trefwoorden: geregelde mechanische systemen / wrijving / niet-lineaire dynamica / stick-  
slip trillingen / systeemidentificatie / regelsysteemontwerp

Subject headings: controlled mechanical systems / friction / nonlinear dynamics / stick-slip  
oscillations / system identification / controller design

Printed by University Press Facilities, Eindhoven, The Netherlands

Cover design by Jan-Willem Luiten

Copyright © by R.H.A. Hensen

All rights reserved. No parts of this publication may be reproduced or utilized in any form or  
by any means, electronic or mechanical, including photocopying, recording or by any infor-  
mation storage and retrieval system, without permission of the copyright holder.

This work forms a part of the research program of the Dutch Institute of Systems and Control  
(DISC).

# **Controlled Mechanical Systems with Friction**

## **PROEFSCHRIFT**

ter verkrijging van de graad van doctor aan de  
Technische Universiteit Eindhoven,  
op gezag van de Rector Magnificus, prof.dr. R.A. van Santen,  
voor een commissie aangewezen door het College voor Promoties  
in het openbaar te verdedigen op  
donderdag 21 februari 2002 om 16.00 uur

door

**Ronnie Herman Anna Hensen**

geboren te Elsloo

Dit proefschrift is goedgekeurd door de promotoren:

prof.dr.ir. M. Steinbuch  
en  
prof.dr. H. Nijmeijer

Copromotor:

dr.ir. M.J.G. van de Molengraft

# Summary

In high-performance motion systems, such as pick-and-place machines, friction can severely deteriorate performance and can introduce negative side effects such as tracking errors, large settling times or limit cycles. It is expected that many of today's high-performance motion systems will gain both speed and accuracy if friction is taken into account in the controller design. To this end it seems useful that the friction present in these systems is modeled with an appropriate friction model and that the corresponding model parameters are identified. The resulting model can be used for either controller synthesis or closed-loop analysis of the occurring friction-related phenomena such as limit cycles.

The scope of this thesis is three-fold and will focus on (i) the development of identification procedures for mechanical systems with friction, (ii) control synthesis for mechanical systems with friction and (iii) the analysis of friction induced hunting limit cycles. The latter is a friction induced phenomenon for a single mass system with friction and a PID controlled regulator task.

To model friction in mechanical systems two grey-box models, which combine physical "white" knowledge of the system at hand with "black" model structures, are presented. The two black-box model structures, i.e., a Neural Network model and a Polytopic Linear Model (PLM), are both capable of identifying friction characteristics that are left unexplained by first principles modeling. In an experimental case-study, both grey-box models are applied to identify a rotating arm subject to friction. An extended Kalman filter is used iteratively and off-line for the estimation of unknown parameters in these models.

In contrast to the above static grey-box models, dynamic friction models, such as the LuGre model, are capable of modeling more practically observed friction phenomena. For example the so-called 'presliding' displacement regime, i.e., spring-like behavior for near zero velocity, is covered by the LuGre model whereas the presented grey-box models both lack this property. For the identification of this 'presliding' displacement regime an efficient frequency domain identification procedure is presented. The identification procedure for the dynamic model parameters of the LuGre model, i.e., (i) the stiffness and (ii) the damping of the presliding phenomenon, is reduced to a single experiment. Time domain validation experiments on a servo mechanism show accurate estimates of the dynamic model parameters for the linearized presliding behaviour.

With respect to the first objective of this work, it can be concluded that both time and frequency domain identification are essential to model and understand all dynamical properties present in a mechanical system with friction. This mixture is most powerful when

both domains are used in a complementary sense.

The dynamic LuGre friction model and the static PLM grey-box model are compared with respect to their performance for servo tasks on mechanical systems that exhibit friction. To this end a classic PID controller combined with mass and friction feedforward is compared to (i) a PID controller combined with a model-based friction compensation using the dynamic LuGre friction model and (ii) a gain-scheduled optimal PD controller based on the PLM. The latter consists of a feedforward part embedding all the system knowledge available in the PLM and a nonlinear feedback part which is designed in an optimal manner. The controllers are compared to the classic PID controller by means of experiments on a rotating arm subject to friction. The performance for third order servo setpoints shows that the gain-scheduled optimal PD controller outperforms the other controllers with respect to settling time and maximal error after setpoint. The tracking performance of the LuGre-based controller and the classic PID controller is similar whereas the tracking performance of the gain-scheduled PD controller is worse.

The limited settling performance of the classic PID controller is shown to be caused by the changing dominant dynamics from a double integrator behaviour in the slip phase to a mass-spring behaviour in the presliding displacement regime. As a consequence, the closed-loop dynamics properties will deteriorate due to a decreasing bandwidth and even decreasing stability margins in the presliding displacement regime. Hence, for a simple PID controller the settling behaviour in terms of static error suppression is limited due to the additional stiffness in the presliding displacement regime.

The third objective of this thesis concerning the friction induced hunting limit cycles is performed by analysis of the nonlinear closed-loop system. The hunting limit cycles are predicted for a simple motion system consisting of a mass system subjected to friction and a PID controlled regulator task. The two friction models used, i.e., (i) the dynamic LuGre friction model and (ii) the static Switch friction model, are compared with respect to the hunting phenomenon. Analysis tools originating from the field of nonlinear dynamics are used to investigate the friction induced limit cycles. For a varying controller gain, stable and unstable periodic solutions are computed numerically with a simple shooting method. The stable and unstable branches are computed with path-following techniques which, together with the stability analysis of the closed-loop equilibrium points, result in a bifurcation diagram. Bifurcation analysis for both friction models indicates the disappearance of the hunting behaviour for controller gains larger than the gain corresponding to the cyclic fold bifurcation point.

In contrast to this computationally expensive bifurcation analysis, the hunting phenomenon is also studied with a more efficient event mapping technique. Two different types of static frictional damping functions, i.e., (i) a Coulomb friction level combined with a discontinuous rise to a larger maximum static friction level and (ii) friction curves with a continuous drop from the maximum static friction level to the lower Coulomb friction level, are used to predict and examine the hunting phenomenon. In particular, a classification with respect to

the ability to predict both stable and unstable limit cycles is obtained. Furthermore, the local stability of the equilibrium points is discussed and attractor basins are given.

The gained insight in the hunting limit cycles is used in an experimental case-study where a linear motor motion system is considered. Besides the velocity dependent friction force the system contains also a nonlinear position dependent cogging force. The existing limit cycles induced by the nonlinear forces in the system in combination with a PID controlled regulator task are analyzed both experimentally and numerically with the event mapping approach.

The used analysis tools, i.e., the path-following and event mapping technique, which originate from the field of nonlinear dynamics, contribute to the understanding and analysis of the hunting phenomenon. For the analysis of the controlled mechanical system as a nonlinear dynamical system the above tools have shown to be indispensable.





# Contents

Summary .....	v
Chapter 1 General Introduction .....	1
<hr/>	
<b>Part I</b>	<b>Identification and Control of Mechanical Systems with Friction</b>
Chapter 2 Introduction .....	15
Chapter 3 Grey-box Modeling of Friction: An Experimental Case-study .....	25
Chapter 4 Frequency Domain Identification of Dynamic Friction Model Parameters .....	41
Chapter 5 High Performance Regulator Control for Mechanical Systems Subjected to Friction .....	51
Chapter 6 In Retrospect .....	71
<hr/>	
<b>Part II</b>	<b>Friction Induced Limit Cycling</b>
Chapter 7 Introduction .....	83
Chapter 8 Friction Induced Hunting Limit Cycles: A Comparison between the LuGre and Switch Friction Model .....	89
Chapter 9 Friction Induced Hunting Limit Cycles: An Event Mapping Approach .....	101
Chapter 10 Analysis of Friction Induced Limit Cycles on an Experimental Linear Motor Motion System .....	121
Chapter 11 In Retrospect .....	143
<hr/>	
Appendix A Terminology .....	153
Bibliography .....	157
Samenvatting .....	167
List of Publications .....	171
Dankwoord .....	173
Curriculum Vitae .....	175



# Chapter 1

## General Introduction

In this introductory chapter the motivation for this work is given and the main topics addressed in this thesis are positioned within the huge amount of research on the subject of friction. The main contributions and outline of the thesis will be presented in addition.

### 1.1 Friction

Friction and friction induced phenomena have been the subject of research for centuries, especially since the important work of Amontons [2] and Coulomb [30]. However, as early as in the days of Leonardo da Vinci, it was observed that friction force is proportional to load, opposes motion and is independent of the (apparent) contact area. Although the research on this topic has been enormous, the interest has continued to increase over the past decades. In fact, this is mainly due to the large number of research fields in which friction and its properties play a prominent role. Important disciplines interested in the friction phenomenon are (i) tribology, (ii) mechanical engineering, (iii) acoustics and (iv) geophysics and/or seismology. The latter is a fairly new research field on the horizon with respect to the friction topic due to the emerging insight in plate tectonics and its tectonic fault dynamics [27], [94]. On the other hand, tribology is probably the field with the most extensive research on friction and studies practically observed friction generated phenomena in terms of surface interactions, both on a macroscopic and microscopic level, using the knowledge of physics and chemistry. Most research fields distinguish themselves from the field of tribology in the fact that they are more interested in incorporating friction as part of the entire dynamical system rather than studying the surface contacts in detail. For example from an acoustics point of view it might be of interest how (i) the screeching noise of a piece of chalk on a blackboard is produced or (ii) the sound of an excited stringed instrument with a fiddle-stick is generated. In mechanical systems, friction is often only one of many forces (torques) present and moreover very often an impediment, which might induce undesirable phenomena such as self-sustaining stick-slip oscillations, e.g., in oilwell drillstrings [74], [119] or in machine tooling [82].

Friction in mechanical systems is the subject of research for several scientific and engineering communities, such as lubrication engineering, applied mathematics, dynamics and

control engineering. Lubrication engineers but also design engineers try to limit the friction in a mechanical system by improving the system itself for instance with better lubricants or a redesign of the system. In contrast to this approach the control community focuses on the modification of the dynamics of the mechanical system by adding a control loop, in order to obtain the desirable closed-loop behaviour. The applied mathematicians and dynamics scientists are primarily interested in the analysis of the nonlinear and discontinuous nature of dynamical systems due to friction.

The increasing interest and research in the class of controlled mechanical systems with friction is mainly caused by the increasing demands for these systems. In high-performance controlled mechanical or motion systems, friction can severely deteriorate performance. In particular, friction induced negative side effects are increasing tracking errors, large settling times or stick-slip oscillations. It is expected that many of today's high-performance motion systems will gain both speed and accuracy if friction is taken into account in the controller design and extensive closed-loop analyzes with respect to occurring friction-related phenomena are conducted. This thesis will contribute to the analysis and synthesis of these controlled mechanical systems with friction. Specific goals and contributions will be given in the next sections of this chapter.

## 1.2 Friction in Controlled Mechanical Systems

Before going into detail a couple of examples are given where friction in controlled mechanical systems can limit the performance and friction should be taken into consideration to meet the predefined specifications. Examples can be found in

- machine tooling, e.g., grinding or microdrilling with very low feed rates [14], [52], machining with single crystal diamond tools [82] or oilwell drilling [119],
- high-performance robotics, both force and position (or trajectory) controlled, e.g., pick-and-place machine for mounting electrical components on Printed Circuit Boards (PCBs) [99] or multi-linked rotational robots used in manufacturing industry [116],
- mechatronics of consumer electronic motion systems, e.g., data storage systems such as disk drives, cd-rom players,
- telescopes or military pointing systems [15].

For each system, the designers have certain goals or tasks in mind and consequently prescribe specifications on the execution of these tasks. For motion systems these tasks are known as controller tasks, which can principally be divided into two groups: (i) regulator tasks, also known as point to point or precision positioning tasks where a constant setpoint is considered and therefore disturbance suppression is of major importance, and (ii) tracking tasks, also known as servo tasks. With respect to friction the latter can be subdivided further into three groups, i.e., (a) tracking with velocity reversal, (b) tracking at low velocities and (c) tracking at high velocities. In the literature survey of Armstrong-Hélouvy et al. [7], which is referred

## 1.2 Friction in Controlled Mechanical Systems

to the reader for a clear synthesis of literature published on the friction subject from a variety of disciplines, for each controller task the friction induced phenomena and/or errors are reported with its responsible dominant frictional contributor, which are recalled in Table 1.1. To understand and reduce the negative side effects of friction, it is of importance to investi-

Task	Control error	Dominant frictional contributor
Regulator	Steady state error or hunting	Stiction
Tracking with velocity reversal	Stand still, lost motion	Stiction
Tracking at low velocities	Stick-slip oscillations	Negatively-sloped Stribeck curve; Stiction
Tracking at high velocities	Large tracking errors	Viscous behaviour of lubricant

Table 1.1 - Friction induced phenomena in controlled mechanical systems.

gate the phenomena both analytically and experimentally. In literature the analysis of friction in mechanical systems is studied by several disciplines for different system settings, with various friction models and analysis tools, and consequently with different results. Especially, the stick-slip oscillations occurring for the tracking task at low velocities have been studied both analytically [6], [38], [49] [105], and experimentally [103], and can be considered as a benchmark for analysis tools and friction models.

### 1.2.1 Friction modeling and identification

The number of friction models proposed in literature is immense, see [7] for a complete literature survey, and can be subdivided with respect to their detail in describing surface contact properties occurring on a microscopic and macroscopic level. In the past decade major effort and contributions [16], [24], [55] are made in the development of friction models, suitable for analysis and controller synthesis, which have limited complexity but a rich similarity to practically observed friction properties. The following qualities of a friction model are considered to be important for controller design, which are encountered when a mechanical system with friction accelerates from zero velocity:

- Presliding displacement (stiction), which is a spring-like behaviour in the stick phase due to limited stiffness of contact asperities [31].
- Static friction, that is assumed to be independent of the velocity, however varies as a function of the dwell-time when sticking and the rate of increase of the applied force [78], [102].
- Stribeck curve [32], [114], i.e., a continuous drop in the friction force for small velocities, which originates from the transition of boundary lubrication to full fluid lubrication through partial fluid lubrication [7].

- Frictional lag, which is a dynamic behaviour that results in a larger friction force for increasing velocities than for decreasing velocities and becomes more apparent for large acceleration and/or deceleration [70], [105].

All these experimentally observed phenomena are necessary to fully understand the problems present in controlled mechanical systems with friction, since a motion system faces one or more of the above described frictional stages for each task as given in Table 1.1. Moreover, the simplest friction model combining all these properties has to contain extra dynamics for the modeling of varying static friction and hysteresis due to frictional lag and should at the same time be nonlinear to capture the Stribeck curve. However, for the analysis of controlled mechanical systems, simplification of the friction model is often necessary due to the limited applicability of the used analysis tools [8], [21], [118]. On the other hand, some friction induced phenomena can successfully be described with less complex friction models, which is desirable from a conceptual point of view and is also an important research issue. Commonly used assumptions to reduce complexity are for instance: infinite stiffness in the presliding displacement regime, which results in the classic concept of (dry) friction, and modeling the continuous Stribeck curve as a discontinuous drop of a constant static friction force to a lower Coulomb friction level [8], [85].

Another aspect in the modeling of the friction is the actual identification of friction present in the mechanical system under consideration. The estimation of the model parameters is important for obtaining quantitatively accurate friction models, which can be used as a mathematical representation of the friction. In general it is not possible to measure the friction force directly and therefore the identification of friction in a mechanical system is far from trivial. Moreover, friction might be introduced by a combination of mechanical elements in the system, e.g., due to several bearings and/or transmissions, which are often lumped into one friction model to reduce model complexity. Since the friction force can not be observed directly, experiments for the identification procedure are performed by sensing quantities that are influenced indirectly by the friction force, such as displacements, velocities or acceleration of the mass connected to the frictional contact surface. To estimate the model parameters, often extended with parameters to describe other dynamics in the system, such as mass and stiffness, different dedicated and time-consuming experiments have to be conducted. Each experiment is designed to visualize one of the friction phenomena as described above by excluding other dynamics in the system. For example for a single mass system with friction it is possible to measure the Stribeck curve by performing a PD position controlled tracking task at different constant velocities. For this specific task the acceleration of the system is equal to zero and the applied feedback controller force at the different constant velocities represents the equivalent friction force. To reveal other frictional properties different experiments have to be conducted and in addition the obtained measurement data is used to estimate the model parameters, where usually some kind of least squares minimization is executed.

However, the time varying nature of friction due to wear and exogenous variables such as changing load or operating temperatures might limit the applicability of an estimated friction

## 1.2 Friction in Controlled Mechanical Systems

model considerably. At a macroscopic level friction forces vary in time due to microscopic effects such as deformation of contact surfaces, accumulation of wear particles or changes in the properties of the lubricant. Since these influences are hard to measure it is also difficult to model these time varying phenomena. Hence, the estimated friction model is expected to capture at best an averaged behaviour of the actual friction over time.

Validation of the friction model with its estimated parameters can either focus on the ability of the identified model to predict the friction characteristics of interest or on the closed-loop performance when the identified friction model is incorporated in the controller design. Roughly speaking, the models can be validated in an open-loop or closed-loop setting and results might be improved, if desirable, in an iterative procedure, by choosing a more complete friction model.

### 1.2.2 Controller design

For mechanical systems, accurate compensation of friction is expected to increase performance considerably, represented for example by smaller tracking errors and/or lower settling times. However, due to the nonlinear (discontinuous) dynamic behaviour of friction, compensation can be difficult for several controller tasks. Especially for controller tasks that encounter stiction or low velocities, friction can be hard to compensate since its nonlinear and discontinuous characteristics can be dominant.

From the literature study [7] a clear distinction can be made between two compensation classes, i.e., non-model-based and model-based compensation for friction. Two of the most widely used controllers are of the first type:

- stiff PD control, which is stable for regulator tasks but will always result in steady-state errors. For tracking tasks at low velocities PD control might exhibit stick-slip oscillations and in recent years it is fully understood how stiff PD control eliminates these oscillations,
- integral control. Steady-state errors which occur for PD control alone can be reduced or eliminated by integral control. Moreover, integral control is favorable and necessary to get a desirable shape of the closed-loop dynamics for fast attenuation of errors and noise at low frequencies. However for a PID controlled regulator task, friction might introduce stick-slip oscillations around the desired position, also referred to as hunting [7].

Other non-model-based compensation methods are for instance dither [28], impulsive control [5], [71], joint torque control [54] and dual mode control [5], [44]. However these techniques as well as their applicability are less general and also less in use.

On the other hand, the model-based methods compensate the friction force by applying an equivalent control (command) force in opposite direction. The most commonly used model-based compensation technique is a fixed compensation based on an identified friction



model. As for other control problems it is possible to compensate for friction in a feedback [77] or feedforward [5], [77] manner. In the feedforward case the desired (commanded) frictional dependencies, such as velocity, position and/or acceleration, are used to compute the compensation control (command) force, whereas in the feedback setting the actual or instantaneous quantities are used. For most applications, only the instantaneous position is measured and consequently for the unmeasured feedback frictional dependencies, like velocity, a reconstruction or estimation problem arises.

Adaptive control [25], [77] and learning control [99] are other model-based compensation techniques, which however are less used and have limited applicability. Adaptive control is desirable when due to influences such as wear or changes in operating conditions the friction force is strong time-varying, which is difficult to capture in a model. Learning control maps unmodelled dynamics such as friction in an iterative way and is especially powerful for applications where repetitive motions have to be performed.

Except for the feedforward approaches, all compensation techniques raise the question of closed-loop stability, which should be incorporated in the controller design and be answered before the controller is implemented in real-life. Moreover, due to the recent use of dynamic friction models with internal states the controller and observer synthesis run in parallel and the closed-loop stability analysis of the combination of both loops is extremely important.

### 1.2.3 Analysis tools

In contrast to the number of friction models, the number of analysis tools is much smaller, where the applicability of each analysis tool with respect to the different types of friction models varies considerably. Especially for complex nonlinear dynamic friction models, the number of appropriate analysis tools is limited and even not fully recognized by involved research fields, such as the control community. Frequently used analysis tools for friction induced phenomena can be summarized as follows:

- Describing Function Analysis (DFA) is mainly used for the analysis of hunting stick-slip oscillations occurring for a regulator task [7] and is found to be inadequate [8] and at best qualitatively predictions are made [45], which is mainly due to its approximating characteristic [21], [118], [8].
- Algebraic analysis is an alternative approach to predict stick-slip oscillations. The idea is to integrate the equation of motion for the closed-loop system in the slip phase and analytically compute the time and state where the system enters the stick phase again. This method is restricted to piecewise linear models where the transition from one phase to another can be determined analytically. However, the obtained results are exact and can often be used as a benchmark for other more sophisticated analysis tools. These exact results, such as the analytic result for a combination of static, Coulomb and viscous friction in [8], can be considered as a special and often limiting case for more general friction models.
- Simulation is a common tool to validate models with respect to experimental results and

## 1.2 Friction in Controlled Mechanical Systems

can be powerful to analyse approximating techniques such as the DFA method. With properly chosen parameter and simulation settings the numerical results can be interpreted just as experiments and as for experimenting a great deal can be learned from these results.

The use of simulation as a tool addresses immediately the problem of numerically solving ordinary differential equations with discontinuous right-hand sides [7], [85]. This discontinuity, introduced by many friction models, can numerically be tackled in various ways and possible solutions include the use of discrete event detection solvers or the use of alternate friction models. The alternate friction models, such as a smooth single-valued friction function [84] or the Karnopp friction model [79], facilitate the numerical implementation and are only approximations of the frictional discontinuity. Moreover, these alternate friction models deal with the problem of existence and uniqueness of solutions, which might be introduced by the discontinuous friction models.

- Phase Plane Analysis (PPA) represents the dynamics of a (non)linear system graphically where the results of extensive simulations are used. The number of states in the system defines the dimensionality of the phase plane and pinpoints the major drawback of this approach which is the applicability only for systems up to order two. For example the Phase Plane Analysis of stick-slip oscillations in case of a PD controlled single mass system with friction is possible [104], [118] but systems with dimension 3 or higher are difficult to visualize.

However in recent years the analysis on stick-slip oscillations in mechanical systems from the fields of nonlinear dynamics and seismology have merged to a more generally usable PPA tool called event mapping [48]. This technique maps a higher dimensional nonlinear discontinuous system into a one-dimensional map, which is constructed by mapping the value of one state variable onto itself for successive stick phases, which is only applicable for frictional systems with sufficient dissipation of energy in the stick phase [48], [81]. In contrast to the simulation tool, this approach is able to find both stable and unstable stick-slip oscillations and on the constructed interval the map defines the complete nonlinear dynamics including possible properties such as chaos [35], [48].

- Analysis tools originating from nonlinear dynamics, such as bifurcation theory, shooting methods and path-following techniques [42]. This set of tools is based on simulations and is capable of finding important properties of general nonlinear dynamical systems with little restrictions. An important feature is the ability to follow branches of stable and unstable periodic solutions for varying model parameters. In combination with Floquet theory [53] these numerical approaches might reveal qualitative changes in the structural behaviour of the system expressed by a bifurcation. The construction of a so-called bifurcation diagram completes the dynamic picture of the system.

The latter together with the event mapping PPA tool appear to be powerful techniques to analyze complex nonlinear dynamic system and phenomena such as friction induced stick-slip oscillations [48], [86]. However only once a PPA technique similar to the event mapping

technique is used for the analysis of a *controlled* mechanical systems with friction, i.e., a PID controlled regulator task on a single mass system is studied for various frictional damping functions in [104]. Controlled mechanical systems with friction are from a dynamics point of view not different from general (nonlinear) dynamic systems if its closed-loop form is considered. Hence, the tools originating from the field of nonlinear dynamics seem to have promising properties to analyze controlled mechanical system with friction and can especially be applicable for the more general complex nonlinear dynamic friction models.

### 1.3 Goals and Main Contributions of the Thesis

The scope of this thesis can be formulated by three goals.

- Development of identification procedures for mechanical systems with friction.
- Control synthesis for mechanical systems with friction.
- Analysis of friction induced stick-slip oscillations, also known as periodic solutions or limit cycles, for controlled mechanical systems with friction.

From the previous introductory sections can be concluded that for controlled mechanical systems with friction none of these goals are fulfilled in a general sense already and especially the strong varying frictional characteristics for different controller tasks, as given in Table 1.1, make it hard to come up with one friction model, one control design and one analysis tool that reaches these goals for a general class of controlled mechanical system with friction. Hence, the focus and contributions throughout this thesis will mainly be limited to one controller task, i.e., the regulator task. Its dominant frictional contributors, i.e., the presliding displacement regime and the negatively-sloped Stribeck curve, as well as the occurrence of hunting stick-slip oscillations for this task hamper all three goals and to some degree interconnect them.

With respect to the first goal an effort is made to reduce the number of time-consuming and dedicated experiments to identify friction phenomena and estimate friction model parameters. The presented friction models are primarily control oriented, i.e., the model structures are chosen to be suitable for controller design, and are therefore mainly validated in a closed-loop manner. Moreover, to reach this goal a standard experimental setting, i.e., a motion system with (i) free adjustable control or command inputs and (ii) instantaneous measurement of rigid body displacements, is kept in mind. For a rotational system with friction the inertia and frictional Stribeck curve are estimated simultaneously using angular position measurements of the system. For this purpose an Extended Kalman Filter is used in an iterative manner to estimate the model parameters of two different friction models. In addition, for the identification of the dynamic properties in the frictional presliding displacement regime an efficient frequency domain identification procedure is presented and applied to the same experimental setup.

## 1.4 Outline of the Thesis

In this thesis the second goal mainly focuses on the evaluation and comparison of different compensation schemes with respect to the regulator task. One of the proposed and identified friction models as will be described in Chapter 3, i.e., a Polytopic Linear Model of the Stribeck curve, is favorable for controller synthesis due to its model structure. This model structure is exploited in the controller design and illustrates the strength of combining model and controller synthesis into one. The resulting model-based compensation controller shows desirable properties in comparison to two other model-based compensation schemes, such as small steady-state errors and small settling times for the regulator task.

The more academic analysis problem of friction induced stick-slip oscillations, in particular hunting limit cycles occurring for a PID controlled single mass system and regulator task, is addressed by the third objective of this thesis. As stated in Section 1.2.3 the promising analysis tools originating from the fields of nonlinear dynamics and seismology are used to analyze this friction induced phenomenon for a controlled mechanical system. A complex nonlinear dynamic friction model is compared to an alternate friction model with respect to this phenomenon and similar results in the form of bifurcation diagrams are found. The disappearance of the limit cycles is predicted for increasing controller gains, which is in line with practice. Moreover, it is shown that the event mapping PPA tool is extremely suitable for the analysis of stick-slip oscillations and reveals completely different closed-loop dynamics for structural variations in the friction model. To conclude this subject, an alternate friction model together with the previously described analysis tools are used to investigate experimentally friction induced stick-slip oscillations for a Linear Motor Motion System (LiMMS). In addition to the nonlinear characteristics of friction this system exhibits extra nonlinear dynamics due to the motor system itself. The insight in the stick-slip oscillations, obtained by the numerical studies, and the use of appropriate analysis tools are shown to be applicable for this more general setting.

Throughout each part of this thesis, the developed theory or performed analysis are put to test with practice, which gives a fair mix of experimental work and theoretical analysis. Experimental research is shown to be extremely important for the validation of the developed models, control schemes, ideas and analysis tools, but raises immediately new unanswered questions which might lead to interesting topics for future research.

## 1.4 Outline of the Thesis

The thesis is organized in two parts and is mainly based on papers which are published or submitted for publication. The main chapters are therefore to some extent self-contained. However, both parts contain an introductory chapter to put the main chapters in a broader context and will be closed with an 'In Retrospect' chapter dealing with summarizing insights, conclusions and recommendations for future research.

The first part, consisting of the three main Chapters 3-5, will deal with the identification and control of mechanical systems with friction and will cover the first two goals of this research

described in the previous section. In the introductory Chapter 2, the increasing interest from the control community in dynamic friction models will be summarized with a brief literature survey on this topic. The identification studies performed in the main chapters of this first part follow in some sense the research line of the development of friction models, i.e., from alternate static friction models in Chapter 3 to the dynamic LuGre friction model in Chapter 4.

Chapter 3 will present two grey-box models, which combine physical "white" knowledge of the system at hand with "black" model structures. The two grey-box alternate model structures, i.e., a Neural Network model and a Polytopic Linear Model (PLM), are both capable of identifying friction characteristics that are left unexplained by first principles modeling. In an experimental case-study, both models are applied to identify a rotating arm subjected to friction. An extended Kalman filter is used iteratively and off-line for the estimation of the unknown model parameters. This chapter has been published in [62].

In contrast to these alternate static friction models, dynamic friction models, such as the LuGre model, are capable of modeling more practically observed friction phenomena. The presliding displacement regime, i.e., spring-like behaviour for near zero velocities, is covered by the LuGre model where the presented grey-box models lack this property. In Chapter 4 an efficient frequency domain procedure for the identification of this presliding displacement regime will be presented. The identification procedure for the dynamic model parameters of the LuGre model, i.e., (i) the stiffness and (ii) the damping of the presliding phenomenon, is reduced to a single Frequency Response Function (FRF) measurement of the phenomenon. The results will appear in [64].

In Chapter 5 the dynamic LuGre friction model and the static alternate friction model based on the PLM will be compared with respect to their performances for regulator tasks on mechanical systems that exhibit friction. To this end a PID controller combined with mass and friction feedforward is compared to (i) a PID controller combined with a model-based friction compensation using the dynamic LuGre friction model and (ii) a gain-scheduled optimal PD controller based on the PLM. The latter consists of a feedforward part embedding all the system knowledge available in the PLM and a nonlinear feedback part which is designed in an optimal manner. The controllers are compared to the PID controller by means of experiments on a rotating arm subject to friction and the differences in settling time and maximal error after setpoint are examined for three third order setpoints. The results are submitted for publication in [65].

This first part will be closed with the 'In Retrospect' Chapter 6, where the obtained results are placed in perspective and summarized. Moreover, recommendations for future research topics will be presented.

The second part of this thesis will be completely devoted to the third objective of this research, i.e., the analysis of friction induced limit cycles for a PID controlled motion system for a regulator task. As for the first part, this part is based on three main Chapters 8-10, an introductory Chapter 7 and a closing 'In Retrospect' Chapter 11. Due to the maybe

## 1.4 Outline of the Thesis

unfamiliar terminology used throughout this second part, Appendix A is suggested to the reader for formal definitions of some frequently used terms such as limit cycle, stability and Floquet Multiplier.

In the introductory Chapter 7, two important friction induced stick-slip oscillations in controlled mechanical systems will be addressed and the present theory, analysis tools and results from different research fields are discussed. The use of analysis tools from the field of nonlinear dynamics for the analysis of the friction induced hunting phenomenon, which is the subject of research in this second part, is motivated by this discussion.

In Chapter 8, two friction models, i.e., (i) the dynamic LuGre friction model and (ii) the static Switch friction model, will be compared with respect to this so-called hunting phenomenon. Analysis tools originating from the field of nonlinear dynamics will be used to investigate the friction induced limit cycles. For a varying controller gain, stable and unstable periodic solutions will be computed numerically with a simple shooting method. The stable and unstable branches will be computed with path-following techniques which, together with the stability analysis of the closed-loop equilibrium points, result in a bifurcation diagram. The results of this chapter have been reported in [67].

In contrast to this computationally expensive bifurcation analysis, the hunting phenomenon is also studied with a more efficient event mapping technique. In Chapter 9, two different types of static frictional damping functions, i.e., (i) a Coulomb friction level plus a discontinuous rise to a larger maximum static friction level and (ii) friction curves with a continuous drop from the maximum static friction level to the lower Coulomb friction level, are used to predict and examine the hunting phenomenon. The local stability of the equilibrium points is discussed and attractor basins are given. This work will be submitted for publication [69].

In Chapter 10, the obtained insight in the hunting limit cycles will be used in an experimental case-study where a Linear Motor Motion System (LiMMS) is considered. Besides the velocity dependent friction force, the system consists also of a nonlinear position dependent cogging force. The existing limit cycles induced by the nonlinear forces in the system combined with a PID controlled regulator task will be analyzed both experimentally and numerically with the event mapping approach and bifurcation diagrams for both the experimental LiMMS setup and the identified model are constructed. The results are in preparation for publication.

In Chapter 11, this thesis will be closed with the 'In Retrospect' chapter, where additional ideas with respect to the analysis of the hunting phenomenon are presented and the obtained results are placed in perspective and summarized. Moreover, recommendations for future research topics for the analysis of friction induced limit cycles will be presented.

## General Introduction

**Part I**

**Identification and Control of  
Mechanical Systems with  
Friction**





# Chapter 2

## Introduction

This introductory chapter will discuss the most widely used friction models as proposed in literature with the main goals, as discussed in Section 1.3, in mind. Therefore, a brief literature review on this topic will be given in Section 2.1, where the results found by Armstrong-Hélouvry et al. [7], Haessig et al. [55] and Olsson et al. [97] will be summarized. In addition the outline of this part will be presented in Section 2.2.

### 2.1 From Static to Dynamic Friction Models

The practically observed friction phenomena as discussed in Section 1.2.1 are considered to be important for accurate friction modeling, analysis of friction related problems and synthesis of controllers. Various mathematical models have been proposed that describe a number of these phenomena. Which model is preferred depends on the purpose of it, but the model that accurately describes all the observed phenomena is in general to be preferred. Besides the question of effectiveness also the model efficiency, e.g., the required computational resources in terms of time, can be of importance when for instance the model will be used in simulation studies. Due to the complexity of the physical mechanisms underlying friction, most models are of an empirical nature. Furthermore, a distinction can be made between ‘static’ and ‘dynamic’ models depending on the inclusion of frictional memory. For static friction models, this frictional memory is omitted, whereas for dynamic friction models this memory behaviour is described with additional dynamics between velocity and the friction force. In the following a brief review of some of the proposed friction models will be given.

#### 2.1.1 Static Friction Models

The observed friction phenomena during the early days of scientific study of friction [2], [30] have led to models of Coulomb, viscous and static friction and its possible combinations, which are often referred to as ‘classical models of friction’. The Stribeck model, which models the Stribeck effect [114], can also be classified nowadays as belonging to this set of models. Three possible combinations are shown in Figures 2.1a) - 2.1c), where the friction force is a static map from the relative velocity  $\dot{x}$  between the two contact surfaces to the friction force  $F_f$ . At rest, i.e.,  $\dot{x} = 0$ , the friction can not be described as a function of only

velocity, but instead as a set-valued function of the sum of external forces  $F$ , where its upper and lower bound is given by the static friction level  $F_s$  and  $F_f \in [-F_s, F_s]$ .

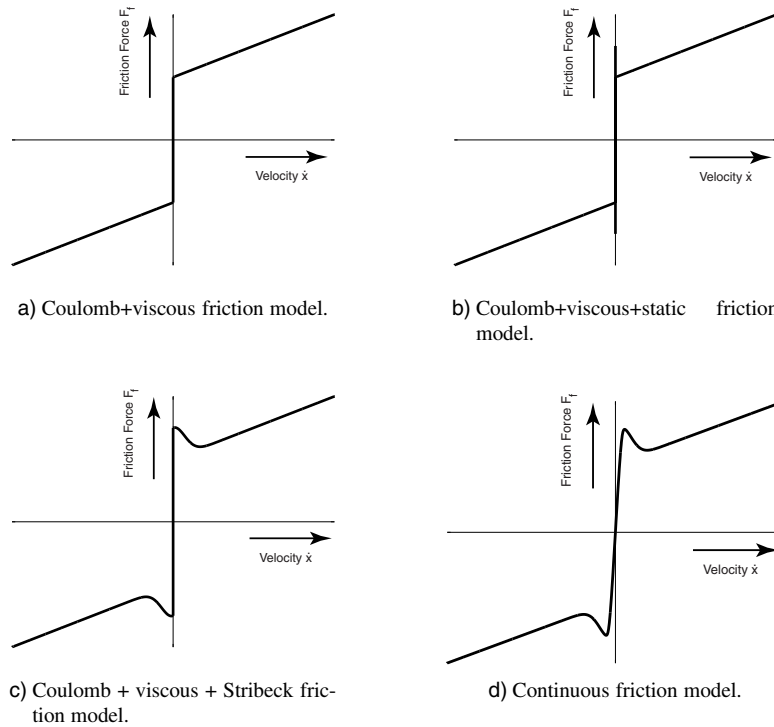


Figure 2.1 - Various combinations of 'static' friction models.

The discontinuity at zero velocity may lead to (i) non-uniqueness of the solutions to the equations of motion for the system [16], [85], which might even occur in real-life and (ii) numerical problems if such a model is used in simulation. For instance, one problem that can arise when using explicit methods for numerical integration is numerical chatter [13]. Precautions have to be taken when numerically integrating a system model that includes discontinuities as introduced by the classical friction models. One approach to overcome the discontinuity is approximating or smoothing the map by a curve with finite slope [55], [84], as depicted in Figure 2.1d). However, a very steep slope around zero velocity can result in very short integration time steps which slows down simulation. Moreover, the body connected to the frictional contact surface will accelerate even if the external forces on the body are less than the peak static friction force  $F_s$  and therefore these alternate friction models will not provide true stiction. Another common technique is to employ a switching function such as

## 2.1 From Static to Dynamic Friction Models

the signum function defined by

$$\text{sgn}(\dot{x}) = \begin{cases} +1 & \forall \dot{x} > 0 \\ 0 & \forall \dot{x} = 0 \\ -1 & \forall \dot{x} < 0 \end{cases},$$

where  $\dot{x}$  is the relative velocity between the two contact surfaces. However for simulation purposes the question arises: At what time instant does zero velocity crossing occur? [8]. Besides possible numerical chattering, this signum model also lacks the notion of true stiction, since external forces in the model smaller than the Coulomb friction level are not compensated at zero velocity by an equivalent friction force.

Recognizing these problems, Karnopp proposed an alternative model to overcome these problems of zero crossing detection and numerical stiffness [79], [55]. To avoid the problem of locating zero velocity with high precision, he defined a small neighbourhood of zero velocity. Outside this neighbourhood friction is the usual function of velocity. Inside this neighbourhood the velocity is considered to be zero and friction is a function of the other forces in the system, forces that are required to hold the system at zero velocity.

$$F_f(\dot{x}, F) = \begin{cases} F_f(\dot{x}) & \forall |\dot{x}| \geq \eta \\ F_f(F) & \forall |\dot{x}| < \eta \end{cases},$$

where  $F$  represents the sum of the other forces in the system,  $\eta$  is the small constant value defining the small neighbourhood. The main advantage of this model is its efficiency in simulation. A drawback of the model is that it is strongly depends on the rest of the system by means of  $F_f(F)$ , which will be different for different system configurations. Moreover, the corresponding set of ordinary differential equations might suffer from numerical instabilities in the stick phase as demonstrated by Sepehri et al. [110]. The so-called Switch friction model, as proposed by Leine et al. [84], overcomes these numerical instabilities and can be considered as an extended version of the Karnopp model. The Switch model describes a system with friction by three different sets of Ordinary Differential Equations (ODEs): one for the slip phase, another for the stick phase and a third for the transition phase for stick to slip. At each time instant the state of the system determines which phase the system is in and the corresponding ODE is chosen to be integrated numerically. The model switches between the different phases by examination of the relative velocity and the sum of the external forces  $F$  acting in the system. If the relative velocity is outside the small neighbourhood  $\eta$  the system is in the slip phase and if the velocity is within this narrow band the system can either be in the stick or in the transition phase. If the system is within the narrow stick band and the external forces are less or equal to the static friction level then the friction model is in the stick phase otherwise it is in the transition phase. In contrast to the Karnopp model, the acceleration of the body is given the following linear behaviour  $\ddot{x} = -\alpha\dot{x}$  to force the relative velocity to zero in the stick mode of the Switch model, which consequently forces the relative velocity to the middle of the narrow stick band. The Switch friction model can be implemented with a pseudo code, i.e., `if then else`-rules, and therefore maintains the continuity of the state vector, which yields a set of ODEs that does not suffer from numerical

instabilities.

One of the major disadvantage of the discussed ‘static’ friction models is the limited richness of the models, which will result in inaccurate friction models for certain regions of interest, such as presliding displacement in the stiction regime or frictional lag for the sliding mode. For the analysis of friction related problems or controller synthesis these phenomena may be of importance, which motivated researchers to make an effort in that direction.

A model that has been devised to include all the relevant observed friction phenomena, as discussed in Section 1.2.1, is the *seven parameter model* [6], [7]. Like the Karnopp model it actually consists of two separate models: one for stiction and one for sliding. During stiction, friction is modeled as a stiff spring

$$F_f(x) = \sigma x$$

to account for presliding displacements. When sliding, the friction is modeled as Coulomb ( $F_c$ ) + viscous ( $F_v$ ) + Stribeck friction with frictional memory:

$$F_f(\dot{x}, t) = \left( F_c + F_v |\dot{x}| + F_s(\gamma, t_2) \frac{1}{1 + \left( \frac{\dot{x}(t - \tau_L)}{\dot{x}_s} \right)^2} \right) \text{sgn}(\dot{x}),$$

where

$$F_s(\gamma, t_2) = F_{s,a} + (F_{s,\infty} - F_{s,a}) \frac{t_2}{t_2 + \gamma}$$

describes the varying friction level at break-away. The level of the static friction force  $F_s$  varies with the time at zero velocity  $t_2$  (dwell time), where a long dwell time gives rise to a high break-away force. The force  $F_{s,a}$  is the magnitude of the Stribeck friction at the end of the previous sliding period;  $\gamma$  is an empirical parameter. The friction force for the sliding mode is equivalent to a static friction model where the velocity has been replaced with a delayed version and which has a time dependent coefficient  $F_s$  [97]. The time delay  $\tau_L$  accounts for the desired frictional memory. When used in simulations some mechanism has to be employed to switch between the two modes for sliding and stiction. Also, the model states  $x$  and  $\dot{x}$  have to be initialized appropriately every time a switch occurs. Although useful for analysis of stick-slip behaviour [6], for simulation purposes the model seems to be less appropriate, at least according to [41] who performed a simulation study employing, amongst several other friction models, the seven parameter model.

## 2.1.2 Dynamic Friction Models

The seven parameter model and similar models try to capture the dynamics of friction by introducing time dependency or a time delay. An alternative approach are the use of dynamic models, which are also often referred to as state variable models. In its general form state variable models were introduced by geophysicists to study stick-slip phenomena. Interest in these phenomena stems from the hypothesis that earthquakes are stick-slip events, in which

## 2.1 From Static to Dynamic Friction Models

the earth's tectonic plates in succession stick and slip [105]. The idea is to introduce extra state variables (or internal states) that determine the level of friction in addition to velocity. The evolution in time of the state variables is governed by a set of differential equations. Often the introduced state variables can be given a physical interpretation, which depends on the friction mechanism that the friction model is supposed to describe. Over the past decades a few friction models belonging to this class have been proposed, i.e., in the late 1960's the Dahl model [33] and in the 80's the state variable model as presented by Rice et al. [105], but only recently interest seems to have increased especially within the control community where several dynamic friction models have been proposed in the 1990's by Haessig et al. [55], Dupont et al. [39], Canudas de Wit et al. [24] and Bliman et al. [16]. Here, the research path which starts with the Dahl model [34] will be discussed in more detail, because it resulted in the nowadays widely used dynamic LuGre friction model [24].

To describe presliding displacements, i.e., elastic and plastic deformations of the asperity junctions before macroscopic sliding [31], Dahl thought of exploiting the stress-strain curve of two surfaces under contact known from solid mechanics [34]. The stress-strain curve can be transformed into a force-displacement curve  $F_f(x)$ . This force-displacement curve is considered to be the solution to a differential equation of the form

$$\frac{dF_f}{dx} = \sigma \left(1 - \frac{F_f}{F_c} \operatorname{sgn}(\dot{x})\right),$$

where  $F_c$  is the Coulomb friction force and  $\sigma$  the stiffness of the asperity junctions at  $F_f = 0$ . Suppose  $\dot{x} > 0$ , then  $F_f(x)$  will behave as a first order system with time constant  $\frac{F_c}{\sigma}$  and a static gain  $F_c$ . With the observation that

$$\frac{dF_f}{dt} = \frac{dF_f}{dx} \frac{dx}{dt},$$

Dahl came to a generalization of ordinary Coulomb friction, a model of the form

$$\frac{dF_f}{dt} = \sigma \left(1 - \frac{F_f}{F_c} \operatorname{sgn}(\dot{x})\right) \dot{x}.$$

This can be rewritten to the following single state friction model

$$\begin{aligned} \dot{\theta} &= \dot{x} - \frac{\sigma |\dot{x}|}{F_c} \theta, \\ F_f &= \sigma \theta. \end{aligned}$$

The nature of the internal state  $\theta$  will be given a physical interpretation later. For now let us assume that the system moves with constant velocity or in other words let us consider the steady-state behaviour of this dynamic friction model. The steady-state friction force is then given by

$$F_f = \sigma \theta = F_c \operatorname{sgn}(\dot{x}),$$

in which the Coulomb friction characteristics can be recognized. Dahl developed the model to describe dry sliding friction in ball bearings, hence other friction phenomena are not

modeled, e.g., the Stribeck effect or static friction. Its simplicity is a nice feature, that caught the attention of other researchers and motivated them to extend the Dahl model to include other observed friction phenomena as well.

The randomness of friction originates from the random distribution of asperities on a surface. A model that tries to capture this behaviour is the bristle model introduced by Haessig et al. [55], that assumes friction between two contact surfaces to be caused by a large number of interacting bristles as shown in Figure 2.2. A bonded bristle acts as a spring and when the

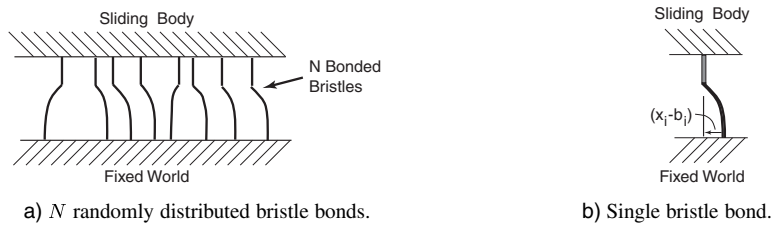


Figure 2.2 - The bristle model.

strain  $|x_i - b_i|$  of a certain bristle exceeds a certain level  $\delta_s$  the bond is broken and a new bond with a randomly distributed strain is established. Friction is made a function of velocity by further assuming that the number of bristles depends on the relative velocity of the opposing surfaces. The friction force is the sum of the individual spring forces, which is given by

$$F_f = \sum_{i=1}^{N(\dot{x})} \sigma_0(x_i - b_i),$$

where  $N$ , the number of bristles, depends on the velocity. The stiffness of the bristles is represented by  $\sigma_0$ ,  $x_i$  is the relative position of the bristles and  $b_i$  is the location of the  $i$ -th bristle which is randomly distributed. Numerically, the bristle model is highly inefficient and will therefore normally not be used in simulations. Its merits are to be found in the interpretation of friction as interacting bristles and the random behaviour it generates. A model feasible for general simulation purposes was subsequently proposed by Haessig et al. [55]: the numerically more efficient reset integrator model, which models the bonding effect during stiction by a single position variable or sliding displacement  $z$ . Hence, the local randomness of friction is modeled by averaging the stochastic properties of the different bristle bonds into this deterministic presliding displacement  $z$ . When a characteristic presliding distance  $z_0$  is exceeded macroscopic sliding starts and the model changes from the stick mode to the slip mode. Again, as was already the case for the Karnopp and the seven parameter model, the friction model consists of two different models and a switching variable. The position variable  $z$  can be considered to be a state variable, and its dynamics is given by the following

## 2.1 From Static to Dynamic Friction Models

differential equation:

$$\frac{dz}{dt} = \begin{cases} 0 & \text{if } (\dot{x} > 0 \text{ and } z \geq z_0) \text{ or } (\dot{x} < 0 \text{ and } z \leq -z_0) \\ \dot{x} & \text{otherwise.} \end{cases}$$

The friction force in either of the two friction modes (stiction or sliding) is given by

$$F_f = \begin{cases} \sigma_0(\dot{x})(1+a)z + \sigma_1 \frac{dz}{dt} & |z| < z_0 \\ \sigma_0(\dot{x})z_0 & |z| \geq z_0, \end{cases}$$

where  $\sigma_1 \frac{dz}{dt}$  is an extra damping term included for the reason of physical realism, i.e., to avoid undamped oscillations during the stick mode. The modulated stiffness  $\sigma_0(\dot{x})$  is an arbitrary function of velocity and the coefficient  $a$  is added to model a higher level of static friction. During stiction, the friction force cancels the driving force through deflection of a spring-damper system. The model is discontinuous in the state variable  $z$  as is evident from the drop in the friction force when switching from stiction to sliding. Numerical stiffness problems may arise for very large spring stiffness and damping values.

A model that is in line with the considerations of the Dahl model and also employs the idea of an averaged characteristic presliding displacement  $z$ , as introduced by Heassig et al. [55], has been proposed by Canudas de Wit et al. [24], where it is presented as the LuGre model. It combines the Dahl model with arbitrary steady-state characteristics such as the Stribeck effect. However, the interpretation of the internal state is that of the bristle model, i.e., friction is visualized as forces produced by bending bristles behaving like springs, but instead of modeling the random behaviour of friction it is based on the average behaviour of the bristles. The average deflection of the bristles is denoted by  $z$  and is modeled as

$$\frac{dz}{dt} = \dot{x} - \sigma_0 \frac{|\dot{x}|}{g(\dot{x})} z,$$

where the arbitrary steady-state behaviour  $g(\dot{x})$  models the Stribeck effect with a Gaussian function

$$g(\dot{x}) = F_c + (F_s - F_c) \exp\left(-\left(\frac{\dot{x}}{v_s}\right)^2\right).$$

The friction force is given as a function of the state variable  $z$  and velocity  $\dot{x}$  by

$$F_f = \sigma_0 z + \sigma_1 \frac{dz}{dt} + b\dot{x}. \quad (2.1)$$

For the same reason as with the reset integrator model an extra damping term is included and viscous friction is represented by  $b\dot{x}$ . The Stribeck effect is reproduced by assuming that the average deflection of the bristles at steady-state motion, and therefore the friction force, decreases with increasing velocity. Thus, neglecting for a moment viscous friction, at steady-state the friction force is given by

$$F_f = \sigma_0 z = g(\dot{x}) \text{sgn}(\dot{x}).$$



The LuGre friction model, as given in Eq. (2.1), is a special case of the model and is denoted as the standard parametrization, which is due to linear viscous friction and a constant bristle damping parameter  $\sigma_1$  [97]. This standard parametrization can be restrictive with respect to the desired passivity property of friction as shown by Barabanov et al. [10]. The authors present necessary conditions for the passivity property to hold for the LuGre model. The conditions are expressed in terms of a simple algebraic inequality involving the parameters of the model. A velocity dependent parametrization of the bristle damping might result in a model which is dissipative [96]. If the damping coefficient  $\sigma_1$  decreases for increasing velocity, e.g.,

$$\sigma_1(\dot{x}) = \sigma_1 \exp -\left(\frac{\dot{x}}{v_d}\right)^2$$

a dissipative model is obtained, which is physically motivated by the change of the damping characteristics as velocity increases, due to more lubricant being forced into the interface of the two contact surfaces.

The LuGre model exhibits a rich behaviour in terms of observed friction phenomena and in particular is able to model: stiction, the Stribeck effect, frictional lag or hysteresis and stick-slip transitions. However some of the practically observed hysteresis related phenomena can not be predicted accurately by the LuGre model as shown by Olsson et al. [97] and Swevers et al. [116]. The latter proposes an extension of the LuGre model to approach these hysteresis problems. The notion of stiction is re-addressed by Dupont et al. [40], who discusses the difference between stiction and presliding displacement. In their analysis both the dynamic Dahl and LuGre friction model are considered to possess presliding displacement but no stiction. A new Elasto-Plastic state variable friction model is proposed which models both stiction and presliding displacement. However, the proposed model by Swevers et al. [116] is more complex than the standard parametrization of the LuGre model due to the use of a hybrid hysteresis model and therefore more difficult to be used for control design and analysis. On the other hand, the Elasto-Plastic state variable friction model proposed by Dupont et al. [40] is mainly based on simulation studies and the presented ideas are not yet confirmed experimentally. Hence, throughout this thesis the standard parametrization of the LuGre model will be used.

Another dynamic friction model inspired by the Dahl model is the Bliman-Sorine friction model [16]. This second order linear dynamic friction model connects a fast and a slow Dahl model in parallel, where the fast model has the highest steady-state friction and the force from the slow model is subtracted from the fast model, which results in a stiction peak. However, comparison studies [46], [97] revealed that the dynamic LuGre model is beneficial with respect to the ability to model rate dependent friction phenomena, such as varying break-away force and frictional lag. Moreover, the model order of the Bliman-Sorine model is higher than for the LuGre model and the damping properties during stiction is numerically more efficient for the LuGre model. Hence, the Bliman-Sorine friction model will not be used further.

## 2.2 Outline of Part I

### **2.2 Outline of Part I**

In the Chapters 3 and 4 identification studies will be performed, which follow in some sense the research line of the discussed friction models in the previous section. In Chapter 3 two black-box ‘static’ friction models are combined with physical “white” knowledge of the system at hand, where an augmented state extended Kalman filter is used iteratively and off-line for the estimation of the unknown model parameters. In contrast to the identification of these static friction models, an efficient frequency domain procedure for the identification of the presliding displacement regime will be presented in Chapter 4. The identification procedure for the dynamic model parameters of the LuGre model, i.e., (i) the stiffness and (ii) the damping of the presliding phenomenon, is reduced from performing several dedicated experiments to one experiment. In Chapter 5 the dynamic LuGre friction model and a static alternate friction model based on the Polytopic Linear Model of the Stribeck effect will be compared with respect to their performance for regulator tasks on mechanical systems that exhibit friction. This first part is closed with the ‘In Retrospect’ Chapter 6, where the obtained results are placed in perspective and summarized. Moreover, recommendations for future research topics will be presented.

Part I - Identification and Control of Mechanical Systems with Friction

## Chapter 3

# Grey-box Modeling of Friction: An Experimental Case-study

### Abstract

Grey-box modeling covers the domain where we want to use a balanced amount of white-box modeling based on first principles and black-box modeling based on empiricism. The two grey-box models presented combine a white-box model with a black-box model, i.e., a Neural Network model and a Polytopic model that are capable of identifying friction characteristics that are left unexplained by first principles modeling.

In an experimental case-study, both grey-box models are applied to identify a rotating arm subjected to friction. An augmented state extended Kalman filter is used iteratively and off-line for the estimation of unknown parameters. For the studied example and defined black-box topologies, little difference is observed between the two models. In addition, the applicability of the identified models is illustrated in a model based friction compensation control scheme with the objective to linearize the system.

---

This chapter has been published in the European Journal of Control [62]. The Extended Kalman Filter tool used in this chapter is documented in more detail in [61].

### 3.1 Introduction

Friction is to some extent present in all mechanical systems. Where this phenomenon is partially neglected, and left unexplained by white-box modeling based on first principles, it can limit the performance of industrial model-based control systems due to increasing tracking errors and limit cycles [7]. Nevertheless, if detailed prior knowledge about the system is available, and white-box modeling is applicable, it might result in complex friction descriptions not very suitable for the purpose of control. It is often a time consuming job to construct these white-box models. On the other hand, black-box models are easier to construct, but purely rely on the data. If data is sparse in some regions of the operating space one may not expect to identify a reliable model. Furthermore, a black-box model does not extrapolate well and the identified parameters in the chosen model structure do not have a physical meaning. Moreover, engineering knowledge is incompatible with most empirical model representations and is therefore difficult to exploit.

Since both white-box and black-box modeling approaches have their merits as well as their drawbacks, there has in recent years been an increasing interest in combining the best of these two approaches. This approach to modeling has been termed grey-box modeling [9], [17], [36], [50].

Since we are interested in identifying a rotational mechanical system (that exhibits several distinct friction phenomena) both for control purposes and qualitative friction analysis we want to use a balanced amount of first principles and empiricism.

Two promising grey-box model structures will be compared on this benchmark system, i.e., a Neural Network model and a Polytopic model. It appears that *a priori* unknown friction characteristics can be modeled such as proposed for instance by [109]. In comparison to the presented theoretical friction models in [7] black-box models approximate any nonlinear function without restricting to known system properties such as equilibrium points and odd friction functions. Here, the grey-box model structure is chosen in such a manner that these *prior* known system characteristics, e.g., odd friction function and equilibrium points of the autonomous system, are met.

In literature, the inertia and friction characteristic are often identified separately, e.g., in the work of Johnson [77] and Held [58]. Here, the well known augmented state Extended Kalman Filter (EKF) [51] is applied for the simultaneous estimation of parameters in both the black-box and white-box part of the model. Since the model parameters enter the models in a nonlinear fashion, the computationally less demanding method proposed by [56] based on the State Dependent Riccati Equation (SDRE) Filtering technique is not applicable. The identification is performed with position sensing and velocity reconstruction, where compared to the work of, for instance, Armstrong-Hélouvy [5] this is done with acceleration sensing. The objective is to identify simulation models, which might give rise to the question whether this is the right objective for modeling for control. Here, the primary goal is to obtain good simulation models and the secondary goal is to perform a closed-loop friction

## 3.2 Rotating Arm Characteristics

compensation law.

The estimated grey-box models can be utilized for the control of the system. A nonlinear state feedback friction compensation [77], [83] will be demonstrated to linearize the system. Other friction compensation designs are described by [97] for dynamic friction models, [73] applying a dithering technique and an acceleration feedback control approach by [117]. Since the main goal is not to design a new friction compensation law, the used compensator is tested for closed-loop responses with (i) step inputs and (ii) velocity reversals (sinusoidal inputs) and compared to the theoretical linear system responses.

In Section 3.2, we will give a description of the rotating arm. The two grey-box models will be discussed in Section 3.3. An EKF is proposed to estimate the unknown parameters of the models in Section 3.4. In Section 3.5 the friction compensation control law is formulated which linearizes the system for the ideal case where the model exactly represents the system. In Section 3.6 experimental results are reported to illustrate the grey-box modeling techniques. The chapter will be concluded in Section 3.7.

## 3.2 Rotating Arm Characteristics

The rotating arm under study can be considered as a nonlinear mechanical system [91]. The state space equations describing the rotating arm system as shown in Figure 3.1 are

$$\frac{d}{dt} \begin{bmatrix} q \\ \dot{q} \end{bmatrix} = \begin{bmatrix} \dot{q} \\ -M^{-1}C(\dot{q}, \theta) \end{bmatrix} + \begin{bmatrix} 0 \\ M^{-1}c_m \end{bmatrix} u \quad (3.1)$$

where

$q$	Angular displacement
$\dot{q}$	Angular velocity
$M$	Effective inertia of the motor-transmission-rotating arm combination
$C(\dot{q}, \theta)$	Friction
$c_m$	Motor gain
$u$	Induction motor input voltage
$\theta$	Parameters

The friction torque  $C(\dot{q}, \theta)$  is assumed to be a function of the angular velocity  $\dot{q}$  and of the model parameters  $\theta$ . Furthermore, it is assumed that the friction can be modeled by an odd continuous function

$$\hat{C}(\dot{q}, \theta) = -\hat{C}(-\dot{q}, \theta) \quad \dot{q} \in \mathbb{R}$$

For angular velocity equal to zero the model friction torque is zero, which results for the model in the same set of equilibrium points as for the system. The friction model does not describe stiction, since the system will always slide (i.e. move) for an applied force  $u$  unequal to zero. The choice for this simplified friction model has two main reasons.

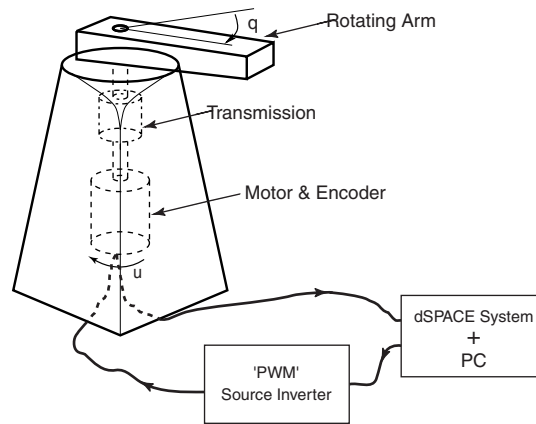


Figure 3.1 - Rotating arm.

- The *stiction* regime will be approximated, if the slope of the friction function near  $\dot{q} = 0$  is very steep. Then the model can still give acceptable simulation results, i.e., angular displacement during stiction is neglectable.
- A continuous friction function will facilitate the numerical solution of the  $2^{nd}$  order differential equation (3.1).

The proposed friction model is static and exhibits no dynamic behaviour, which has received a lot of research interest [16], [24], [55] over the last few years. Practically observed dynamic friction phenomena, e.g., presliding displacement [31] and frictional lag [57], are not observable in the experimental setup due to the accuracy of the encoder used. Hence, dynamic friction models can not be identified on the setup and are therefore not used.

The resolution of the encoder used to measure the angular displacement is  $1.9175 \cdot 10^{-4}$  [rad]. The induction motor is supplied by a 'Pulse Width Modulation' source inverter which translates the input signal, i.e., the desired torque expressed in a voltage, into three phase signals with a fundamental frequency. This source inverter actually controls the torque produced by the motor to the desired torque. The input signal of the source inverter and the TTL encoder signals are respectively send and read by a dSPACE system [37]. During the experiments the sample frequency is set to 1 [kHz].

### 3.3 Grey-box Modeling

Grey-box modeling covers the region, where we want to use a balanced amount of first principles and empiricism. In this case, the mechanical model structure is known but the

### 3.3 Grey-box Modeling

friction component is left unexplained and also the inertia ( $M$ ) has to be estimated. Despite of their fixed topology, the grey-box models have to be compatible with prior knowledge and observed data. Two different grey-box models will be demonstrated to model the rotating arm, i.e., (i) the Neural Network model (NN) [89] and (ii) the Polytopic model.

The NN model uses a decomposition of the system in principal functional components. These functional components can be white-box parts or unknown black-box parts. The white-box part of the model consists of the known functional components defined by Eq. (3.1). The NN modeling approach utilizes a neural network to approximate the friction function  $C(\dot{q}, \theta)$  globally. Since a neural network is a universal approximator [72], it increases the accuracy of the grey-box model.

In the case of the Polytopic modeling, the operating space is decomposed into operating regions. For every operating region a model is defined together with a model validity function. The locally valid models are combined in the operating space to obtain one globally valid nonlinear model. The model structure satisfies the universal approximation property [76], [121]. Since the system is defined by a convex combination of affine models one can associate with this model a polytope in the model parameter space. Therefore, this model type will be called a Polytopic model. The Polytopic model generalizes various model types, e.g., Fuzzy Models [115] and Local Model Networks [75], which all have an equivalent mathematical structure. Furthermore, it should be emphasized that the polytopic model is a different model type than a Radial Basis Function (RBF) model. The RBF model forms an interpolation of constants, where the polytopic model is defined as a convex combination of affine models. Moreover, the weight or basis functions are not normalized in the RBF case which is an essential difference, see [112].

#### 3.3.1 Neural network

The neural network consists of two layers, i.e., one hidden layer and one output layer. The neural network represents a nonlinear mapping from the network input  $\mathbb{R}^r$  into the network output  $\mathbb{R}^s$ . Here, this mapping is from angular velocity  $\dot{q}$  ( $\mathbb{R}$ ) to friction model torque  $\hat{C}(\dot{q}, \theta)$  ( $\mathbb{R}$ ). Defining the weight matrices for the first and second layers as  $W_1$  and  $W_2$ , one can write the neural network output as

$$\hat{C}(\dot{q}, \theta) = W_2^T \Sigma(W_1 \dot{q} + b_1) + b_2$$

where  $b_i$  represents the bias value for the neurons in the  $i$ -th layer and  $\Sigma(\cdot)$  is a nonlinear operator with  $\Sigma(\underline{z}) = [\sigma(z_1), \dots, \sigma(z_v)]^T$ ,  $\sigma(\cdot)$  a differentiable, nonlinear, monotonic increasing function and  $v$  is the number of hidden neurons.

To assure the system properties described in Section 3.2 to hold, the following restrictions are posed on the neural network topology.



## Part I - Identification and Control of Mechanical Systems with Friction

- Choose an odd function for  $\sigma(\cdot)$  which is equal to zero if its argument is zero.

$$\sigma(z_i) = 1 - \frac{2}{e^{2z_i} + 1}$$

- The first choice together with the set of equilibrium points for the system implies that the bias terms should be zero. Here, the assumption is made that there is no bias in the reconstructed angular velocity  $\dot{q}$ .

These two restrictions result for the neural network friction approximator in

$$\hat{C}(\dot{q}, \theta) = W_2^T \Sigma(W_1 \dot{q})$$

The linear part of the system dynamics, i.e., the viscous damper characteristic and the input term are described by two other principal functional components. In state space description the grey-box model becomes

$$\begin{bmatrix} \dot{q} \\ \ddot{q} \end{bmatrix} = \underbrace{\begin{bmatrix} 0 & 1 \\ 0 & -\frac{b}{M} \end{bmatrix}}_{\text{white-box component}} \begin{bmatrix} q \\ \dot{q} \end{bmatrix} - \underbrace{\begin{bmatrix} 0 \\ \frac{W_2^T \Sigma(W_1 \dot{q})}{M} \end{bmatrix}}_{\text{black-box component}} + \underbrace{\begin{bmatrix} 0 \\ \frac{c_m}{M} \end{bmatrix}}_{\text{white-box component}} u$$

where  $b$  is the viscous damper constant of the system. For the model parameters this results in

$$\theta = [W_1^T \quad W_2 \quad b \quad \hat{M}]^T$$

### 3.3.2 Polytopic model

The polytopic model is composed of several locally valid models. The structure of each model is chosen equal to the topology of an mechanical system, i.e.,  $\dot{x} = A_i x + C_i + B_i u$  with  $x = [q \quad \dot{q}]^T$ . With each local model a model validity function  $\rho_i : \mathbb{R}^p \rightarrow [0, 1]$  is associated which, by definition, is close to 1 for those regions in the input and state space where the corresponding local linear model is valid. Here, the partitioning only depends on the angular velocity  $\dot{q}$  due to the choice of the nonlinear friction torque as a function of  $\dot{q}$ . A typical choice for the validity function  $\rho_i$  is the Gaussian function

$$\rho_i(\dot{q}, \theta) = e^{-\frac{1}{2} \frac{(\dot{q} - c_i)^2}{\sigma_i}}$$

where  $c_i$  is the center and  $\sigma_i$  is the variance of the Gaussian function. Now a set of normalized validity functions  $w_i : \mathbb{R} \rightarrow [0, 1]$  can be defined

$$w_i(\dot{q}, \theta) = \frac{\rho_i(\dot{q}, \theta)}{\sum_{j=1}^N \rho_j(\dot{q}, \theta)}$$

where  $N$  is the number of local models used to compose one global model. This definition implies that  $\sum_{i=1}^N w_i(\dot{q}, \theta) = 1 \forall \dot{q}$ . The polytopic friction model becomes

$$\hat{C}(\dot{q}, \theta) = \sum_{i=1}^N w_i(\dot{q}, \theta) (a_i (\dot{q} - c_i) + b_i)$$

### 3.4 Estimation of the Model Parameters

where  $a_i(\dot{q} - c_i) + b_i$  is the affine model of the friction locally valid around velocity  $c_i$ . For the identification of the Polytopic model, the centers  $c_i$ , slopes  $a_i$  and offsets  $b_i$  of the linear models and the variance  $\sigma_i$  of the Gaussian validity functions have to be estimated.

One way to construct an odd function with the polytopic model is to:

- Choose an odd number of local models, where one locally valid model has no offset, i.e.,  $b_1 = 0$  and the corresponding center  $c_1 = 0$ . Again, the assumption of an unbiased reconstruction of the angular velocity  $\dot{q}$  is adopted here.
- The other  $N - 1$  models are divided in pairs of two, where the centers are opposite  $c_{2i} = -c_{2i+1}$ , the variances are equal  $\sigma_{2i} = \sigma_{2i+1}$  as well as the slopes  $a_{2i} = a_{2i+1}$  and the offsets are again opposite  $b_{2i} = -b_{2i+1}$  with  $i = 1, \dots, \frac{N-1}{2}$ . An advantage of this construction is the reduction of parameters by a factor 2.

These conditions assure an odd function which gives zero if  $\dot{q}$  is zero in order to guarantee the equilibrium property. The state space representation of the polytopic model becomes

$$\begin{bmatrix} \dot{q} \\ \ddot{q} \end{bmatrix} = \sum_{i=1}^N w_i(\dot{q}, \theta) \left\{ \begin{bmatrix} 0 & 1 \\ 0 & -\frac{a_i}{M} \end{bmatrix} \begin{bmatrix} q \\ \dot{q} \end{bmatrix} + \begin{bmatrix} 0 \\ \frac{a_i c_i - b_i}{M} \end{bmatrix} + \begin{bmatrix} 0 \\ \frac{c_m}{M} \end{bmatrix} u \right\}$$

where the first term on the right-hand side are the normalized validity functions and the second term between the brackets the locally valid linear mechanical models. For the polytopic grey-box model, the model parameters become

$$\theta = [a_1 \ a_{2i} \ b_{2i} \ c_{2i} \ \sigma_1 \ \sigma_{2i} \ \hat{M}]^T \quad i = 1, \dots, \frac{N-1}{2}$$

So, the modeling problem is reduced to dividing the operating space of the system into a set of operating regimes and identifying with every operating regime a locally valid mechanical model together with a corresponding validity function.

Although the proposed black-box models, motivated by the properties of the general model classes, have limited complexity, the models show clear resemblance with the properties of the underlying mathematical fields.

### 3.4 Estimation of the Model Parameters

The rotating arm will be identified with the objective to obtain simulation models that yield accurate long-term prediction. The model parameters are estimated with an algorithm that minimizes an output error criterion. Due to the smoothness of the proposed nonlinear grey-box models the Extended Kalman Filter (EKF) seems a suitable technique for estimating the model parameters [51]. The filter is able to reconstruct the state of the continuous-time system with discrete-time measurements of the system outputs. This technique, which is based on the assumption that all errors are stochastic, minimizes the variance of the

reconstruction error, i.e., the difference between the actual state  $x$  and the estimated state  $\hat{x}$ .

The nonlinear parameter estimation procedure for continuous-time mechanical models, Eq. (3.1), with discrete measurements will be outlined shortly. First the state  $x = [q \ \dot{q}]^T$  is augmented with the unknown parameters,  $\theta \in \mathbb{R}^k$  such that the new state  $x^* = [x \ \theta]^T$ . The parameter estimation problem is converted into a state ( $x^*$ ) reconstruction problem. Consequently, Eq. (3.1) has to be augmented with  $k$  trivial differential equations  $\dot{\theta} = 0$ , which marks the parameters as constants.

Here, the model errors are considered to be zero mean gaussian noise having intensity matrices  $Q(t)$  for the state equation error and  $R(t)$  for the measurement error. Furthermore, the errors are assumed to be uncorrelated. The uncertainty in the initial state estimate  $\hat{x}^*(0)$  can be expressed by the diagonally chosen initial covariance matrix  $P(t_0)$ . The EKF technique is, in contrast to Least Squares (LS) methods, able to incorporate model uncertainties by the model errors. Moreover, the model validation is possible during Extended Kalman Filtering by inspection of the innovation signal on the state equations. Deterministic behaviour of the innovation sequence indicates model errors.

For a start, the EKF technique was implemented off-line. However in principle, the EKF approach can be applied on-line in real-time applications. First, an experiment must be performed to obtain measured experimental data. These data should excite all system dynamics we are interested in. Second, the data are passed through the filter several times until the parameter estimates converge. After each filter pass, the initial system states  $x$  and the corresponding covariance matrices are re-initialized with the initial estimates of the first pass. The parameters  $\theta$  and the corresponding covariance matrix are reset to the final estimates of the previous filter pass. When the parameters have become constant, after applying the iterative EKF, the estimates can be considered as smoothed estimates [51] which implies that effectively an output error criterion is minimized.

### 3.5 Nonlinear State Feedback Friction Compensation

If the frictional characteristic of the rotating arm is identified accurately, a nonlinear compensation law can be designed. Here, a nonlinear state feedback friction compensation will be used to linearize the system, which is shown in Figure 3.2. This compensation law results in the closed-loop behaviour:

$$M\ddot{q} = -C(\dot{q}) + \hat{C}(\dot{q}) + \hat{M} \left[ -k_1\dot{q} - k_2\ddot{q} + u^* \right]$$

In the ideal case where  $\hat{M} = M$ ,  $\dot{\hat{q}} = \dot{q}$  and  $\hat{C} = C$ , which results in full nonlinear compensation, the closed-loop system is described by the linear system

$$\ddot{q} + k_2\dot{q} + k_1q = u^*$$

### 3.6 Experimental Study

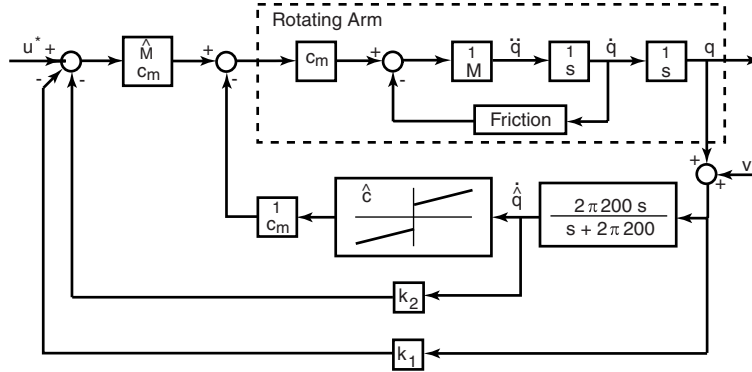


Figure 3.2 - Nonlinear state feedback friction compensation.

## 3.6 Experimental Study

In this section an experimental study will be reported, where the parameters of the two proposed models are estimated with experimental data obtained from the rotating arm.

The rotating arm is excited by a motor torque  $c_m u$  which together with the measured angle and arm velocity responses of the system are depicted in Figure 3.3. Here, we are mainly interested in the friction phenomenon and non-zero angular velocities. The measured angle is differentiated numerically by a high pass filter with a cut-off frequency of 200 [Hz] to reconstruct the angular velocity. The measurement noise is not visible on the scale of the plots.

For the parameter estimation, the two model structures have to be specified, i.e., the number of neurons for the NN and the number of linear models for the polytopic model have to be chosen. Both the number of neurons and the number of linear models are set to 3. Hence, the total number of parameters to be estimated for the NN model becomes 8; 6 parameters for the neural network, one for the viscous damping and one for the inertia. For the polytopic model 7 parameters have to be determined; 6 for the polytopic friction model and one for the inertia. The motor constant  $c_m$  is in both cases assumed to be exactly known and set to 16 [N·m/V].

The initial state of the system is known, but the model parameters are not known. The initial model parameters are chosen in such a manner that physical known properties, e.g., positive inertia value or positive viscous damper value, are met. Hence, the error variance for the initial state estimates is small while we are not sure of the initial estimates for the model parameters. These considerations lead to the initial variance matrix  $P(t_0) = \text{diag}(0, 0, 1, \dots, 1)$  where the non-zero elements correspond to the variance of initially uncertain parameters. The matrix  $Q(t)$  can be seen as the variance of the

## Part I - Identification and Control of Mechanical Systems with Friction

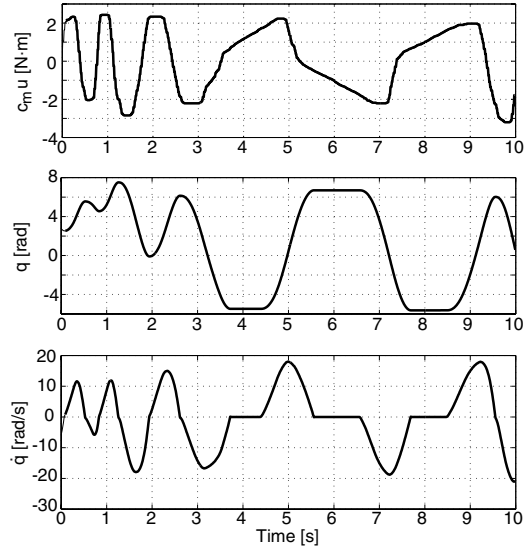


Figure 3.3 - Experimental data.

augmented state model errors. Here the assumption is that the model errors are not cross-correlated. Furthermore the model equations describing constant model parameters and  $\frac{d}{dt}q = \dot{q}$  from Eq. (3.1) are regarded as true. Combined this gives a diagonal matrix with  $Q(t_0) = Q(t) = \text{diag}(0, Q_{22}, 0, \dots, 0)$  where  $Q_{22} = 0.001$ . Due to the finite encoder resolution of  $1.9175 \cdot 10^{-4}$  [rad] and the differentiation scheme an uncertainty on the angular velocity reconstruction is introduced. To take this into account the variance matrix  $R(t)$  is constructed by a diagonal matrix  $R(t) = \text{diag}(0.001, 0.01)$  where 0.001 corresponds to the uncertainty in the angle measurement and 0.01 to the uncertainty in the arm velocity reconstruction. The filter tuning is mainly based on experience and trial and error. It is important that the parameters converge to constant values. Different filter tunings will result in different convergence speeds and even parameter divergence can occur.

After 10 filter passes the parameter estimates become constant and the sum of eigen-values of the covariance matrix  $P(t)$  is minimal. The identified inertia value is the same for both models, i.e.,  $0.0292$  [kg·m<sup>2</sup>/rad]. In Figure 3.4 both the estimated neural network and polytopic friction model, as a function of the angular velocity  $\dot{q}$ , are shown. The following different friction phenomena can be distinguished from the estimated friction models: (i) coulomb friction, (ii) static friction, (iii) stribek effect for low velocities and (iv) viscous friction for high velocities.

The validation of the models is two-folded: (i) examination of the filter innovation on the second state for constant model parameters and (ii) performing a validation experiment where the system response is compared to the model responses. First, the innovation

### 3.6 Experimental Study

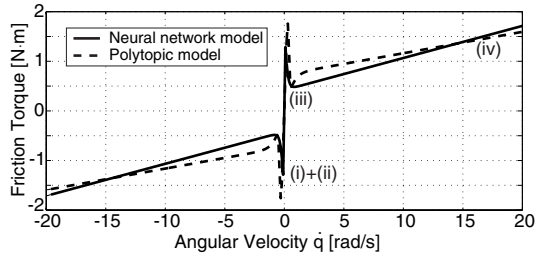


Figure 3.4 - Identified friction models.

sequences on the two models are given in Figure 3.5. In the upper part the innovation signal on the second state equation of the Polytopic model is depicted, which is large for the transitions from the stick phase to the sliding phase. In the lower part of the figure the innovation signal on the second state equation of the Neural Network model is shown, which is much smaller for the mentioned regime. This implies a better stick-slip approximation for the Neural Network model. To get an idea of the accuracy of the models, the innovation signals have to be compared to the angular velocities that occur during the identification. Since the angular velocities vary from  $-20$  to  $20$  [rad/s], i.e., approximately 100 times the level of innovation, the models can be considered as very accurate. The obtained simulation models are also validated by another experiment. The results of the validation experiment and simulated model responses are shown in Figure 3.6. Here the solid lines are the experimental validation data, the dashed lines the Neural Network response and the

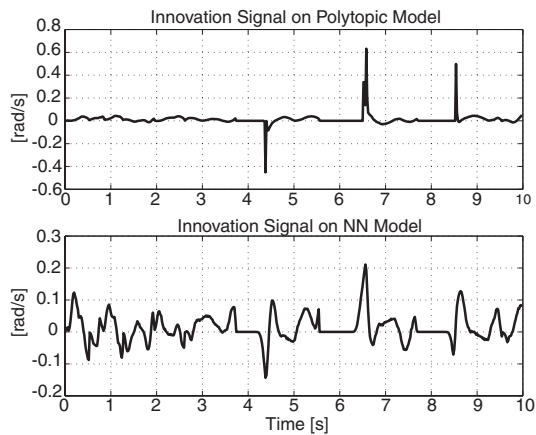


Figure 3.5 - Innovation signals on second state.

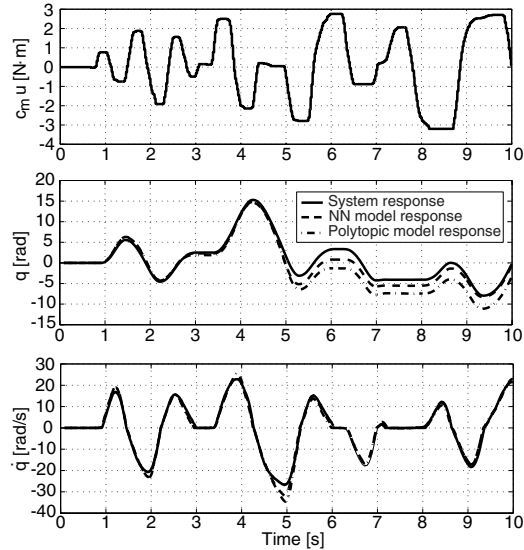


Figure 3.6 - Validation of identified models.

dash-dotted lines the Polytopic model response. For high velocities, i.e.,  $|\dot{q}| \geq 20$  [rad/s], which were not present in the training data, the displacement errors become large. Hence, the models exhibit poor extrapolation and good generalization behaviour. The assumption of the continuous friction function, made in Section 3.2, is justified by the validation responses. For velocities near zero the displacement is indeed much smaller than for high velocities.

An unexpected change of the friction characteristic of the system was recorded due to maintenance effort. This change was investigated by applying the same input torque as for the validation, as shown in Figure 3.7. The dashed lines represent the new system responses, which indicate a change of the friction characteristic. A new identification experiment was performed to get appropriate measurements of the new system behaviour. The inertia was estimated within 2% difference of the earlier identified inertia. New friction models were identified with the earlier identified friction models as initial estimates and the same identification procedure as above. The static friction is not present any more resulting in a friction characteristic describing: (i) coulomb friction and (ii) viscous friction, as shown in the lower plot of Figure 3.7. The black-box models are able to identify different friction characteristics, as shown in Figure 3.4 and Figure 3.7, without changing the black-box topology, i.e., number of neurons for the NN and number of local models for the Polytopic model. To give insight in the accuracy of the identified friction models the reconstructed friction torque from the identification experiment is also plotted in Figure 3.7. The assumption that the friction is an odd function seems to be justified. The neural network friction model gives a slightly better fit of the experimental data than the polytopic friction model. A change in

### 3.6 Experimental Study

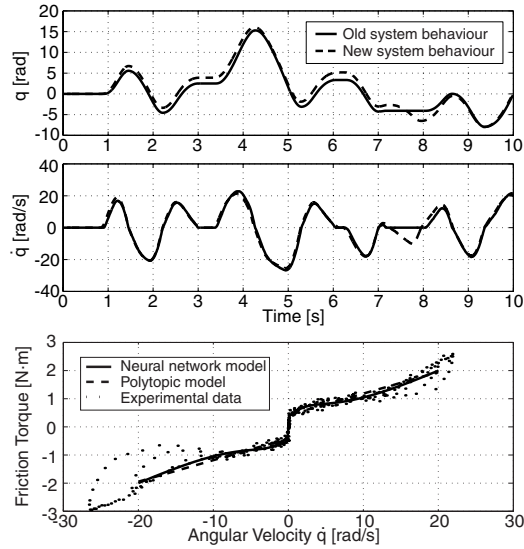


Figure 3.7 - Changed system characteristics and new identified friction models.

the topology of the polytopic model, e.g., five linear models, might allow us to identify a better friction model due to more freedom in the model. Furthermore, hysteresis curves for high angular velocities are recorded which would prefer dynamic friction models instead of static friction models.

The change in the system characteristics and the poor extrapolation behaviour of the models would prefer an on-line implementation of the EKF to adapt to changes in friction, which will be an important topic in future work.

To test the friction compensation law, the closed-loop responses are compared to the theoretical responses for the following two compensation tasks:

- step response performed with  $u^* = 100\varepsilon(t - 2)$ , where  $\varepsilon(\tau)$  is the Heaviside function:

$$\varepsilon(\tau) = \begin{cases} 0, & \forall \tau < 0 \\ 1, & \forall \tau \geq 0 \end{cases}$$

- velocity reversal response performed with  $u^* = -100 \sin(1.5t)$ .

The friction compensation tasks were performed directly after the second identification procedure. Both the closed-loop parameters  $k_1, k_2$  are set to 10. In Figure 3.8 the responses for the positioning task are shown where the solid line is the response of the linear model and the dashed line the experimentally observed response of the friction compensation with different models. With friction compensation a more accurate step response can be observed



## Part I - Identification and Control of Mechanical Systems with Friction

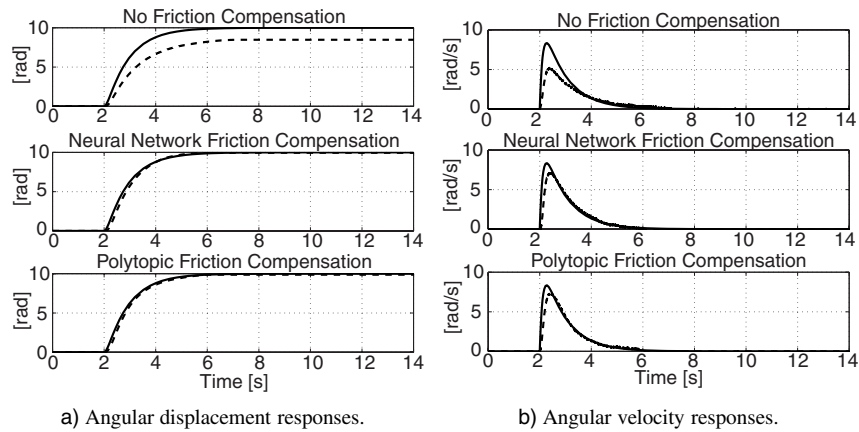


Figure 3.8 - Step input responses.

than without friction compensation. The responses for the velocity reversal task are shown in Figure 3.9 where the same line definitions hold as for Figure 3.8. During the velocity reversal

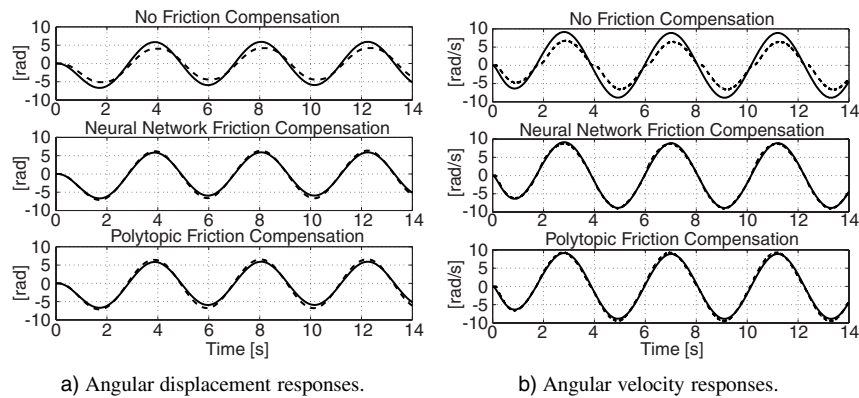


Figure 3.9 - Sinusoidal input responses.

task no stiction is recorded for the friction compensation with both grey-box models, but the stiction is considerable without friction compensation. Hence, the performance for both the tasks can be improved by using a friction compensation based on the grey-box models. To compare the two grey-box models the angular displacement errors and velocity errors for the velocity reversal task are depicted in Figure 3.10. The difference in performance is minimal and little can be said about which model is best. The assumption that the angular velocity

### 3.7 Conclusions

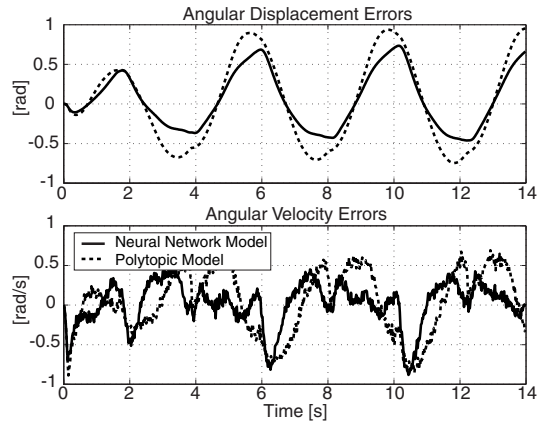


Figure 3.10 - Error responses.

reconstruction is unbiased seems to be untrue according to Figure 3.10, since differentiation of the angular displacement errors (upper plot Figure 3.10) is not equal to the angular velocity errors (lower plot Figure 3.10), where the reconstructed angular velocity  $\hat{q}$  is used. This can be solved by adding a bias term  $d$  to the function argument, i.e.,  $\hat{q}$  becomes  $\hat{q} - d$ , in the friction model equations given in Section 3.3.

### 3.7 Conclusions

The identification of grey-box models presented in this chapter yields good results for an experimental study on a rotating arm which exhibits friction. Although the two proposed grey-box modeling approaches, i.e., Neural Network modeling and Polytopic modeling, are different from a theoretical point of view, both approaches are able to identify a continuous friction function that by construction models *a priori* known system characteristics, e.g., equilibrium points. The friction models can physically be interpreted where friction phenomena such as static friction and the stiction effect are observed. The black-box elements can represent different friction characteristics without changing the black-box topology. Hence, the proposed grey-box models are favourable for the identification of systems with unknown friction characteristics. This ability to represent the friction characteristic accurately results in simulation models that have good long-term prediction with good interpolation and poor extrapolation properties. In future work the choice of the black-box model topology will be investigated and an extension to dynamic friction models will be made.

The iterative EKF approach appears to be a useful identification tool for the proposed nonlinear continuous-time modeling techniques where discrete-time measurements are available. The filter tuning is an important aspect of the model identification due the possible divergence of the parameter estimates. The EKF is able to identify the friction models based

## Part I - Identification and Control of Mechanical Systems with Friction

on angular displacement measurements and velocity reconstruction. Due to the time-varying friction characteristics an on-line implementation of the EKF is of future interest.

The friction compensation demonstrated in the previous section gives an illustration of the use of the identified grey-box models. Although the objective of identifying simulation models is not the same as the objective of identifying models for closed-loop control, the friction compensation exhibits good results for different tasks and a considerable improvement is achieved compared to no friction compensation. The difference in the closed-loop performance between the two grey-box models is small and to give a qualitative better comparison additional closed-loop experiments with varying input frequencies and amplitudes should be done. This will also give insight in the accuracy of the linearization of the system.

## Chapter 4

# Frequency Domain Identification of Dynamic Friction Model Parameters

### Abstract

This chapter presents a frequency domain identification of dynamic model parameters for frictional presliding behaviour. The identification procedure for the dynamic model parameters, i.e., (i) the stiffness and (ii) the damping of the presliding phenomenon, is reduced from performing several dedicated experiments to one experiment where the system is excited with random noise and the Frequency Response Function (FRF) of the phenomenon is measured. Time domain validation experiments on a servo mechanism show accurate estimates of the dynamic model parameters for the linearized presliding behaviour.

## 4.1 Introduction

Over the past decade the use of dynamic friction models has grown immensely [16], [24], [55]. The LuGre model [24], that is closely related to the work of [33], [55], is a commonly used model for friction (i) compensation [24], [26], [47], (ii) simulation [46], [55] and (iii) observer design [92], [96]. The strength of the dynamic LuGre friction model is the ability to describe a large number of practically observed friction phenomena; for references of these phenomena see [7]. One of the interesting observed frictional properties is the presliding displacement [31], i.e., spring-like behaviour for near zero relative velocity (stiction). Here, we are interested in the identification of this phenomenon, which is also described by the dynamic LuGre model.

The identification of the LuGre model is described in [25], [46]. The idea is to estimate the model parameters in different friction regimes, i.e., (i) in the sliding phase and (ii) in the stick phase, by performing appropriate experiments in each regime. The estimation of the sliding parameters in the Stribeck friction curve can be done by various techniques, e.g., a least-squares method [25] or Extended Kalman Filtering [62]. However, the identification of the presliding phenomenon is far from trivial and performing suitable experiments is time-consuming as discussed in [25]. Furthermore, the dynamic parameter corresponding to the damping of the elastic bristles is often given a value instead of being estimated such that a well damped behaviour is obtained for zero velocity crossing [45]. Another drawback of the proposed identification procedures [25], [45] is the need for measurement or reconstruction of the relative velocity. Here, the second order description of the linearized LuGre model in the stiction regime will be used to perform a frequency domain identification of the dynamic parameters. The advantage of this technique is that the necessary measurements are solely the sampled system position and input. Thus time-consuming experiments are replaced by a single experiment where the system is excited with random noise and the Frequency Response Function (FRF) of the system is measured. Moreover, both the stiffness and damping of the presliding behaviour can be estimated from the measured FRF. To perform this technique a high-resolution encoder is used to observe the presliding behaviour. Furthermore, a comment on the linearization of the LuGre friction model in the stick phase will be given and the notion of *generalized differentials* [29] will be addressed to obtain the linearization.

The outline of this chapter is as follows. In Section 4.2, we will give a short description of the dynamic LuGre model, the linearization and the presliding phenomenon. The experimental setup used for the presliding measurements will be described in Section 4.3. The frequency domain identification and time domain validation will be discussed in Section 4.4. In Section 4.5 this chapter will be concluded and further research topics will be addressed.

## 4.2 The LuGre Model and Presliding Behaviour

### 4.2 The LuGre Model and Presliding Behaviour

In the LuGre model, the friction force during stiction is modeled as the average force applied by a set of elastic springs under a tangential microscopic displacement. An interpretation of these elastic springs can be given under the assumption that the two moving surfaces are in contact by a large number of bristles with a certain stiffness [55], which can be represented as depicted in Figure 4.1. To incorporate this phenomenon in a continuous friction model

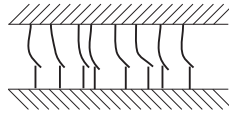


Figure 4.1 - The friction interface between two surfaces is thought of as a contact between bristles, where the bristles on one surface are shown as being rigid.

extra dynamics describing the average bristle displacement is needed. Hence, extra model parameters, i.e., bristle stiffness and damping, are introduced to model these dynamics. The LuGre friction model implements it as:

$$F = \sigma_0 z + \sigma_1 \dot{z} + \sigma_2 \dot{x} \quad (4.1)$$

$$\dot{z} = \dot{x} - \frac{|\dot{x}|}{g(\dot{x})} z = f(\dot{x}, z) \quad (4.2)$$

where  $F$  is the tangential friction force,  $z$  the average bristle deflection,  $\dot{x}$  the relative velocity between the two surfaces,  $g(\dot{x})$  the Stribeck curve for steady-state velocities,  $\sigma_2$  the viscous damping-coefficient and the dynamic model parameters: (i) the bristle stiffness  $\sigma_0$ , (ii) the bristle damping  $\sigma_1$ .

In [24] the presliding behaviour of the model is investigated and it is concluded that the phenomenon qualitatively describes the experimentally observed results in [31]. The model lacks the plastic deformation property that is hard to capture in one model describing both the sliding phase and stick phase. A simulated presliding displacement of the LuGre model

Parameter	Value	Unit
$\sigma_0$	$10^5$	[N/m]
$\sigma_1$	$\sqrt{10^5}$	[N·s/m]
$\sigma_2$	0.4	[N·s/m]
$F_c$	1	[N]
$F_s$	1.5	[N]
$v_s$	0.001	[m/s]

Table 4.1 - Parameter values used in simulation.

## Part I - Identification and Control of Mechanical Systems with Friction

is shown in Figure 4.2a), 4.2b) for model parameters as given in Table 4.1. A unit mass subjected to friction is considered where an external force  $u$  - slowly ramped up to 95% of the static friction  $F_s$  - is applied with an initial state of the system equal to zero  $[x \ \dot{x} \ z]^T = \underline{0}$ . Then the force is decreased slowly to the negative counterpart of the maximal applied force, i.e.,  $u = -1.425$  [N], and this cycle is repeated.

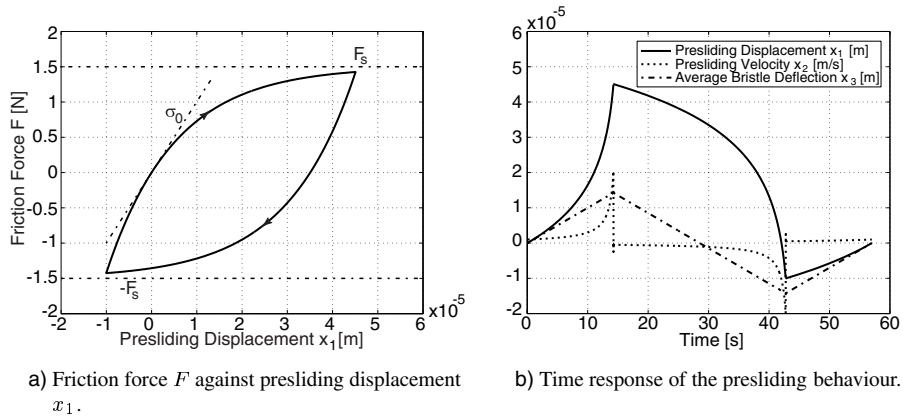


Figure 4.2 - Presliding behaviour of dynamic LuGre friction model.

The vectorfield  $f(\underline{x}, u)$  for this simple mass system subjected to the LuGre friction model reads

$$\begin{aligned} \dot{\underline{x}} &= f_{LuGre}(\underline{x}, u) \\ &= \begin{bmatrix} x_2 \\ -\sigma_0 x_3 - \sigma_1 \left( x_2 - \frac{|x_2|}{g(x_2)} x_3 \right) - \sigma_2 x_2 + u \\ x_2 - \frac{|x_2|}{g(x_2)} x_3 \end{bmatrix} \end{aligned}$$

where  $x_1 = x$ ,  $x_2 = \dot{x}$  and  $x_3 = z$  as in the LuGre friction description given above,  $u$  the applied force and the Stribeck curve  $g(x_2)$  is defined as

$$\sigma_0 g(x_2) = F_c + (F_s - F_c) e^{-(x_2/v_s)^2}$$

with  $F_s$  the static friction,  $F_c$  the coulomb friction and  $v_s$  the Stribeck velocity.

An interesting point in the stress-strain curve of Figure 4.2a) is the initial state  $\underline{x} = \underline{0}$ . In this initial state, where Figure 4.2b) shows the time responses of the states, the time derivatives of  $x_1$  and  $x_3$  are visibly equal. Furthermore, the state after one cycle of  $u$  is again zero and illustrates the lack of the ability to model plastic deformations.

### 4.3 Experimental Setup

Due to the non-smoothness of the LuGre model, i.e., the presence of an absolute-value operator on the relative velocity  $\dot{x}$  in Eq. (4.2), the derivation of the linearization about the initial state needs special attention. Obviously, the right-hand side of Eq. (4.2) is not absolutely differentiable at  $\dot{x} = 0$ . However, it possesses a left and right derivative defined as

$$f'_- = \lim_{\dot{x} \uparrow 0} \frac{f(\dot{x}, z) - f(0, z)}{\dot{x}}, \quad f'_+ = \lim_{\dot{x} \downarrow 0} \frac{f(\dot{x}, z) - f(0, z)}{\dot{x}}$$

The subdifferentials of Clarke [29], also called *generalized differentials*, can be used in this case and states that the *generalized derivative* of vectorfield  $f$  at state  $\underline{x}$  is declared as *any* value  $f'_q(\underline{x})$  included between its left and right derivative. The closed convex hull of the derivative extremes is called the *generalized differential* of  $f$  at  $\underline{x}$ .

$$\begin{aligned} \partial f &= \overline{\text{co}}\{f'_-, f'_+\} \\ &= \{f'_q(x) | f'_q(x) = (1 - q)f'_- + qf'_+, \forall q | 0 \leq q \leq 1\} \end{aligned}$$

Now, the generalized differential of the vector field  $f_{LuGre}(\underline{x})$  with respect to  $\underline{x}$  can be regarded as the generalized Jacobian  $\tilde{J}$  in the sense of Clarke

$$\tilde{J} = \partial_{\underline{x}} f_{LuGre} = (1 - q)J_- + qJ_+, \quad 0 \leq q \leq 1$$

where  $J_-$  and  $J_+$  are respectively the left and right Jacobian matrices. The generalized Jacobian matrix in the zero state  $\underline{x} = \underline{0}$  becomes

$$\tilde{J}(\underline{0}) = \begin{bmatrix} 0 & 1 & 0 \\ 0 & -\sigma_2 - \sigma_1 & -\sigma_0 \\ 0 & 1 & 0 \end{bmatrix}$$

which is independent of  $q$ , i.e., no convex combination of left and right Jacobian matrices. This is due to the fact that for this special situation the left and right Jacobian are equal. However, it should be emphasized that this is not always the case for non-smooth differential equations and then the notion of subdifferentials is essential. Returning to the linearized system, the observed initially equal time derivatives of  $x_1$  and  $x_3$  in Figure 4.2b) is mathematically shown since  $\dot{x}_1 = \dot{x}_2 = \dot{x}_3$ . Now the substitution of  $x_3 = x_1$  is possible and the linearization of the unit mass subjected to LuGre friction for zero state reads

$$\dot{x}_1 = x_2 \tag{4.3}$$

$$\dot{x}_2 = -\sigma_0 x_1 - (\sigma_1 + \sigma_2)x_2 + u \tag{4.4}$$

where  $\sigma_0$  represents the stiffness and  $\sigma_1 + \sigma_2$  the damping of the linearized system.

### 4.3 Experimental Setup

A rotating arm system consisting of (i) an induction motor, (ii) a low backlash planetary transmission and (iii) a rotating arm will be considered here. Due to the bearings and seals



in the motor and transmission, the inertia of the total system, i.e., the combined inertia of the separate elements, is subjected to friction. The angular displacement of the system is measured with a high-resolution encoder that produces two sinusoidal signals as output. These two 90 degrees in phase-shifted signals, i.e., an analog sine and an analog cosine, are interpolated and digitized into two 90 degrees in phase-shifted square-wave pulse trains, i.e., two TTL signals. The interpolation degree is set to 40, which results in a resolution of  $8e5$  increments per revolution of the motor shaft. Due to a gear ratio of the transmission of 8.192 the resolution of the angular arm displacement measurements becomes  $6.5536e6$  increments per revolution. The induction motor is supplied by a 'Pulse Width Modulation' source inverter which translates the input signal, i.e., the desired torque expressed in a voltage, into three phase signals with a fundamental frequency. This source inverter actually controls the torque produced by the motor to the desired torque. The input signal of the source inverter and the TTL encoder signals are respectively sent and read by a dSPACE system [37]. During the experiments the sampling frequency of the dSPACE system is set to 10 [kHz]. To perform on-line frequency domain measurements, the input signal and the angular displacement are processed by a SigLab system [113]. A schematic representation of the setup is given in Figure 4.3 and the specifications of the separate experimental elements are given in Table 4.2.

Element	Brand	Model-type
Encoder	Heidenhain	ERN 480
Interpolator	Leonard+Bauer	GEL 214
AC Motor	AMK Pumasyn	Unknown
Source Inverter	AMK Pumasyn	Pus 3
Transmission	Alpha Gear	SPF"'"M"
dSPACE	dSPACE	DS1103
SigLab	DSP Technology	20-42

Table 4.2 - Specification of the apparatus.

## 4.4 Frequency Domain Identification and Time Domain Validation

The system under consideration can be modeled as

$$J\ddot{\alpha} = -F + c_m u \quad (4.5)$$

where  $J$  is the effective inertia of the motor-transmission-rotating arm combination,  $\alpha$  the angular displacement,  $u$  the input voltage,  $c_m = 16$  [N·m/V] the motor constant and  $F$  the friction torque that is modeled by the dynamic LuGre model Eqs. (4.1-4.2). Linearizing Eq. (4.5) as presented in Section 4.2 for the stiction regime and zero state the linearized system

#### 4.4 Frequency Domain Identification and Time Domain Validation

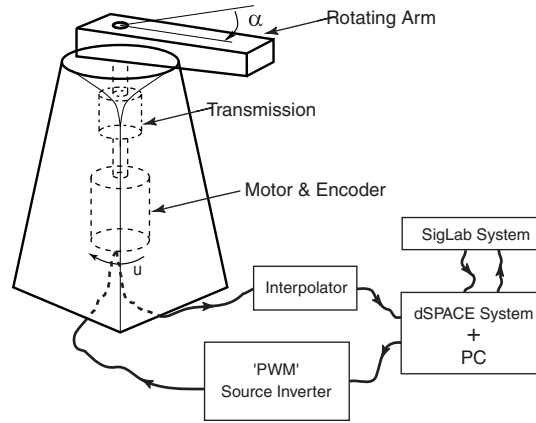


Figure 4.3 - Experimental setup.

in frequency domain reads

$$\frac{A(j\omega)}{U(j\omega)} = H(j\omega) = \frac{c_m}{-J\omega^2 + (\sigma_1 + \sigma_2)j\omega + \sigma_0}$$

To estimate this frequency response function (FRF)  $H(j\omega)$ , the system is excited with a PRBS signal of a bandwidth up to 500 [Hz] and a RMS level below the static friction  $F_s$ . The measured FRF  $G(j\omega)$  is obtained by averaging 50 time series of 8192 samples at a sampling frequency of 10 [kHz] with a Hanning window and 50% overlap.

Since the linearization Eqs. (4.3-4.4) is only locally valid, the nonlinear behaviour is investigated on by varying the RMS level of the noise within the static friction of the system. In Figure 4.2a) the dynamic parameter  $\sigma_0$  is depicted as the stiffness of the friction torque for small variations of the presliding displacement  $x_1$  under small variations of the applied torque  $c_m u$ . Hence, the noise level used during the experiment should be very small to obtain valid measurements for the linearized model. A noise level up to the static friction  $F_s$  will give an 'averaged' stiffness lower than the real stiffness. In Figure 4.4a) this nonlinear behaviour is shown for increasing noise levels. The magnitude of the various FRFs for frequencies approaching zero represent the gain  $|G(j0)| = \frac{c_m}{\sigma_0}$  of the presliding behaviour. In Table 4.3 the rough estimates of the stiffness for the different noise levels are given. As expected, the stiffness  $\sigma_0$  decreases, i.e.,  $\frac{c_m}{\sigma_0}$  increases, as the level of excitation increases. To estimate a second order FRF  $H(j\omega)$  from the measured  $G(j\omega)$  with the smallest noise level, an iterative procedure of convex combination steps similar to the SK-iteration of Sanathanan and Koerner (1963) [23] is used. Inspection of the measured FRF shows high order behaviour for frequencies above 150 [Hz]. Since it is not our goal to identify this behaviour, the focus will be on the second order dynamics up to 150 [Hz]. The measured

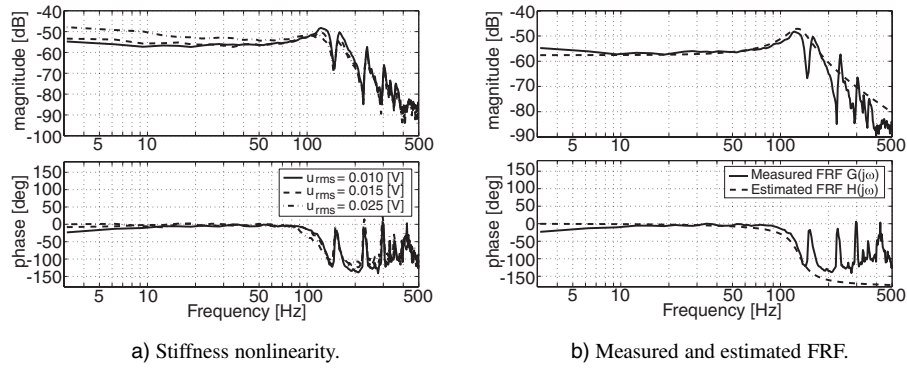


Figure 4.4 - Frequency response functions of presliding behaviour.

RMS noise level [V]	Estimated $\sigma_0$ [N·m/rad]
0.010	$1.2e+04$
0.015	$9.6e+03$
0.025	$6.3e+03$

 Table 4.3 - Stiffness  $\sigma_0$  for different noise levels.

$G(j\omega)$  and estimated  $H(j\omega)$  are depicted in Figure 4.4b). The estimated dynamic LuGre parameters become (i)  $\sigma_0 = 1.21e4$  [N·m/rad], (ii)  $\sigma_1 + \sigma_2 = 4.47$  [N·m·s/rad] and the estimated inertia  $J = 0.018$  [kg·m<sup>2</sup>/rad]. Here, the parameters have to be considered as the lumped compliance and impedance of the total system rather than the stiffness and damping of the friction alone. Hence, in the sequel of the chapter the parameters will be addressed as the dynamic model parameters for the frictional presliding behaviour.

The obtained dynamic model parameters are validated by two time domain experiments, i.e., (i) a break-away experiment and (ii) sinusoidal excitation of the system in the stick regime. First a ramp input is used to perform a break-away experiment, where the voltage applied is given by  $u = 0.001t$ . The measured and simulated responses are depicted in Figure 4.5, where in the upper part the macroscopic displacement is given and in the lower part the microscopic or presliding displacement. From the lower part can be concluded that the estimated dynamic model parameters and the LuGre model are valid for the linearization described in Section 4.2, since the slope of the measured response and the LuGre model response are equal for small input torques. In comparison to the LuGre model shows the system response larger presliding displacements for larger input torques. The reason is yet unclear but might be explained by: (i) plastic deformation or creep of the system is not

#### 4.4 Frequency Domain Identification and Time Domain Validation

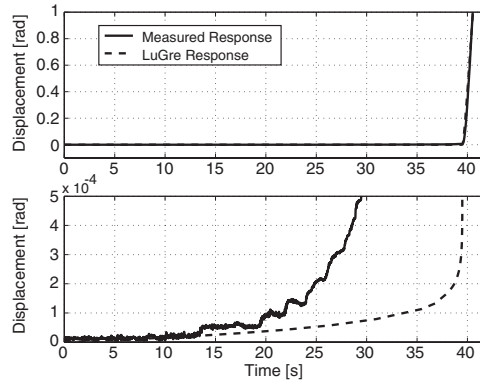


Figure 4.5 - Break-away experiment.

incorporated in the LuGre model and (ii) the LuGre model structure is too limited to describe the presliding behaviour accurately, e.g., the stiffness  $\sigma_0$  might be a nonlinear function in  $z$  or  $\dot{x}$ . On the other hand the macroscopic differences are very small.

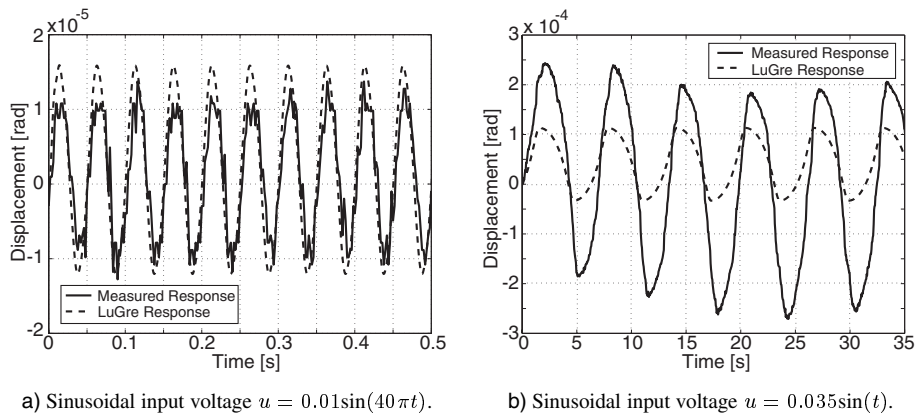


Figure 4.6 - Sinusoidal validation.

To investigate the obtained dynamic model parameters and the LuGre model for the presliding behaviour more extensively, the system is excited with two sinusoidal input torques. In Figure 4.6a) the applied torque has a frequency of 20 [Hz] and an amplitude of 0.01 [V] that is equal to the noise level used for the identification procedure. Again the estimated dynamic model parameters and the LuGre model are able to predict the presliding behaviour very accurately. In Figure 4.6b) the results of a second sinusoidal experiment is shown with

a frequency of  $\frac{1}{2\pi}$  [Hz] and an amplitude of 0.035 [V], i.e.,  $\pm 90\%$  of the static Friction  $F_s$ . For these larger input torques the system response gives again larger microscopic displacement than the LuGre model. The reason for this difference in the presliding behaviour can be sought in the arguments given above.

## 4.5 Conclusions

This chapter demonstrates a frequency domain identification technique for the dynamic model parameters in the frictional presliding behaviour. To perform this frequency domain identification the dynamic LuGre friction model is linearized to obtain a linear second order description that is locally valid in the stick regime. The identification procedure is reduced from performing several dedicated experiments to one experiment where the system is excited with random noise and the Frequency Response Function (FRF) of the system is measured. The measured FRF is used to estimate both dynamic model parameters, i.e., (i) the stiffness  $\sigma_0$  and (ii) the damping  $\sigma_1 + \sigma_2$ . Excitation of the presliding behaviour outside the linearization shows a nonlinear behaviour that describes a decreasing stiffness for an increasing applied torque. This phenomenon is also incorporated in the dynamic LuGre friction model.

Time domain validation experiments show accurate estimation of the dynamic model parameters for the linearized presliding behaviour, i.e., locally valid around zero presliding displacement and zero applied force. However, the applicability of the dynamic LuGre friction model for the description of the entire presliding phenomenon, i.e., the total stick regime for an applied force  $u$  lower than the static friction  $F_s$ , is limited. Extensive evaluation of the presliding behaviour will be a topic of future research as well as the modification of the LuGre model to obtain a more accurate dynamic friction model for the description of the presliding phenomenon.

## Chapter 5

# High Performance Regulator Control for Mechanical Systems Subjected to Friction

### Abstract

In this chapter several control strategies are compared with respect to their performance for regulator tasks on mechanical systems that exhibit friction. For this purpose a classic PID controller combined with mass and frictional feedforward is compared to (i) a PID controller combined with a friction compensation based on the dynamic LuGre friction model and (ii) a gain-scheduled optimal PD controller based on a Polytopic Linear Model (PLM). The latter consists of a feedforward part and an optimal nonlinear feedback part.

The controllers are compared to the classic PID controller by means of experiments on a rotating arm subjected to friction. The performance for three third order servo setpoints shows that the gain-scheduled optimal PD controller outperforms the other controllers with respect to settling time and maximal error after setpoint, i.e., regulator performance. For the tracking performance during the different setpoints comparable results for both the LuGre-based controller and the classic PID controller are found where the tracking performance of the gain-scheduled PD controller is limited.

---

This chapter is submitted for publication in IEEE Transactions on Robotics and Automation [65]. Parts of this chapter have been presented at the Mathematical Theory of Networks and Systems (MTNS 2000) conference in Perpignan, France [63] and at the IEEE Conference on Control Applications (CCA 2001) in Mexico City, Mexico [66].

## 5.1 Introduction

Friction is to some extent present in all mechanical systems. In motion systems this phenomenon can limit the performance considerably due to increasing tracking errors and limit cycles. In this chapter the focus will be on regulator or point to point movements where the dominant frictional contributor is stiction and the main control errors are (i) steady-state errors and (ii) hunting, i.e., limit cycle around the desired position [7]. The friction induced hunting limit cycling is an undesirable phenomenon in controlled motion systems due to its oscillatory and persistent behaviour. Friction induced limit cycles are mainly due to the combination of the difference in static and Coulomb friction and integral control in the control loop. One way of avoiding hunting limit cycles is the use of PD control only, which consequently implies steady state errors in the presence of friction. However, if the steady state errors are larger than for instance the desired accuracy of the positioning task, these controllers are found to be inadequate.

Here, a widely used PID controller in combination with properly tuned feedforwards is compared to two more sophisticated friction compensation schemes. The first one consists of an observer-controller scheme based on the dynamic LuGre friction model [24]. The second is a gain-scheduled optimal PD controller based on a Polytopic Linear Model (PLM). The latter consists of a feedforward part and an optimal nonlinear feedback part.

In industry, the most commonly used strategy in the presence of friction is a classic PID controller in combination with mass and friction feedforward. The PID controller is classically tuned in frequency domain with the objective of an as high as possible closed-loop bandwidth with sufficient stability margins. Especially for positioning tasks, the integral action should be tuned desirable large in the presence of friction for fast attenuation of static errors. However, in practice the speed of attenuation of static errors is limited and degenerates the regulator performance unacceptably. Moreover, as mentioned before integral control in combination with friction might cause the closed-loop system to limit cycle. Therefore, the performance of the closed-loop system should be evaluated closely to ensure this does not occur.

In contrast to this classic approach, the increased interest on the modeling of frictional phenomena [16], [24], [33], [55] over the past decade, especially at or near zero relative velocity, has resulted in the promising dynamic LuGre friction model [24]. This model incorporates a large number of practically observed frictional properties, e.g., frictional lag and varying break-away, and models the friction force near zero velocity like a stiff spring. As presented in [24], [25], this model can be used to design an observer for position control of mechanical systems subjected to friction. Near zero relative velocity, the more complete LuGre friction model is able to predict the friction force more accurate and desirable reduce static errors faster in comparison to the classic PID controller. This dynamic friction observer-controller scheme is used here and compared to the classic PID controller with feedforwards. In the ideal case where the friction is perfectly compensated, integral action in the feedback loop is not necessary. However, over or under estimation and time-varying

## 5.2 Friction Compensation Controllers

friction characteristics will introduce low frequent errors which are attenuated slowly without integral control. Hence, integral control is incorporated in the feedback loop and to have a good comparison with the classically tuned controller the LuGre-based feedback loop controller has equal settings.

Another approach to suppress steady state errors, as discussed in the literature survey on friction in [7], is to use stiff PD controllers. However, high gains may lead to closed-loop instabilities and unacceptable controller efforts. Here, a gain-scheduled PD controller [63], based on a Polytopic Linear Model (PLM) of the system [62], is used in such a way that for low velocities the PD gain can be increased and closed-loop stability (and performance) is guaranteed. Two desirable properties of the proposed controller design are: (i) a high-gain controller where it is needed, i.e., for low velocities where the friction is important, and (ii) the stability of the closed-loop system is guaranteed and limit cycling is avoided. The controller design consists of two parts, i.e., (i) feedforward control on the basis of estimated PLM parameters and (ii) a nonlinear optimal controller for the remaining error dynamics [4], [63]. This PLM-based control strategy is also compared to the performance obtained with the classic PID controller in combination with mass and friction feedforward.

The outline of this chapter is as follows. In Section 5.2, the various friction compensation techniques and their tuning will be discussed. The experimental results consisting of (i) the experimental setup, (ii) the specific tuning of the various friction compensation controllers and (iii) a comparison of the different controller performances for three servo setpoints will be given and discussed in Section 5.3. Conclusions will be presented in Section 5.4.

## 5.2 Friction Compensation Controllers

A general description of a simple motion system subjected to friction can be given as follows:

$$J \frac{d^2 q(t)}{dt^2} = -f(t) + c_m u(t), \quad (5.1)$$

where  $q(t)$  is the generalized coordinate or the position of the system,  $J$  is the mass,  $f(t)$  the friction force,  $c_m$  the motor gain and  $u(t)$  the system input. Equation (5.1) will be used as a starting point for the different controllers proposed in the sequel and the time argument ( $t$ ) is omitted where possible for brevity.

### 5.2.1 Classic PID Controller plus Feedforward

In industry, a commonly used friction compensation technique is a standard PID controller in combination with properly tuned feedforwards. The linear part of the system, i.e., the double integrator behaviour and the higher order dynamics due to eigenfrequencies of the system, will be visualized by performing a frequency domain analysis and used for feedback control design.



### Frequency domain PID controller tuning: loop-shaping

Standard control of motion systems is PID control, where its design objectives can generally be described as (i) obtain a stable closed-loop system with an as high as possible bandwidth given (ii) predefined phase and gain margins. For the analysis of the closed-loop stability and its stability margins it is of major importance to have accurate information on the linear dynamics of the motion system under consideration. A standard procedure to obtain this information is to measure the Frequency Response Function (FRF) of the system. However, simple frequency domain identification by excitation of the motion system within a certain frequency range in open-loop is in general impossible due to nonlinear friction effects. One way of shutting out the friction phenomenon from experimental data is to measure the sensitivity FRF  $S(j\omega)$  of a stable closed-loop system with a known controller  $C(j\omega)$ , as depicted in Figure 5.1. By exciting the closed-loop system with a Pseudo Random Binary Signal

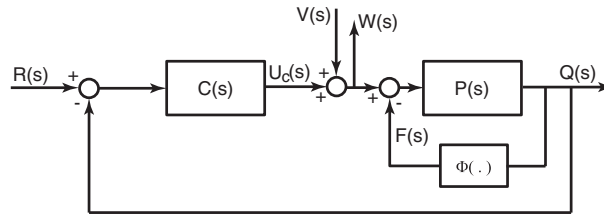


Figure 5.1 - Closed-loop configuration

(PRBS) for a certain frequency range at signal  $v$  and by measuring  $w = u_c + v$  it is possible to write  $W(s)$  as

$$W(s) = \frac{V(s)}{1 + P(s)C(s)} + \frac{C(s)R(s)}{1 + P(s)C(s)} + \frac{P(s)C(s)}{1 + P(s)C(s)}F(s) \quad (5.2)$$

$$W(s) = S(s)V(s) + S(s)C(s)R(s) + T(s)F(s) \quad (5.3)$$

where  $P(s)$  is the linear part of the system,  $S(s)$  is the sensitivity of the closed-loop system,  $T(s)$  is the complementary sensitivity of the closed-loop system,  $R(s)$  the reference of the closed-loop system and  $F(s)$  the friction force. The nonlinear operator  $\Phi(\cdot)$  is a function of  $q$  and describes the nonlinear dynamics of the friction. The influence of the last two terms of Eq. (5.3) on the measurement, i.e., (i) a force necessary to follow the desired reference and (ii) a term that compensates the friction force  $F$  during the setpoint, can be eliminated by choosing an appropriate reference signal. Here, a ramp function is used as a reference, i.e., the motion system should move with constant velocity unequal to zero, since in this case the force due to inertia is zero and the friction force is assumed to be constant. For this reference both terms become stationary, i.e., consider these expressions for  $\lim_{s \rightarrow 0} s[C(s)S(s)R(s) + T(s)F(s)]$ , and equal to zero under the assumption that the dominant dynamics of  $P(s)$  is a double integrator and  $C(s)$  consists of a PD controller or PID controller. Then, from Eq. (5.3) an estimate  $S(j\omega) = w(j\omega)/v(j\omega)$  can be obtained, which can be used to reconstruct the FRF of the system since the controller  $C(j\omega)$  is known.

## 5.2 Friction Compensation Controllers

The controller used during this measurement can be any controller as long as the closed-loop system is stable. Normally, a simple PD controller with a low gain is used which can easily be used to reconstruct the systems FRF  $P(j\omega)$ .

After the reconstruction of the linear dynamics of the system, i.e., inertial properties, higher order dynamics and possible time-delays, a PID controller of the following form

$$C(s) = K \left( \frac{\tau_i s + 1}{\tau_i s} \right) \left( \frac{\tau_d^z s + 1}{\tau_d^p s + 1} \right) \left( \frac{\omega_{lp}^2}{s^2 + 2\beta_{lp}\omega_{lp}s + \omega_{lp}^2} \right) \quad (5.4)$$

is used to tune the closed-loop characteristics. This controller consist of proportional ( $K$ ), lead-lag ( $\tau_d^z$ ,  $\tau_d^p$ ) and integral ( $\tau_i$ ) control combined with a low-pass filter ( $\beta_{lp}$ ,  $\omega_{lp}$ ) to suppress measurement noise. Here, the controller parameters are tuned with the objective to obtain the highest possible bandwidth, 30 [deg] phase margin and 6 [dB] gain margin for the loop-gain  $L(j\omega) = P(j\omega)C(j\omega)$ .

### Feedforwards

To improve the performance of the tracking behaviour of the closed-loop system the following feedforwards are commonly added:

1. mass feedforward, which can be based on the reconstructed linear dynamics of the system. The dominant double integrator behaviour of the system is used to identify a second order transfer function on the measured FRF of the system. The estimated mass is used in the feedforward as follows

$$c_m u_{feedforward}^{mass} = J \ddot{q}_d,$$

where  $J$  is the estimated mass of the system and  $\ddot{q}_d$  is the reference acceleration.

2. friction feedforward, which consists of Coulomb and viscous friction feedforwards and can be described as

$$c_m u_{feedforward}^{friction} = F_c \text{sign}(\dot{q}_d) + \sigma_2 \dot{q}_d,$$

where  $F_c$  is the estimated Coulomb friction level,  $\sigma_2$  the estimated viscous damping coefficient,  $\dot{q}_d$  the reference velocity and the sign for zero velocity is defined as zero. These estimated friction force parameters can be obtained by construction of a friction-velocity or Stribeck map measured for references with constant velocity. For different constant velocity levels, both positive and negative, closed-loop experiments with a PD controller are performed, where the averaged applied forces and averaged velocities are used to construct a friction-velocity map. The friction feedforward parameters are estimated from these experimental data with a least-squares minimization as demonstrated in [25].

This feedforward tuning method is one of many possible techniques. Other methods proposed in literature are mainly stepwise time domain procedures for individually identifying the parameters of the inertia and friction characteristics, such as presented in [77]. A simultaneous approach for the identification of both the inertia and friction characteristics is presented in [62], where an Extended Kalman Filtering technique is used iteratively.

The total control law is a combination of the feedback controller Eq. (5.4) and both feedforwards, i.e.,

$$u(t) = c(t) * e(t) + \frac{1}{c_m} [J\ddot{q}_d(t) + F_c \text{sign}(\dot{q}_d(t)) + \sigma_2 \dot{q}_d(t)],$$

where the tracking error  $e(t) = q_d(t) - q(t)$ ,  $c(t)$  is the inverse Laplace transformation of  $C(s)$ , i.e.,  $c(t) = \mathcal{L}^{-1}[C(s)]$  and  $c(t) * e(t)$  the convolution product.

### 5.2.2 Friction Compensation based on the Dynamic LuGre Model

The dynamic LuGre friction model [24] models the friction force  $f$  in Eq. (5.1) as a continuous function of the velocity  $\dot{q}$  and the friction internal state  $z$ , which can be interpreted as the average deflection of the contact surfaces during the *stiction* regime. The LuGre friction force is given by

$$\dot{z} = \dot{q} - \frac{\sigma_0 |\dot{q}|}{g(\dot{q})} z \quad (5.5)$$

$$f = \sigma_0 z + \sigma_1 \dot{z} + \sigma_2 \dot{q}, \quad (5.6)$$

where  $f$  is the friction force,  $z$  the friction internal state,  $\dot{q}$  the (relative) velocity between the contact surfaces,  $\sigma_2$  the viscous friction coefficient,  $\sigma_0$  the stiffness of the microscopic displacements of  $z$  and  $\sigma_1$  the corresponding damping coefficient. The function  $g(\dot{q})$  defines the Stribeck curve as

$$g(\dot{q}) = F_c + (F_s - F_c) \exp\left(-\left(\frac{\dot{q}}{v_s}\right)^2\right), \quad (5.7)$$

where  $F_c$  is the Coulomb friction level,  $F_s$  the static friction level and  $v_s$  the Stribeck velocity.

To design a LuGre model-based friction compensation scheme the internal state  $z$  has to be known. Since the state  $z$  is not measurable, the following observer for closed-loop use can be designed as presented in [24], [25], under the assumption that the model parameters are known:

$$\dot{\hat{z}} = \dot{q} - \frac{\sigma_0 |\dot{q}|}{g(\dot{q})} \hat{z} - k e, \quad k > 0 \quad (5.8)$$

$$\hat{f} = \sigma_0 \hat{z} + \sigma_1 \dot{\hat{z}} + \sigma_2 \dot{q}, \quad (5.9)$$

where  $k$  is the observer gain and the following control law is used

$$c_m u(t) = -c_m c(t) * e(t) + \hat{f}(t) + J\ddot{q}_d(t), \quad (5.10)$$

## 5.2 Friction Compensation Controllers

where  $e(t) = q(t) - q_d(t)$  is the position error and  $q_d(t)$  the reference signal which is assumed to be two times differentiable,  $\hat{z}$  is the observed internal state and  $\hat{f}(t)$  is the friction estimate. Again  $c(t)$  is the inverse Laplace transformation of  $C(s)$ , i.e.,  $c(t) = \mathcal{L}^{-1}[C(s)]$  and  $c(t) * e(t)$  the convolution product. For the closed-loop system, i.e., the system described in Eqs. (5.1), (5.5-5.6) combined with the friction observer Eqs. (5.8-5.9) and control law (5.10) with a linear controller  $C(s)$ , a sufficient stability condition can be derived as presented in [24] and states that the linear system

$$G(s) = \frac{\sigma_1 s + \sigma_0}{Js^2 + c_m C(s)} \quad (5.11)$$

should be strictly positive real (SPR).

As for the previous proposed control schemes, model parameters are important with respect to the overall performance of the proposed observer-controller scheme. Here, the dynamic friction parameters, i.e., the frictional stiffness  $\sigma_0$  and frictional damping  $\sigma_1$ , will be identified with frequency domain measurements in the presliding displacement regime [64]. Additionally, the estimation of the parameters in the Stribeck function in Eq. (5.7) can be done by various techniques, e.g., a least-squares method [25] or Extended Kalman Filtering [62]. Again, the friction-velocity map will be used to estimate the Stribeck parameters in Eq. (5.7) by performing the least-squares method where the estimated mass  $J$  from the frequency domain analysis is used.

### 5.2.3 Inverse Optimal Control based on a Polytopic Linear Model

Over the last few years promising approaches for the modeling and control of nonlinear systems have emerged [88]. The unified idea is to represent a nonlinear dynamic system by a 'global' model which is the result of taking convex combinations of locally valid affine models. Two desirable properties are (i) the richness of this model class to approximate a large class of nonlinear systems arbitrarily close [4], [121] and (ii) the fact that the model structure is suitable for system analysis and controller synthesis based on linear matrix inequalities (LMIs) [20]. Here, a polytopic grey-box model [62] will be used to design a gain-scheduled optimal controller. This polytopic model is a convex combination of locally valid linear models and therefore the model is named a Polytopic Linear Model (PLM).

### PLM Design for Mechanical Systems Subjected to Friction

Here, the friction force  $f(t)$  as described in Eq. (5.1) is assumed to be a nonlinear function of the velocity  $\dot{q}$  and of the model parameters  $\theta$ , i.e.,  $f = f(\dot{q}, \theta)$ . This friction model is static and does not describe *stiction*, meaning that for an applied force  $u$  unequal to zero the system will always (start to) move. This simplified friction model will facilitate the numerical solution of the 2<sup>nd</sup> order differential Eq. (5.1), due to the continuity of the friction function. By choosing a steep slope for the friction function near  $\dot{q} = 0$ , the *stiction* regime can be approximated. Such a model can still give acceptable simulation results, in the sense

## Part I - Identification and Control of Mechanical Systems with Friction

that the angular displacement near  $\dot{q} = 0$  can be negligibly small [62].

The nonlinear friction force will be modeled with a PLM as

$$f(\dot{q}, \theta) = \sum_{i=1}^N w_i(\dot{q}, \theta) (a_i(\dot{q} - c_i) + b_i) \quad (5.12)$$

with the normalized Gaussian validity function

$$w_i(\dot{q}, \theta) = \frac{e^{-\frac{1}{2} \frac{(\dot{q} - c_i)^T (\dot{q} - c_i)}{d_i}}}{\sum_{j=1}^N e^{-\frac{1}{2} \frac{(\dot{q} - c_j)^T (\dot{q} - c_j)}{d_j}}},$$

where  $w_i : \mathbb{R} \rightarrow [0, 1]$  for all  $i$ , and  $a_i(\dot{q} - c_i) + b_i$  is the affine model of the friction locally valid around velocity  $c_i$ . For the identification of the PLM, the center  $c_i$ , slope  $a_i$  and offset  $b_i$  of the linear models and the variance  $d_i$  of the Gaussian validity functions have to be estimated.

Here, the friction PLM is chosen as follows; Choose an even number of local models  $N$ , which models are divided in pairs of two. The centers are chosen opposite  $c_i = -c_{2i}$  where the variances are chosen equal  $d_i = d_{2i}$  with  $i = 1, \dots, N/2$ . To be able to estimate different frictional characteristics for positive and negative velocities, the slopes  $a_i$  and the offsets  $b_i$  can be chosen freely for all linear models. An advantage of this construction is a reduction of the number of parameters describing the normalized Gaussian validity functions. The state space representation of the second order mechanical system Eq. (5.1) with friction model Eq. (5.12) becomes

$$\begin{bmatrix} \dot{q} \\ \ddot{q} \end{bmatrix} = \sum_{i=1}^N w_i(\dot{q}, \theta) \left\{ \begin{bmatrix} 0 & 1 \\ 0 & -\frac{a_i}{J} \end{bmatrix} \begin{bmatrix} q \\ \dot{q} \end{bmatrix} + \begin{bmatrix} 0 \\ \frac{a_i c_i - b_i}{J} \end{bmatrix} + \begin{bmatrix} 0 \\ \frac{c_m}{J} \end{bmatrix} u \right\}$$

or

$$\dot{x} = \sum_{i=1}^N w_i(x, \theta) \{A_i(\theta)x + C_i(\theta)\} + Bu, \quad x = \begin{bmatrix} q \\ \dot{q} \end{bmatrix}. \quad (5.13)$$

For the PLM, the model parameters become

$$\theta = [J \ a_i \ b_i \ c_j \ d_j]^T \quad i = 1, \dots, N, \quad j = 1, \dots, \frac{N}{2} \quad (5.14)$$

The parameters given in Eq. (5.14) will be estimated on the basis of a friction-velocity map as described in Section 5.2.1 and the frequency domain estimate of  $J$  will be used as the mass parameter.

## 5.2 Friction Compensation Controllers

### Inverse Optimal Control

The objective of the closed-loop system is to perform a high precision regulator or positioning task. Hence, the controller consists of (i) a feedforward part  $u_{feedforward}$  and (ii) a (nonlinear) optimal regulator  $u_{feedback}$  for the remaining error dynamics. The controller is derived by choosing a proper Lyapunov function for the tracking error dynamics as suggested in [63].

The "feedforward" control part, which is based on the model class of Eq. (5.13), can be written as

$$u_{feedforward} = (B^T B)^{-1} B^T \left[ \dot{x}_d - \sum_{i=1}^N w_i(x, \theta) \{A_i(\theta)x_d + C_i(\theta)\} \right]$$

where  $x_d$  are the desired state trajectories and  $(B^T B)^{-1} B^T$  is the (pseudo) inverse of  $B$ . The feedforward term is given in quotation marks since the normalized validity functions  $w_i(x, \theta)$  are a function of the actual state  $x$  which makes the feedforward also a kind of feedback. This scheduling of the feedforward over the actual state  $x$  is necessary to be able to perform an optimal controller synthesis for the remaining error dynamics. With  $u = u_{feedforward} + u_{feedback}$  the remaining error dynamics become

$$\dot{e} = \sum_{i=1}^N w_i(x, \theta) \{A_i(\theta)e\} + B u_{feedback} \quad (5.15)$$

where the tracking error  $e = x - x_d$ . To apply this feedforward successfully, i.e., to obtain error dynamics which have  $e = 0$  as an equilibrium, the constant vector fields  $C_i$  should be in the range of  $B$  for all  $i$ .

By solving an inverse optimal control problem it can be shown [4], [63] that the following nonlinear feedback control law

$$\begin{aligned} u_{feedback} &= u_{optimal} \\ &= - \sum_{i=1}^N w_i(x, \theta) R_i^{-1} B^T P e, \quad R_i > 0 \quad \forall i \end{aligned}$$

is optimal under the condition that there exists a  $P = P^T > 0$  satisfying the following set of Algebraic Riccati Equations (AREs)

$$Q_{ij} + P A_i(\theta) + A_i^T(\theta) P - P B R_j^{-1} B^T P = 0, \quad \forall (i, j) \quad (5.16)$$

where  $Q_{ij}$  and  $R_j$  are symmetric weight matrices. These matrices balance the accumulated deviation of the state error  $e$  from zero and the accumulated amplitude of the feedback control input  $u_{feedback}$  in a quadratic cost function

$$\begin{aligned} J &= J(e, u_{feedback}) \\ &= \int_0^\infty \left( \sum_{i,j=1}^N w_i(x, \theta) w_j(x, \theta) e^T Q_{ij} e + u_{feedback}^T \left( \sum_{j=1}^N w_j(x, \theta) R_j^{-1} \right) u_{feedback} \right) dt \end{aligned}$$

## 5.3 Experimental Results

In this section the experimental results will be discussed for the various controllers. First, the experimental setup will be described with a specification of the different elements in the apparatus. Second, the tuning of the different control strategies will be discussed for this specific experimental setup. The experimental results for different servo tasks, i.e., three different third order setpoints, will be given and discussed in the last part of this section.

### 5.3.1 Experimental Setup

A rotating arm system consisting of (i) an induction motor, (ii) a low backlash planetary transmission and (iii) a rotating arm is considered here. Due to the bearings and seals in the motor and transmission, the inertia of the total system, i.e., the combined inertia of the separate elements, is subjected to friction. The angular displacement of the system is measured with a resolution of  $2e4$  increments per revolution of the motor shaft. Due to a gear ratio of the transmission of 8.192 the accuracy of the angular arm displacement measurements is  $3.835e-5$  [rad]. The induction motor is supplied by a 'Pulse Width Modulation' source inverter which translates the input signal, i.e., the desired torque expressed in a voltage, into three phase signals with a fundamental frequency. This source inverter actually controls the torque produced by the motor to the desired torque. The source inverter shows linear behaviour between voltage and shaft-torque for angular velocities lower than 12 [rad/s]. The input signal of the source inverter and the TTL encoder signals are respectively sent and read by a dSPACE system [37]. During the experiments the sampling frequency of the dSPACE system is set to 5 [kHz]. To perform on-line frequency domain measurements, the input signal and the angular displacement are processed by a SigLab system [113]. A schematic representation of the setup is given in Figure 5.2 and the specifications of the separate experimental elements are given in Table 5.1.

Element	Brand	Model-type
Encoder	Heidenhain	ERN 480
Interpolator	Leonard+Bauer	GEL 214
AC Motor	AMK Pumasyn	Unknown
Source Inverter	AMK Pumasyn	Pus 3
Transmission	Alpha Gear	SPF"M"
dSPACE	dSPACE	DS1103
SigLab	DSP Technology	20-42

Table 5.1 - Specification of the apparatus.

### 5.3 Experimental Results

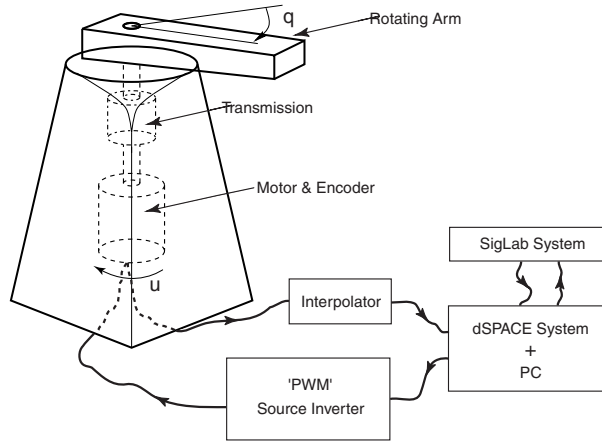


Figure 5.2 - Experimental setup.

#### 5.3.2 Controller Tuning

##### Frequency domain analysis and tuning

To get an idea of the linear properties of the rotating arm the frequency domain analysis as described in Section 5.2.1 is performed with a known (stable) PID controller and a reference ramp  $R$  with a slope (or velocity) of 0.5 [rad/s]. To estimate the sensitivity FRF  $S(j\omega)$ , the closed-loop system is excited at the signal  $v$ , see Figure 5.1, with a PRBS signal of a bandwidth up to 500 [Hz] and a RMS level of 0.5 [V]. The measured FRF  $S(j\omega)$  is obtained by averaging 50 time series of 8192 samples at a sampling frequency of 10 [kHz] with a Hanning window and 50% overlap. Using this measured sensitivity FRF and the known controller, the linear dynamics of the system, i.e.,  $P(j\omega)$ , can be reconstructed, as depicted in Figure 5.3a). The reconstructed system FRF  $P(j\omega)$  shows a double integrator behaviour up to 150 [Hz] where the first eigenfrequency of the system is located. The second and third eigenfrequencies are located over 200 [Hz]. By looking at the phase of this FRF a considerable time-delay can be noticed which is due to the source inverter. The control scheme of the source inverter, i.e., the control of the linear relation between desired torque and applied torque, is running at a sampling frequency of approximately 500 [Hz]. This sampling frequency manifests itself as a pure time-delay in the systems dynamics as recorded in the phase.

This reconstructed FRF  $P(j\omega)$  with its phase-lag and eigenfrequencies is used for tuning a PID controller in combination with a second order low-pass filter as given in Eq. (5.4). In Figure 5.3b) the nyquist plot of the tuned loop-gain  $L(j\omega) = P(j\omega)C(j\omega)$  is shown with the obtained gain and phase margins, i.e., 7.7 [dB] gain margin and 31.9 [deg] phase margin. The bandwidth of the closed-loop system is mainly limited due to the phase-lag introduced by the source inverter and is tuned at 24.2 [Hz] located at 0 [dB] loop-gain. This tuned linear controller  $C(s)$  will be used in the classic PID control scheme and in the observer-controller



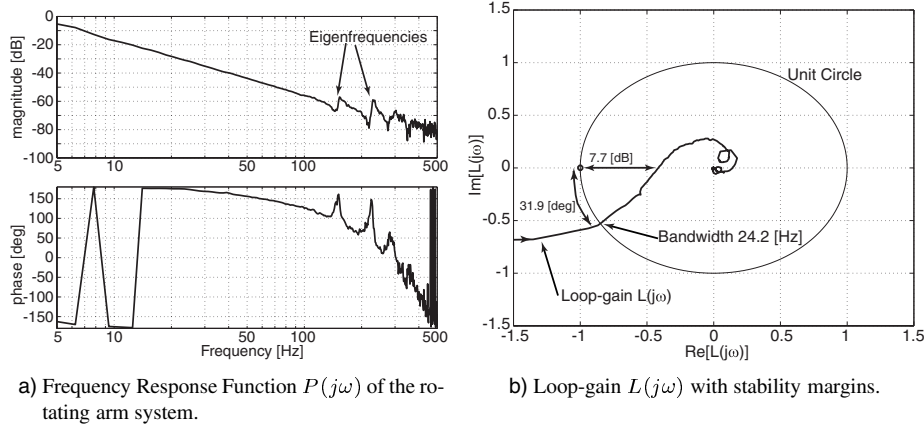


Figure 5.3 - Frequency domain analysis and controller tuning of the linear dynamics of the rotating arm system.

scheme based on the LuGre friction model in Eq. (5.10). In addition to this controller tuning a second order system, i.e.,  $\hat{P}(j\omega) = \frac{c_m}{J(j\omega)^2}$ , is estimated on the reconstructed FRF  $P(j\omega)$  with  $c_m = 16$  [N·m/V]. The estimated  $J$  is equal to 0.026 [kg·m<sup>2</sup>/rad] and will be used for all three control strategies as the inertial estimate.

### Friction-velocity map

To identify the different static friction curves used in the various compensation techniques discussed in Section 5.2 a friction-velocity map is generated. For this purpose the frequency domain tuned PID controller  $C(s)$  is used to control the system for reference functions with different constant velocities. For both negative and positive reference velocities, the applied torque and obtained velocity are averaged to reduce noise and position dependent frictional effects. The averaged applied torques at the different averaged velocities are depicted in Figure 5.4 with circles. The various parameters for the different friction models are obtained by minimization of the following quadratic cost function

$$\min_{\theta} \sum_{k=1}^M [F_{ss}(\dot{q}_k) - F_{model}(\dot{q}_k, \theta)]^2,$$

where  $F_{ss}(\dot{q}_k)$  are the friction torques measured during constant velocities  $\dot{q}_k$  and  $M$  is the number of measured data points. The number of model parameters  $\theta$  varies for each model type  $F_{model}(\dot{q}_k, \theta)$ . The estimated parameters are given in Table 5.2 and the resulting friction curves for the different models are shown in Figure 5.4 with solid lines. For the identified PLM Stribeck curve the number of local models used is set to 4 which are denoted with LM

### 5.3 Experimental Results

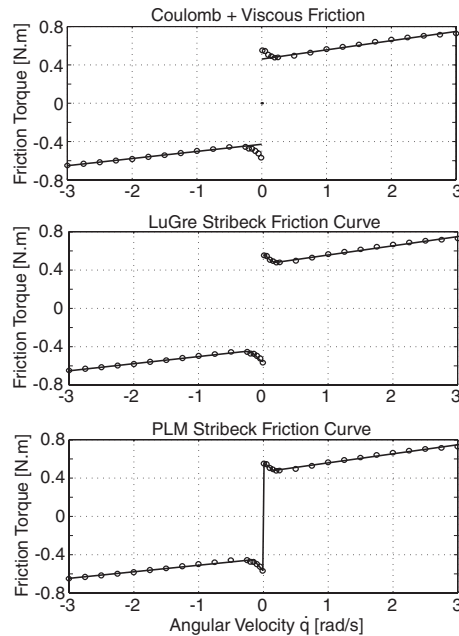


Figure 5.4 - Friction-velocity map and the estimated friction curves.

in Table 5.2. The friction parameters are direction dependent for all model types due to a clear difference in frictional behaviour for positive and negative angular velocities.

#### Classic PID control plus friction feedforward

The tuning for this control scheme was completed in the previous two subsections, where it should be emphasized that the friction curve in the upper-left plot of Figure 5.4 is only used as a feedforward where for zero desired velocity the friction feedforward is set to zero.

#### LuGre-based controller

As for the classic PID controller the LuGre-based observer-controller scheme is completely determined by the parameter estimates in Table 5.2 and the frequency domain tuned linear controller  $C(s)$  described previously in this subsection. It should be emphasized that for an ideal friction compensation scheme integral control is not necessary. However, due to possible under or over compensation of the friction force errors in the low frequency range will not be attenuated without integral control. Therefore, the PID controller tuned in the frequency domain as presented earlier is used here. However, for the estimated model parameters and tuned PID controller the sufficient closed-loop stability condition Eq. (5.11) as discussed in Section 5.2.2 is not satisfied and therefore stability of the closed-loop system

## Part I - Identification and Control of Mechanical Systems with Friction

Classic	$\dot{q} > 0$	$\dot{q} < 0$
$F_c$ [N·m]	0.461	0.428
$\sigma_2$ [N·m·s/rad]	0.096	0.075

LuGre	$\dot{q} > 0$	$\dot{q} < 0$
$F_c$ [N·m]	0.461	0.428
$F_s$ [N·m]	0.555	0.552
$v_s$ [rad/s]	0.105	0.135
$\sigma_0$ [N·m/rad]	1.2e4	1.2e4
$\sigma_1$ [N·m·s/rad]	4.39	4.39
$\sigma_2$ [N·m·s/rad]	0.096	0.075

PLM	LM 1	LM 2	LM 3	LM 4
$a$ [N·m·s/rad]	0.069	-0.773	-0.527	0.095
$b$ [N·m]	-0.441	-0.571	0.563	0.464
$c$ [rad/s]	-1	-0.05	0.05	1
$d$ [rad <sup>2</sup> /s <sup>2</sup> ]	0.008	8.9e-5	8.9e-5	0.008

Table 5.2 - Friction model parameters.

can not be proven. On the other hand, in [25] it is shown that this sufficient condition is in general conservative and in practice this condition may be relaxed. So, though at this stage stability of the closed-loop system can not be proved, controller Eq. (5.10) will be applied to the experimental setup.

### Gain-scheduling optimal PD controller

As presented in Section 5.2.2 the PLM control scheme consists of (i) a "feedforward" based on the identified PLM of the friction and mass of the system and (ii) a nonlinear optimal feedback law. The feedforward is completely determined by the parameter estimates in Table 5.2 whereas for the feedback part an inverse optimal control problem has to be solved. To solve the inverse optimal control problem the set of AREs as given in Eq. (5.16) have to be satisfied for all  $(i, j) = 1, \dots, 4$ , under the condition that there exists a  $P = P^T > 0$ . The matrices  $A_i(\theta)$  are determined by the parameter estimates and used to design the optimal controller part. The optimal controller design boils down to a nonlinear equivalence of the LQ-design in linear system theory. Likewise the LQ-theory, the system according to Eq. (5.13), should be stabilizable [20], which is satisfied since a stabilizability condition [4], i.e., the identified PLM is stabilizable if there exists a matrix  $Q = Q^T > 0$  and a scalar  $\sigma$  such that

$$A_i Q + Q A_i^T - \sigma B B^T < 0, \quad \forall i = 1, \dots, 4,$$

### 5.3 Experimental Results

can be checked easily and confirms that the AREs admit a solution.

Here, the optimal controller part  $u_{feedback}$  is designed with the objective of obtaining a high gain PD controller for low velocities to reduce the steady state error. For this situation the input weights  $R_j$ ,  $j = 1, \dots, 4$  can be chosen differently and determine the different gains of the feedback controller in the various regimes of the state space. Clearly, the number of AREs to be solved for this inverse optimal problem is  $N^2 = 16$ . However, the validity functions  $\rho$  are chosen symmetrically around zero angular velocity, i.e., for the centers  $c_1 = -c_4$ ,  $c_2 = -c_3$  and for the variances  $d_1 = d_4$ ,  $d_2 = d_3$ . Especially around zero velocity, i.e., models 2 and 3, a higher gain is desirable and therefore different input weights  $R_j$  are only considered for the model pairs (1,4) and (2,3). Hence, the number of AREs to be solved reduce to  $N(N/2) = 8$ .

To solve this inverse optimal control problem a seemingly ad hoc approach will be performed, since first a static gain PD controller, i.e., one input weight  $R$  for all models, will be derived. This will result in (i) a positive-definite matrix  $P$  for one  $R$  and (ii) 4 different positive-definite matrices  $Q_i$ ,  $i = 1, \dots, 4$ . Secondly by altering only the input weights  $R$  corresponding to the model pair (2,3) it is shown that the found  $P$  matrix is also a solution for the gain-scheduled PD controller. Hence, the first step is to find a static gain PD controller, i.e., one input weight  $R$  for all models. For this problem, the number of AREs to be solved reduce to  $N = 4$  and the following AREs have to be solved

$$Q_i + PA_i(\theta) + A_i^T(\theta)P - PBR^{-1}B^T P = 0 \quad (5.17)$$

for all  $i = 1, \dots, 4$ , where  $P > 0$ ,  $Q_i > 0$ ,  $R > 0$ . To assure acceptable input torques, the ARE corresponding to model 4, which is valid for large positive velocities, is solved yielding a  $P$  for given  $R$  and  $Q_4$ . Next, given  $R$  and  $P$ ,  $Q_i$  for  $i = 1, \dots, 3$  are computed from Eq. (5.17). If  $Q_i > 0$ ,  $\forall i = 1, \dots, 3$  a solution  $P$  has been found that satisfies all four AREs. Here, the weight matrices  $Q_4$  and  $R$  are chosen after an iterative process, where the matrices are initialized as suggested in [19]. For the solution of this ARE we found a  $P$  and the matrices  $Q_i$ ,  $i = 1, \dots, 3$  are found to be positive definite for this  $P$  and  $R$ . Hence, an optimal static gain state feedback law is obtained. Returning to the gain-scheduling control problem this result can be used to derive the gain-scheduled state feedback controller

$$u_{feedback} = - \sum_{i=1}^4 w_i(x, \theta) R_i^{-1} B^T P e,$$

where  $R_1 = R_4$  and  $R_2 = R_3$ . For this problem the following AREs have to be solved

$$Q_{ij} + PA_i(\theta) + A_i^T(\theta)P - PBR_j^{-1}B^T P = 0$$

for all  $i = 1, \dots, 4$ ,  $j = 1, 2$ . If we denote the input weight  $R$  from the previous controller design as  $R_1$ , and  $Q_i$  as  $Q_{i1}$  for  $i = 1, \dots, 4$  we have to find  $R_2$ ,  $Q_{i2}$  for  $i = 1, \dots, 4$  for the given  $P$ . Due to the fact that by using the weights  $R_1$  and  $Q_{i1}$ ,  $i = 1, \dots, 4$  and the optimal  $P$  the other four AREs are satisfied, we propose for  $R_2$

$$R_2 = \alpha R_1 \quad 0 < \alpha \leq 1.$$

With  $\alpha$  small we obtain a high gain controller for the low velocity regime corresponding to the model pair (2,3). In practice, the design variable  $\alpha$  can not be chosen too small due to the fact that high gain control will amplify measurement noise, and due to the fact that the control torque  $u$  is bounded. For the low velocity regime this stiff PD controller is favorable in order to reduce steady state errors due to static friction.

### 5.3.3 Experimental Results

The different friction compensation techniques are compared for three third order setpoints where the classic PID controller combined with feedforwards serves as a reference. For a third order setpoint the reference position  $q_d(t)$ , velocity  $\dot{q}_d(t)$  and acceleration  $\ddot{q}_d(t)$  are continuous. The desired jerk  $\dddot{q}_d(t)$  is the first discontinuous derivative in the setpoint. As discussed earlier, the rotating arm system is limited with respect to the maximum allowable angular velocity. To express this limitation, the setpoints used have a maximal reference velocity of 10 [rad/s]. Other bounds imposed on the setpoints are a maximal acceleration of 100 [rad/s<sup>2</sup>] and a maximal jerk of 1000 [rad/s<sup>3</sup>]. The different setpoints are given in Figure

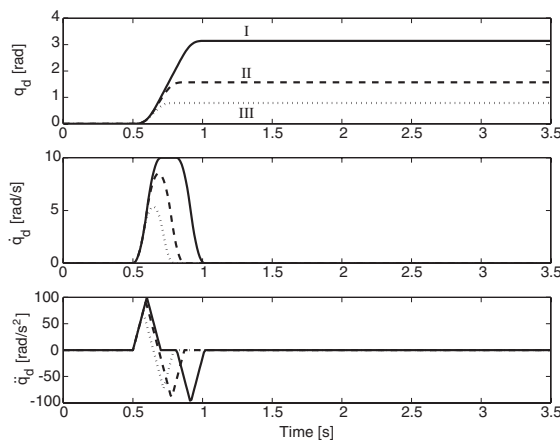


Figure 5.5 - Three different third order setpoints.

5.5 where the reference position, velocity and acceleration are depicted. The first setpoint (solid lines) reaches the maximal allowable velocity, acceleration and jerk, where the second (dashed lines) and third setpoint (dotted lines) have lower maximal velocities, acceleration and jerks. For the first setpoint there is clearly a period with constant velocity where for the second and third setpoint the system is expected only to accelerate and decelerate.

In the upper-plots of Figure 5.6 a), b) and c) the LuGre controller performances, depicted with dashed lines, are compared to the classic PID controller performances, depicted with solid lines. In the lower-plots the PLM controller performances, depicted with dashed lines, are also compared to the classic PID controller performances, again depicted with solid lines.

### 5.3 Experimental Results

The vertical dashed lines define the starting point and end point of the different setpoints.

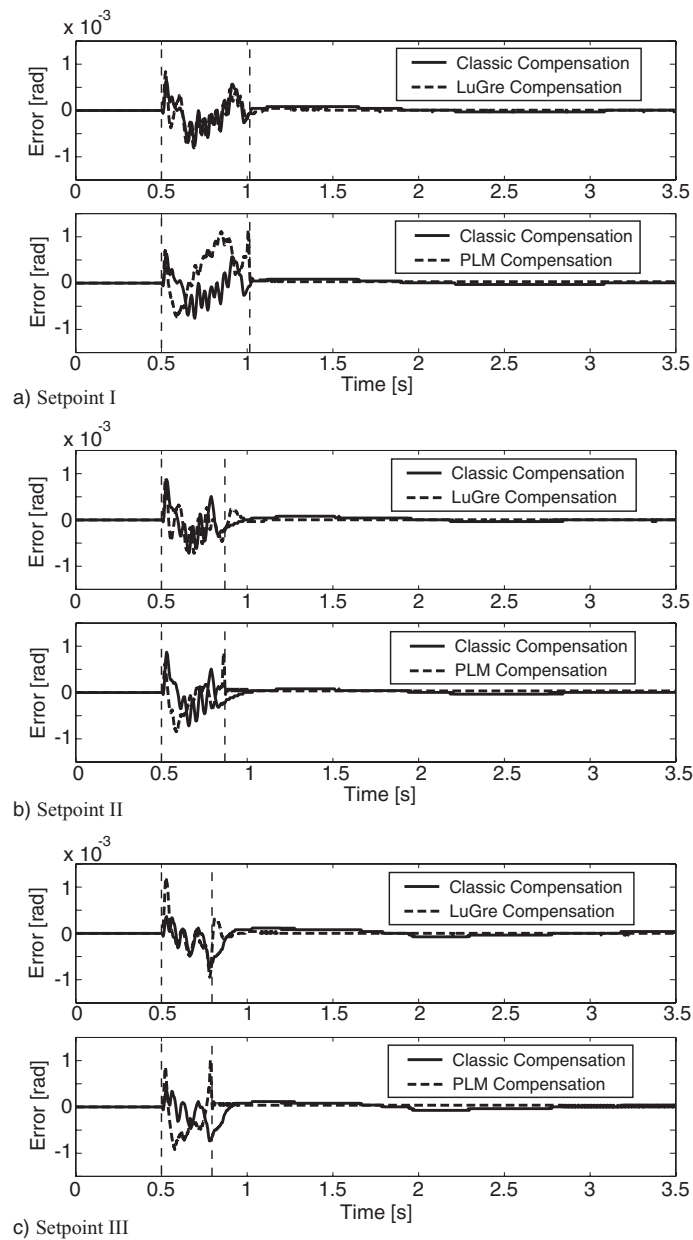


Figure 5.6 - Comparison of controller performances.

## Part I - Identification and Control of Mechanical Systems with Friction

In Table 5.3 (i) the error at the end of the setpoint, (ii) the settling time, here defined as the time necessary after the end of the setpoint to reach the desired reference position within one increment or  $\pm 3.835e-5$  [rad] (together the regulator performance), and (iii) the maximal error during the setpoint (tracking performance), are given for the three different controllers and the three different setpoints.

Controller	Error after setpoint in $1e-5$ [rad]		
	Setpoint 1	Setpoint 2	Setpoint 3
PID	-6.95	-22.64	-65.01
LuGre	-3.10	-22.64	-34.30
PLM	18.4	15.0	7.49

Controller	Settling time [s]		
	Setpoint 1	Setpoint 2	Setpoint 3
PID	0.641	0.671	1.507
LuGre	0.450	0.133	0.196
PLM	0.194	0.132	0.152

Controller	Maximum error in $1e-4$ [rad]		
	Setpoint 1	Setpoint 2	Setpoint 3
PID	6.5	8.7	-7.3
LuGre	8.5	9.0	11.8
PLM	11.5	8.6	10.2

Table 5.3 - Controller performances for three different setpoints.

The high gain parameter  $\alpha$  in the PLM control scheme is set to 0.2 where the innovation gain  $k$  in the LuGre observer is set to 5. Due to the higher gain at low velocities for the PLM controller the static error is immediately reduced at the end of the setpoints. The PID controller performs well during the setpoints however after the setpoints the integral action is still present for a long time and the static errors are attenuated slowly in comparison to the other two schemes. The LuGre observer-controller scheme is comparable to the classic PID controller during the setpoint however after the setpoint the static error is compensated faster.

To give a better comparison of the controller performances presented in Table 5.3, the results are translated into three indices, i.e., one for the settling time, one for the error after setpoint and one for the maximal error during setpoint. The indices are defined as follows

$$I = 100(1 - RE),$$

where  $I$  is the corresponding index and  $RE$  is the relative performance of the controllers with respect to the performance obtained with the classic PID controller in combination with mass

## 5.4 Conclusions

and friction feedforward. The relative performance  $RE$  is averaged over the three different setpoints. Figure 5.7 gives the indices for (i) the LuGre controller-observer scheme and (ii) the gain-scheduled PD controller. A positive performance index indicates an improvement, where  $I = 100$  is the desired performance and a negative performance index indicates a deterioration with respect to the classic PID controller plus feedforwards.

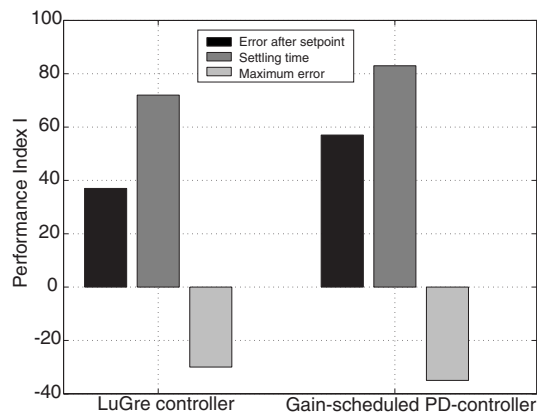


Figure 5.7 - Comparison of controller performances expressed in performance indices.

## 5.4 Conclusions

In this chapter, different control schemes have been compared with respect to their performance for regulator or point to point tasks on a rotating arm system subjected to friction. Frequency domain analysis of the system reveal important aspects of the linear dynamics of the rotating arm, i.e., location of eigenfrequencies and presence of time-delay. A linear PID controller was tuned in the frequency domain to obtain a closed-loop system with an as high as possible bandwidth under certain stability margins. Construction of a friction-velocity map gives insight in the frictional characteristic of the system and is used to identify different friction curves for three different friction compensation schemes, i.e., (i) classic PID controller in combination with Coulomb plus viscous friction feedforward, (ii) an observer-controller scheme based on the dynamic LuGre friction model and (iii) a gain-scheduled optimal PD controller based on a Polytopic Linear Model of the friction.

Experimental results on the rotating arm show the favorable property of the gain-scheduled PD controller to suppress static errors for low velocities. Another advantage of this PLM-based control scheme is the fact that at the end of the setpoint the controller is very fast. Hence, with respect to regulator performances the PLM-based scheme shows the best results, whereas the tracking performance during setpoint is limited for this controller scheme. The LuGre-based scheme performs well both during the setpoint and after the setpoint where



## Part I - Identification and Control of Mechanical Systems with Friction

errors are attenuated considerably faster than with the standard PID controller. Hence, if a combination of servo and point to point movements are considered the LuGre-based scheme gives the best for both worlds. Furthermore, the relaxation of stability condition with respect to the LuGre observer design raised in Section 5.2.2 is also applicable for this system since no unstable responses of the closed-loop system were encountered during the experimental work.

# Chapter 6

## In Retrospect

In this chapter, the main contributions with respect to the development of identification procedures and control synthesis for mechanical systems with friction are summarized and topics for further research are presented. However, first additional remarks on the used theory and methods are given to clarify some aspects of the presented results in this first part.

### 6.1 Notes and Comments

#### 6.1.1 Extended Kalman Filter

The use of the Extended Kalman Filter estimator in Chapter 3 calls for some additional comments. The assumption that the technique minimizes the variance of the reconstruction error, as stated in Section 3.4, is only satisfied for the linear case and under the assumption that the model errors and measurement errors have white noise properties. For the nonlinear case the Extended Kalman Filter technique turns out to be a sub-optimal estimator due to the nonlinear model structures used, where the propagation of the estimated state  $\hat{x}$  and the corresponding covariance matrix  $P(t)$  are based on linearizations. Moreover, the assumption that the model errors can be modeled as zero mean gaussian noise with intensity  $Q(t)$  is a heavy one, since model errors in general will exhibit a dominant deterministic part due to, for instance, the presence of unmodeled higher order dynamics in the real system. For example, the experimental setup used throughout this first part is modeled in Chapter 3 as a second order system, but the reconstructed FRF of the linear part of the system in the slip phase, as depicted in Figure 5.3a), clearly shows higher order dynamics due to flexibility in the system. Hence, the influence of these unmodeled higher order dynamics, that will show an error on the second model equation of Eq. (3.1) in the Chapter 3, is assumed to possess zero mean gaussian noise properties. This is of course a severe assumption due to the local effect of unmodeled higher order dynamics in the frequency domain.

As for many optimization techniques, the stochastic Kalman filtering technique has also a deterministic counter approach. If the model errors and measurement errors are regarded as deterministic errors, the least-squares minimization of the sum of the weighted squares of these deterministic errors will result in an estimator algorithm identical to the Kalman

filter algorithm. In this deterministic approach the weighting matrices are the counterparts of the intensity matrices  $Q(t)$  and  $R(t)$  in the stochastic case and balances the certainty or uncertainty in the model equations and the measurements. Therefore, in contrast with the statement made in Section 3.4, the EKF technique can also be seen as a least-squares technique. However, in contrast to output-error least-squares techniques, where only uncertainty in the measurements are modeled, the EKF technique is also able to incorporate uncertainties in the model equations in the optimization.

### 6.1.2 Generalized differentials

In Chapter 4, the non-smooth LuGre friction model was linearized to obtain a second order linear description of a mass system connected to a frictional surface in the presliding displacement regime. To this end the non-smooth calculus of *generalized differentials* [29] was used to obtain this linearization, where the closed convex hull of the left and right derivatives defines the *generalized differential*. However, for this specific case where the system is linearized about an internal friction state  $z = x_3 = 0$ , the left and right derivative become equal, i.e.,  $f'_- = f'_+$ . Hence, the use of the non-smooth calculus of *generalized differentials* is not necessary to obtain the linearization about  $z = x_3 = 0$  as presented in Chapter 4.

On the other hand, if the internal friction state  $z$  is unequal to zero and the velocity  $\dot{x}$  becomes zero the left and right derivative will be different due to the non-smoothness in the LuGre friction model. Returning to the stress-relaxation simulation as described in Section 4.2 this can be seen in Figure 4.2, where interesting points in the graphs are those at velocity reversals or extrema of the displacement  $x_1$ . At these points, the linearization of the friction force with respect to the state  $\underline{x}$ , where the velocity is equal to zero and  $z = x_3$  different from zero, is clearly multiple-valued, i.e., sharp corner in the force-displacement curve of Figure 4.2a) and jumps in the time response of the velocity  $x_2$  as shown Figure 4.2b) at approximately  $t = 14$  [s] and  $t = 42$  [s]. Hence, the non-smooth calculus of *generalized differentials* might be useful for the case where for the LuGre friction model the internal state  $z$  is different from zero and the velocity  $\dot{x}$  becomes zero. In the second part of this thesis, we will encounter an example where this special situation occurs for a set of equilibrium points and the notion of *generalized differentials* will be used to analyze the local stability of the equilibrium set.

### 6.1.3 Controller performance in the presliding displacement regime

The comparison study in Chapter 5 shows an improvement of the regulator performance, i.e., in terms of smaller settling times and smaller errors after setpoint, for both the proposed PLM based controller and the LuGre based compensation scheme with respect to the regulator performance obtained with the classic PID controller plus feedforwards. However, these two friction compensation schemes are far more complex in terms of implementation, controller synthesis and stability analysis than the classic PID controller with feedforwards. Hence, it is of interest to understand the limiting factors of the regulator performance for this

## 6.1 Notes and Comments

widely used classic approach.

To this end we return to the regulator performance obtained for the first third order setpoint with the classic PID controller with mass and Coulomb plus viscous friction feedforward as discussed in Section 5.3.3 and shown again in Figure 6.1. In the upper plot the error is shown, where the vertical dashed lines define the start and the end of the setpoint. In the lower plot the corresponding controller effort is depicted, where during setpoint the feedforward part contributes besides the feedback part to the applied torque whereas after the setpoint the feedback controller is the only remaining active controller part. Hence, the settling behaviour of the error after setpoint, which mainly determines the settling time, is completely defined by the closed-loop dynamics. From the settling behaviour of the error it can be seen that the occurring error after setpoint is suppressed very slowly and its low frequent oscillation, with an approximate frequency of 1/3 [Hz], indicates a closed-loop dynamics with a much lower bandwidth than the bandwidth of 24 [Hz] as discussed in Section 5.3.2.

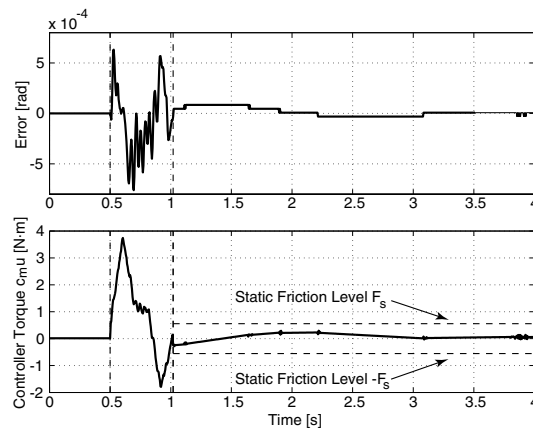


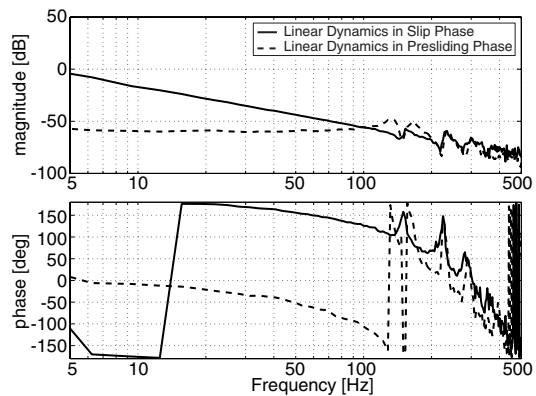
Figure 6.1 - Time responses of the position error and the controller effort.

In Section 5.2.1, the tuning of the implemented feedback controller was discussed, which aimed at an as high as possible closed-loop bandwidth while guaranteeing sufficient stability margins. To this end, a frequency domain controller synthesis was performed with the linear dynamics of the system in the slip phase as reconstructed in Section 5.3.2. However, as can be seen in the lower plot of Figure 6.1, the controller torque after setpoint is constantly within the static friction level (depicted with horizontal dashed lines), which indicates together with the very small and slow varying error that the system is in the presliding displacement regime and **not** in the slip phase. Therefore, the closed-loop dynamics after setpoint is determined by the tuned feedback controller in combination with the dynamics of the presliding displacement regime and **not** with the dynamics of the slip phase.

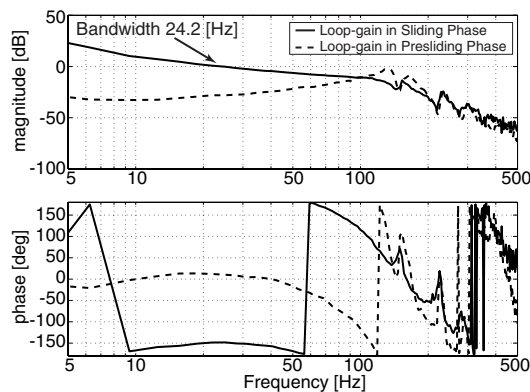
To analyse the influence of these changing closed-loop dynamics the FRF measurements of

## Part I - Identification and Control of Mechanical Systems with Friction

the linear part of the dynamics for the two different phases are shown together in Figure 6.2a), where the solid line depicts the linear dynamics in the slip phase and the dashed line represents the linear dynamics in the linearized presliding displacement regime, as measured in Chapter 4. The figure shows clearly the change from a double integrator behaviour in



a) Varying linear dynamics of the system.



b) Loop-gain for varying closed-loop dynamics.

Figure 6.2 - Frequency domain analysis of the varying linear (closed-loop) dynamics of the rotating arm system.

the slip phase to a mass-spring behaviour in the presliding displacement regime. Next, the closed-loop dynamics for both regimes are compared, where the linear feedback controller is used to reconstruct the loop-gain of the varying closed-loop dynamics. In Figure 6.2b), the loop-gain for the slip phase, which is depicted with the solid line, shows the tuned bandwidth of 24 [Hz] together with the desired stability margins and is the same loop-gain as shown

## 6.1 Notes and Comments

in the corresponding Nyquist-plot of Figure 5.3b). However, in the presliding displacement regime the shape of the loop-gain, which is depicted with the dashed line, is completely different and deteriorates the closed-loop dynamics due to the strong change of the dynamical behaviour. For instance, the closed-loop dynamics around the first eigenfrequency of the system, i.e., approximately at 150 [Hz], is altered due to the additional stiffness in the presliding displacement regime and nearly results in unstable closed-loop dynamics in the presliding displacement regime. Moreover, the bandwidth of the closed-loop dynamics in the presliding displacement regime has dropped immensely and lies outside the range of the picture. Therefore additional closed-loop FRF measurements in the presliding displacement regime are performed to measure the low frequency range of interest. In Figure 6.3, the loop-gain in the presliding displacement regime is depicted for frequencies up to 10 [Hz] and indicates a bandwidth of approximately 0.2 [Hz], which is consistent with the measured settling behaviour of the error after setpoint.

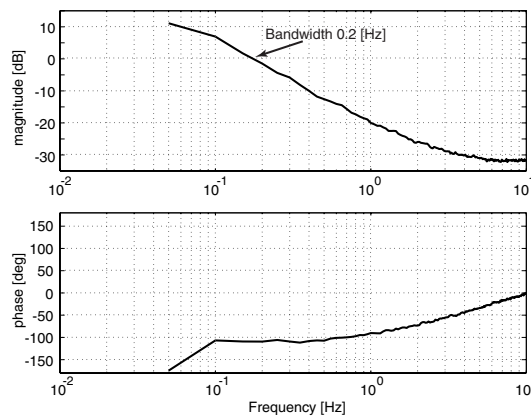


Figure 6.3 - Low frequency behaviour of loop-gain in the presliding displacement regime.

Here, it should be emphasized that the dynamics in the presliding displacement regime in general is nonlinear and therefore the depicted FRF measurements are only valid locally in the presliding displacement regime, as discussed in Chapter 4. However, these FRF measurements play an important role in the understanding of the degenerating settling behaviour in the presliding displacement regime for the classic PID controller. Hence, it is advisable to incorporate the dynamics of the presliding displacement regime into the design of the PID controller. However, due to the strongly varying dynamical properties a single PID controller will not have desirable closed-loop properties, such as an as high as possible bandwidth with sufficient stability margins, for both the slip phase and the presliding displacement regime. A solution might be the use of two different linear feedback controllers, i.e., one for the slip phase and one for the presliding displacement regime. However, the switching between the different controllers needs an extremely accurate detection of the different dynamical phases of the system, which might be a function of both the velocity and the applied forces. An

accurate real-time measurement of very low velocities is still an open issue and needs to be solved before such switching controllers can be successfully implemented.

## 6.2 Summary of Contributions

In this section, the main contributions made in this part with respect to the first two research goals as discussed in Section 1.3 will be summarized.

### 6.2.1 Identification techniques

Throughout this first part, various identification techniques have been discussed and used for the estimation of model parameters of mechanical systems with friction. A clear distinction can be made between the used identification methods, i.e., methods based on (i) time domain measurements, such as the Extended Kalman Filtering technique in Chapter 3 and (ii) frequency domain measurements as used to reveal the linear part of the dynamics in the presliding displacement regime and the slip phase in Chapters 4 and 5. In general, all identification procedures consist of four different stages, i.e.,

- a modeling stage, where an appropriate model has to be chosen with respect to the system or dynamics under consideration,
- an experimental stage, where the system has to be excited - either in open-loop or closed-loop configuration - in such a way that all the relevant phenomena are present in the measured data,
- an identification stage, where an estimation algorithm has to be chosen depending on the model structure and used to estimate the model parameters and
- a validation stage, where the model is either auto- or cross-validated with the system. The model might be tested satisfactory for the intended purpose or not, where in the latter case one or all of the previous stages have to be reconsidered.

The first three stages strongly depend on one another and therefore the order of execution is not fixed. For frequency domain identification, the modeling stage is of course restricted to linear dynamics and therefore for nonlinear systems, such as the here discussed mechanical systems with friction, these measurements can only be used to model the linear aspects of the system. However, some influences of nonlinear phenomena might be measured with FRF measurements, for instance as shown in Chapter 4, where the dependence of the input amplitude on the “averaged” stiffness in the presliding displacement regime has been observed. Moreover, for a real-life system each physical component, e.g., motor, transmission and bearings, contributes to important dynamical properties, such as mass, stiffness and damping. For frequency domain measurements, the various dynamical properties of the different physical elements are lumped into one or more sources. Hence, from measured FRFs it is hard or even impossible to pin-point the dynamical properties of the separate

## 6.2 Summary of Contributions

components.

In Chapter 3, the iterative EKF approach has shown to be a useful identification tool for two proposed nonlinear static friction models, which were embedded in a second order model of the mechanics. The identification stage is performed with discrete-time measurements of the angular displacement and reconstructed angular velocities. Moreover, both the proposed neural network model structure and the Polytopic Linear Model have a rich and flexible topology, that is able to model the nonlinear Stribeck phenomenon. Moreover, the EKF approach enables the user to estimate all model parameters simultaneously, which reduces the number of experiments.

In Chapter 4, frequency domain measurements have been used to identify the linear dynamics in the presliding displacement regime of friction, as modeled by the dynamic LuGre friction model. In this way the important parameters in this dynamic friction model, i.e., the bristle stiffness and damping, could be estimated from a single experiment. As a spin-off of this research, the expected nonlinear nature within the presliding displacement regime has been confirmed with FRF measurements, which have been conducted at different amplitude levels of the input within the presliding displacement regime and indicated the expected decreasing “averaged” presliding stiffness.

A mixture of time and frequency domain measurements have been utilized to estimate model parameters of various friction models and other system dynamics in Chapter 5. An appropriate reference trajectory has been chosen to isolate the linear dynamics of the closed-loop system from the nonlinear friction phenomenon during the experiments. For stable closed-loop dynamics and a known controller the linear dynamics of the system in the slip phase could be reconstructed, which revealed important aspects of the system, such as location of eigenfrequencies and an apparent time delay in system. On the other hand, to estimate the nonlinear phenomenon of friction present in the system time domain experiments have been performed, which resulted in the identification of the Stribeck friction curve for various friction models.

Overall, it can be concluded that both time and frequency domain identification are essential to model and understand all dynamical properties present in a mechanical system with friction. Moreover, both domains should be used in a complementary sense, where the strength of each domain has to be exploited over the limitations of the other. In the second part, i.e., in Chapter 10, this mixture of time domain and frequency domain identification will be illustrated once more for a more complex dynamical system.

### 6.2.2 Presliding displacement regime versus slip phase

The frequency domain identification of the linear dynamics in (i) the presliding displacement regime, as presented in Chapter 4, and (ii) the slip phase of the system, as presented in Chapter 5, have contributed to the understanding of the changing dominant dynamics from a double integrator behaviour to a mass system connected to the fixed world with a finite



stiffness. Figure 6.2a), depicting the FRFs of the linear dynamics for both frictional regimes, has visualized this notion, where for the low frequency range up to the eigenfrequency of the dynamics in the presliding displacement regime the difference in dynamics is prominent. For the high frequency range, i.e., above the eigenfrequency of the dynamics in the presliding displacement regime, the dynamics are again equivalent. For the considered experimental setup, all differently located components that contribute to the friction, such as bearings and transmission, have been lumped into one friction source collocated at the motor (and encoder) side of the system.

In Chapter 10 of the thesis, this change of the dominant linear dynamics due to changing frictional regimes will be illustrated once again for a more complex dynamical system with similar results.

### 6.2.3 Controller synthesis and performance

In Chapter 5, three different control schemes have been compared with respect to their performance for regulator or point to point tasks. The controller design and synthesis of each friction compensation scheme can be summarized as follows:

- for a classic PID controller in combination with mass and Coulomb plus viscous friction feedforward, the FRF measurement of the linear dynamics of the system in the slip phase has been used to tune a PID controller with the objective to obtain a closed-loop system with an as high as possible bandwidth under certain stability margins. In this way the linear higher order dynamics and phase-lag due to the time-delay in the system have been incorporated in the controller synthesis. To increase the expected controller performances mass and friction feedforwards have been added, that are based on the low frequent double integrator behaviour of the measured FRF and a measured friction-velocity map,
- for an observer-controller scheme based on the dynamic LuGre friction model, an observer has been used to reconstruct the not measurable internal friction state  $z$  of the dynamic friction model. This model-based compensation scheme is composed of a linear feedback controller, which in practice has been tuned in the same way as the classic PID controller, and a nonlinear friction feedback compensation, which is based on the identified dynamic LuGre friction model. Stability issues of the complete closed-loop observer-controller scheme are still an open issue, but were found not to be restrictive in the experimental study,
- for a gain-scheduled optimal PD controller based on a Polytopic Linear Model of the system, the measured friction-velocity map and measured FRF of the linear dynamics have been used to determine the PLM parameters. The PLM structure has been shown to be extremely suitable for controller synthesis, which fact has been exploited resulting in a PLM-based inverse optimal controller design. The derived controller consists of (i) a feedforward part, where both mass and friction components are present, and

### 6.3 Recommendations for Future Research

- (ii) a (nonlinear) optimal feedback PD controller with variable gain as a function of velocity.

Due to the use of model-based compensation schemes, the earlier discussed identification procedures have been extremely important for controller synthesis and will determine to some extent the performance that can be obtained with the compensation schemes.

The experimental results have indicated that the gain-scheduled PD controller, where for low velocities the controller gain has been increased, has the favorable property of suppressing static errors. Another advantage of this PLM-based control scheme is the fact that at the end of setpoint the controller is very fast. Hence, with respect to regulator performance the PLM-based scheme has shown the best results, whereas the tracking performance during setpoint has been limited for this controller scheme. The LuGre-based scheme performs well both during setpoint and after setpoint where errors have been attenuated considerably faster than with the classic PID controller. Hence, if a combination of servo and point to point movements are considered the LuGre-based scheme will give the best for both worlds.

In Section 6.1.3, the limited settling performance of the classic PID controller has been shown to be caused by the changing dominant dynamics from a double integrator behaviour in the slip phase to a mass-spring behaviour in the presliding displacement regime. As a consequence, the closed-loop dynamics properties will deteriorate due to a decreasing bandwidth and even decreasing stability margins in the presliding displacement regime. Hence, for a simple PID controller the settling behaviour in terms of static error suppression is limited due to the additional stiffness in the presliding displacement regime.

## 6.3 Recommendations for Future Research

In connection to the present work the following research topics might be of future interest.

### 6.3.1 Presliding displacement dynamics

In Chapter 4, the dynamic LuGre friction model has been used to analyse the dynamics within the presliding displacement regime. However, time domain validation of the identified linear behaviour within this regime has shown good correspondence to the real system. Only one discrepancy has been recorded outside this very locally valid regime. The dynamic LuGre friction model has limited applicability for the description of the entire presliding phenomenon, i.e., the total stick regime for an applied force lower than the static friction. Extensive evaluation of the presliding behaviour will be necessary in future research as well as the modification of the LuGre model to obtain a more accurate dynamic friction model for the description of the presliding phenomenon. In Chapter 2, extensions of the standard parametrization of the dynamic LuGre friction model were briefly addressed and might be used as a starting point for this research.

### 6.3.2 Switching linear controllers

As discussed in Section 6.1.3, the use of two different linear controllers, i.e., one for the slip phase and one for the presliding displacement regime, might improve the regulator performance considerably in terms of settling behaviour and disturbance attenuation. However this approach will encounter the following open problems:

- How to detect the change in dominant dynamics? That is, when is the system in the presliding displacement regime and when in the slip phase? This will certainly require an accurate measurement of the instantaneous velocity and especially of very low velocities. Moreover, the switching surface might be a complex nonlinear function of applied forces, velocity and the non-measurable presliding displacement.
- How to switch between two different linear controllers? Switching forth and back between linear dynamic controllers raises the question how to re-initialize the state of each controller after a switch has occurred. Various techniques have already been studied in gain-scheduling literature [87], [107], but the issue of stability has not been sufficiently addressed yet.

**Part II**

# **Friction Induced Limit Cycles**



# Chapter 7

## Introduction

This second part will start with a short review on friction induced stick-slip oscillations in controlled mechanical systems and its analysis in Section 7.1. An outline of this second and last part of the thesis will be given in Section 7.2. Appendix A is recommended for formal definitions of some frequently used terms, such as limit cycle, bifurcation or Floquet multipliers.

### 7.1 Friction Induced Stick-Slip Oscillations in Controlled Mechanical Systems

A friction induced phenomenon for controlled mechanical systems that deserves extra attention is stick-slip oscillations, for which rigid body elements alternately stick and slip with respect to each other, which is caused by the fact that friction is not constant as a function of velocity, i.e., loosely speaking, the friction force is larger at rest than during motion. Stick-slip oscillations always have and still do attract a sure amount of interest, as is evident from the huge amount of literature describing this phenomenon.

For controlled mechanical systems with friction two important types of friction induced stick-slip oscillations for two different controller tasks can be distinguished as reported in Table 1.1, i.e.,

- stick-slip oscillations for a tracking controller task at low velocities with a PD controller, which can be traced back to the negatively-sloped Stribeck curve for low velocities in combination with stiction,
- hunting oscillations, which are friction induced limit cycles, i.e., periodic solutions of the nonlinear autonomous closed-loop system, for a PID controlled regulator task. About this type of stick-slip oscillations little is known and its elimination in practice for increasing controller gains is not explained and fully understood yet.

For both phenomena the most simple motion system consists of a single mass system subjected to friction, where each controller task introduces its own friction induced stick-slip oscillations. The variation in friction induced oscillations is not limited to these two types

## Part II - Friction Induced Limit Cycling

of limit cycles, e.g., in [18], [49], [95] and [98] a fourth order system (two mass system) subjected to friction is considered for various dynamical settings. However, before getting into these more complex mechanical systems with friction in our opinion it is extremely important to fully understand the mechanism behind the occurrence of the two fairly simple looking friction induced phenomena as mentioned above. Hopefully, the obtained insight can be extended and applied to more general mechanical systems with friction.

The objective of this part is to investigate the second type of stick-slip oscillations also referred to as hunting [7]. However, let us first summarize the known results with respect to the first type of friction induced limit cycles to get an idea about the effect of the dominant frictional contributors on stick-slip oscillations. As for many friction related subjects as discussed in Chapter 1, these specific stick-slip oscillations are of interest for many different research communities expressed by a vast amount of literature on the subject ranging from the fields of tribology [103], control community [6], [38], geophysics [105], nonlinear dynamics [49], [35]. The majority of the researchers consider stick-slip oscillations for a mass-spring-damper system attached to a slowly moving belt or slider mechanism as shown in Figure 7.1a), which is equivalent to a PD controlled mass system with a low constant velocity tracking task of which the kinematic mirror is depicted in Figure 7.1b).

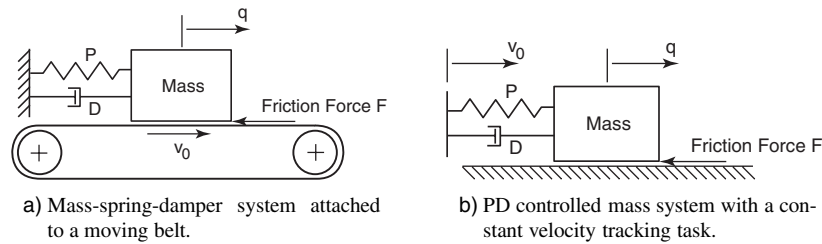


Figure 7.1 - Two equivalent systems that are able to show friction induced stick-slip oscillations.

The equilibrium point for the moving belt system is given by

$$\begin{bmatrix} q \\ \dot{q} \end{bmatrix}_{eq} = \begin{bmatrix} -\frac{F(-v_0)}{P} \\ 0 \end{bmatrix}$$

and the equilibrium point with respect to the tracking error  $e = v_0 t - q$  of the PD controlled system can be described as

$$\begin{bmatrix} e \\ \dot{e} \end{bmatrix}_{eq} = \begin{bmatrix} \frac{F(v_0)}{P} \\ 0 \end{bmatrix}.$$

For control engineers, important questions to be answered with respect to the stick-slip oscillations induced by the PD controlled system are [7]:

## 7.1 Friction Induced Stick-Slip Oscillations in Controlled Mechanical Systems

- Do stick-slip oscillations exist and for what system and control parameter values will they be stable?
- For what system parameter values the equilibrium motion  $\dot{q} = v_0$  is stable?

In control literature, these questions are addressed separately. This literature investigates either (i) the existence and stability of stick-slip oscillations, e.g., Armstrong-Hélouvy [6] applies a perturbation analysis for a non-dimensionalized friction model with Coulomb, viscous and Stribeck friction with frictional memory and rising static friction, or (ii) the local stability of the equilibrium motion, e.g., [38] performs a stability analysis of the equilibrium motion for a state variable friction model, which finds its origin in the geophysics community [106]. The motivation for incorporating these dynamic friction models into the analysis is the practically observed dependency of the existence of stick-slip limit cycles on the stiffness or proportional gain in the system, i.e., by increasing the stiffness stick-slip oscillations can be eliminated as shown by [103]. Moreover, it has been shown both experimentally [103] and analytically [38] that these oscillations can also be eliminated, besides by altering the stiffness, by increasing the damping in the system or by increasing the desired tracking velocity  $v_0$ , which from a control point of view is often not desirable. By increasing the damping, the equilibrium motion  $\dot{q} = v_0$  becomes stable if the negatively-sloped Stribeck curve is compensated for at low velocities. By increasing the desired tracking velocity  $v_0$ , the equilibrium velocity is pushed outside the negatively-sloped region of the Stribeck curve and therefore becomes stable. If the equilibrium motion becomes stable it is not clear whether the stable stick-slip oscillation has disappeared, since the stability analyses presented in the above mentioned literature are only based on local considerations. Hence, the complete dynamic picture giving answer to both questions simultaneously has not yet been presented in the control literature.

However, for the field of nonlinear dynamics these two questions go hand in hand and are considered as one general problem, which can be phrased as:

- What kind of solutions with what kind of local stability properties exist for the closed-loop system and how do they change as a function of the system parameters; for example for the damping value  $D$  in the moving belt system?

In [49] a frictional damping function with a negative slope for low velocities is considered. There, for varying damping values the existing solutions are determined using nonlinear analysis tools as described in Chapter 1. As expected, for damping values lower than a critical value  $D < D_{cr}^1$ , where the critical value represents the amount of damping added that is equal to the destabilizing negative damping at the equilibrium velocity  $\dot{q} = 0$  of the moving belt system, the equilibrium point is locally unstable and there also exists a stable limit cycle due to the stiffness in the system. The limit cycle is characterized by its maximum positive velocity amplitude, which is equal to  $v_0$  for the moving belt system. At the critical value  $D = D_{cr}^1$  the equilibrium point becomes stable due to the occurrence of a so-called subcritical Hopf bifurcation [108], which predicts the creation of an unstable limit cycle beyond it. At the bifurcation point, the already existing stick-slip oscillation remains



locally stable and for increasing values of  $D > D_{cr}^1$ , there coexist a stable and unstable limit cycle as well as a locally stable equilibrium point. For increasing damping values the amplitude of the unstable limit cycle increases and the stable and unstable limit cycle coincide at a second critical value  $D = D_{cr}^2$ , which represents a so-called fold bifurcation. However, this fold bifurcation is 'non-smooth' or better a discontinuous fold bifurcation as explained in more detail in the work of Leine [86], who considers a comparable system and finds similar results as Galvanetto et al. [49]. For damping values  $D > D_{cr}^2$ , there exists only a stable equilibrium point and stick-slip oscillations are absent. The complete dynamics featuring stable and unstable periodic solution and stability property of the equilibrium point can be depicted in one so-called bifurcation diagram as shown in Figure 7.2. This picture

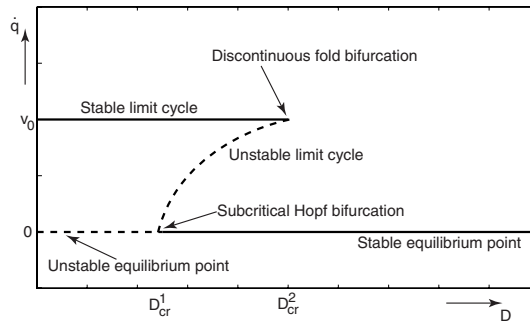


Figure 7.2 - Bifurcation diagram for varying damping values, which defines the maximal positive velocity amplitude of the existing solutions.

clearly shows the reason why it is important to address both questions as mentioned earlier simultaneously, since for a locally stable equilibrium point their might still exist a locally stable periodic solution and consequently for this second order system an unstable periodic solution in between.

For a more complete dynamic friction model, which incorporates both tangential and normal dynamics, Dankowicz et al. [35] show a numerically computed bifurcation diagram predicting different types of bifurcations and also the disappearance of stick-slip oscillations for increasing stiffness in the system.

Returning to the goal of this last part, i.e., analysis of the hunting phenomenon, it is clear that analysis tools originating from the field of nonlinear dynamics might reveal important aspects of the closed-loop dynamics. Moreover, due to the fact that the hunting phenomenon only arises in controlled systems and no equivalent dynamical representation of interest is known from the fields of nonlinear dynamics or tribology, little literature on the subject is present. However, important contributions from the control community on this problem are (i) an algebraic analysis performed for a friction model with static and Coulomb friction in [8] and (ii) the use of a Phase Plane Analysis tool for various frictional damping functions in [104]. Here, these results are extended for more complete friction models. Moreover, other analysis tools, such as the construction of bifurcation diagrams, are used to get a better

## 7.2 Outline of Part II

understanding of the phenomenon and the closed-loop dynamics.

## **7.2 Outline of Part II**

This part is organized as follows. With respect to the hunting phenomenon the dynamic LuGre friction model will be compared to the static Switch friction model in Chapter 8 using analysis tools originating from the field of nonlinear dynamics. In Chapter 9 for various frictional damping functions incorporated in the Switch friction model, bifurcation diagrams will numerically be computed for a varying controller gain using a Phase Plane Analysis tool called event mapping. In Chapter 10 experimentally observed friction induced limit cycles for a Linear Motion Motor System (LiMMS) will be analysed using the presented event mapping tool. Summarizing thoughts, concluding remarks and recommendations for future research on these stick-slip oscillations will be presented in the 'In Retrospect' chapter.

## Part II - Friction Induced Limit Cycling

## Chapter 8

# Friction Induced Hunting Limit Cycles: A Comparison between the LuGre and Switch Friction Model

### Abstract

In this chapter friction induced limit cycles are predicted for a simple motion system consisting of a PID controlled motor-driven inertia subjected to friction and a regulator task. The two friction models used, i.e., (i) the dynamic LuGre friction model and (ii) the static Switch friction model, are compared with respect to the so-called hunting phenomenon. Analysis tools originating from the field of nonlinear dynamics will be used to investigate the friction induced limit cycles. For a varying controller gain, stable and unstable periodic solutions are computed numerically which, together with the stability analysis of the closed-loop equilibrium points, result in a bifurcation diagram. Bifurcation analysis for both friction models indicates the disappearance of the hunting behaviour for controller gains larger than the gain corresponding to the cyclic fold bifurcation point.

---

This chapter is accepted for publication in *Automatica* [67]. A more elaborated version of this work can be found in [68]. The author is grateful to Dr. Remco Leine for his contribution to this chapter.

## 8.1 Introduction

In mechanical servo or tracking systems friction can severely limit the performance in terms of increasing tracking errors and the occurrence of limit cycles, i.e., periodic solutions of the nonlinear autonomous system. In particular, limit cycling is an undesirable phenomenon in controlled servo systems because of its oscillatory and persistent behaviour. Limit cycling can be caused by the combination of the difference in static and Coulomb friction and integral action in the control loop. A regulator task might end up in a stick-slip oscillation around the target position, which is called hunting [7].

To predict and simulate hunting in mechanical systems with friction, an appropriate friction model should possess (i) a drop of the friction force from a static friction level to a lower Coulomb friction level [8], [104] and (ii) a good stiction approximation since the dominant frictional contributor for hunting is stiction [7]. Here, the LuGre friction model [24] and the Switch friction model [84], both of which possess these properties, will be compared with respect to the hunting phenomenon, since we are interested in the computationally most efficient friction model that will describe the occurrence of closed-loop limit cycles.

The hunting cycle phenomenon has already been extensively studied in literature, see e.g. [7] for an overview. We will mention the papers that are most closely related to our work. In [46], a describing function analysis was performed based on the LuGre model, which resulted in only qualitative prediction of limit cycles. In [104], a phase plane analysis of the hunting behaviour was performed on the basis of various discontinuous friction models. Only stable periodic solutions were found in this way, whereas the equilibrium points were assumed to be stable. In [8], exact algebraic analysis based on a discontinuous friction model was performed and compared to describing function analysis for a PID controlled system. This paper states that the controlled system will always show a limit cycle if the static friction level has a discontinuous drop to a lower constant Coulomb friction level, which result is inadequate to practical observation where hand-tuned PID controllers indeed eliminate hunting.

The main objective of this chapter is to improve on the above results with respect to the following items.

- Quantitatively describe both stable and unstable limit cycles.
- Study the change in closed-loop dynamics as a function of control parameters.
- Use a continuous friction model instead of a discontinuous one, in particular, the LuGre and Switch model will be compared.

To reach this goal we will use analysis tools originating from nonlinear dynamics, such as bifurcation theory, shooting methods and path-following techniques [53]. These tools have already been used to study mechanical systems with friction ([35], [48], [84]), but not with respect to the hunting phenomenon. The advantage of this approach is that even for sophisticated friction models accurate prediction of limit cycles is obtained and information

## 8.2 Hunting

on local stability is provided. Furthermore, the possible disappearance of limit cycles for certain controller settings is indicated by the bifurcation diagram.

The outline of this chapter is as follows. In Section 8.2, we will give a description of the hunting phenomenon. A qualitative comparison with respect to hunting between the LuGre model and the Switch model will be given in Section 8.3. For both systems, stable and unstable branches of periodic solutions will be computed in Section 8.4, which together with the stability analysis of the equilibrium points will result in a bifurcation diagram. Section 8.5 will conclude this chapter.

## 8.2 Hunting

Consider a simple motion system model consisting of a motor-driven rotating inertia  $J$  subjected to friction, i.e.,  $J\ddot{\theta} = -F + c_m u$ , where  $\theta$  is the angle of rotation,  $F$  the friction torque,  $c_m$  the motor constant and  $u$  the input motor torque. For a regulator task, the desired angle  $\theta_d$  is constant in time. The use of a PD controller would lead to a steady state error due to the presence of friction. Therefore, a PID type controller will be used here with a fixed controller structure. The controller is composed of a proportional gain  $K$ , a derivative and an integral controller part, where only the controller gain  $K$  can be altered. In the time-domain the closed-loop system becomes

$$J\ddot{\theta} + c_m K \left[ \left(1 + \frac{\tau_d}{\tau_i}\right) (\theta - \theta_d) + \tau_d \dot{\theta} + \frac{1}{\tau_i} \int_0^t (\theta - \theta_d) d\tau \right] = -F, \quad (8.1)$$

where  $\tau_i$  determines the integral part and  $\tau_d$  the derivative controller part. In the sequel of this chapter the following fixed controller shape will be utilized, i.e.,  $\tau_i = \tau_d = \frac{1}{2\pi}$ .

For an experimental motion system which can be modeled by Eq. (8.1), the fixed controller is used for a regulator task with  $\theta_d = 1$  [rad] and  $K = 0.04$ . In Figure 8.1, the measured angular displacement  $\theta$ , angular velocity  $\dot{\theta}$ , integral term  $\int_0^t (\theta - \theta_d) d\tau$  and applied control effort  $u$  are depicted. The response of the system has entered a hunting behaviour and will not reach the desired angular position. However, the stick-slip oscillation does not become stationary, since its amplitude and frequency varies with time, which is due to the systems time varying, direction and position dependent frictional behaviour.

Throughout the chapter, the states of the closed-loop system are defined as

$$x_1 = \theta - \theta_d, \quad x_2 = \dot{\theta}, \quad x_3 = \int_0^t x_1 d\tau.$$

## 8.3 Comparison of Friction Models

In the past decade, the interest in dynamic friction models increased and resulted in a number of dynamic friction models based on the Dahl model [33]. The LuGre model [24] is such a

## Part II - Friction Induced Limit Cycling

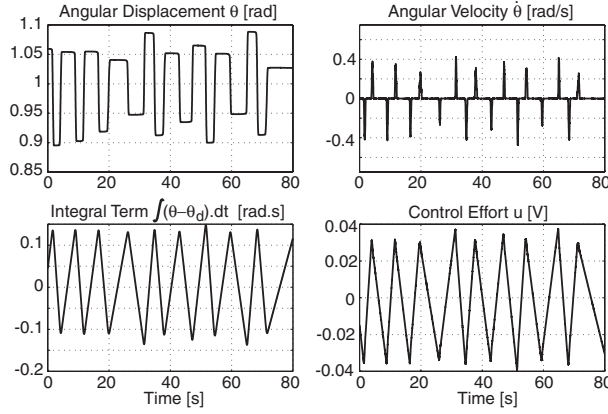


Figure 8.1 - Hunting behaviour of experimental setup.

dynamic friction model and exhibits a rich behaviour of friction phenomena, e.g., presliding displacement, frictional lag and varying break-away force, which have all been observed in practice. Here, the LuGre model will be used to predict and simulate hunting limit cycles. The friction force is described as

$$F = \sigma_0 z + \sigma_1 \frac{dz}{dt} + \sigma_2 x_2 \quad \text{and} \quad \frac{dz}{dt} = x_2 - \frac{|x_2|}{g(x_2)} z \quad (8.2)$$

where  $z$  is an extra state representing the average microscopic deflection of the so-called bristles located between the two sliding surfaces,  $x_2$  the relative velocity between the moving parts,  $g(x_2) = F_c + (F_s - F_c) \exp(-(\frac{x_2}{v_s})^2)$  the Stribeck curve,  $\sigma_0$  the stiffness of the bristles,  $\sigma_1$  the damping of the bristles,  $\sigma_2$  the viscous friction coefficient and  $v_s$  the Stribeck velocity. The autonomous system consisting of the model Eq. (8.1) and the friction model Eq. (8.2) can be written as a set of continuous non-smooth stiff differential equations, i.e.,

$$\begin{aligned} \dot{\underline{x}} &= f_{LuGre}(\underline{x}) \\ &= \begin{bmatrix} x_2 \\ -\frac{2Kc_m}{J}x_1 - (\frac{Kc_m}{2\pi J} + \frac{\sigma_2 + \sigma_1}{J})x_2 - \frac{2\pi Kc_m}{J}x_3 - \frac{\sigma_0}{J}(1 - \frac{\sigma_1|x_2|}{g(x_2)})x_4 \\ x_1 \\ x_2 - \sigma_0 \frac{|x_2|}{g(x_2)}x_4 \end{bmatrix} \end{aligned}$$

where  $x_4 = z$  and  $\underline{x} = [x_1 \ x_2 \ x_3 \ x_4]^T$ .

In contrast to the dynamic friction model mentioned above, the Switch model [84] is a static friction model that can be considered as a modified version of the Karnopp model [79]. The idea is to approximate the friction force during stiction as a set-valued function at  $x_2 = 0$ :

$$F(x_2, c_m u) = \begin{cases} g(x_2) \text{sgn}(x_2), & \forall x_2 \neq 0 \quad \text{Slip} \\ \min(|c_m u|, F_s) \text{sgn}(u), & \forall x_2 = 0 \quad \text{Stick} \end{cases}$$

### 8.3 Comparison of Friction Models

where  $u$  is the applied control effort,  $F_s$  is the static friction and  $g(x_2)$  is the same Stribeck curve as used in the LuGre model. The state equation, describing the closed-loop system, reads

$$\dot{\underline{x}} = f_{Switch}(\underline{x}) = \begin{bmatrix} x_2 \\ c_m u - F(x_2, c_m u) \\ x_1 \end{bmatrix}$$

where the control effort  $u = -K(2x_1 + \frac{1}{2\pi}x_2 + 2\pi x_3)$  and  $\underline{x} = [x_1 \ x_2 \ x_3]^T$ . As for the Karnopp friction model, a narrow band  $\eta$  around zero velocity is introduced to numerically integrate the system of equations of the Switch model. The model distinguishes three situations: (i) the slip phase, (ii) the stick phase and (iii) the transition phase, which are described by ordinary differential equations (ODEs). The transition phase describes the transition from stick to slip or velocity reversals without stiction. In the stick phase, the acceleration of the mass is set to  $-\alpha x_2$  and forces the velocity  $x_2$  to zero for  $\alpha > 0$ . This acceleration term ensures that the ODE belonging to the stick phase does not suffer from numerical instabilities as in the Karnopp friction model.

The identification of the friction models is not the subject of this chapter. However, it is very important to identify the various friction parameters accurately to obtain good quantitative predictions. To compare both models in terms of the hunting behaviour, the same regulator task  $\theta_d = 1$  [rad] as given in Figure 8.1 is considered. The closed-loop responses for both models end up in a hunting limit cycle, see Figure 8.2. Contrary to the time varying hunting behaviour of the experimental setup the predicted limit cycles are symmetric and the closed-loop dynamics is time invariant. Therefore, a good comparison with experimental data is difficult. However, one approximately symmetric period of the experiment response, i.e., from  $\pm 55$  [sec] to  $\pm 65$  [sec], is shown also in Figure 8.2. The phase portrait of the first three

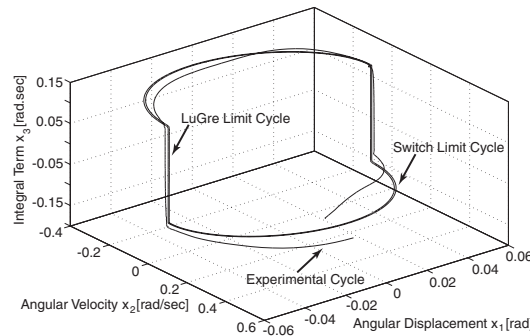


Figure 8.2 - Hunting limit cycle.

states of this experimental hunting cycle is compared with (i) the LuGre closed-loop system and (ii) the Switch closed-loop system. The experimentally observed cycle can be predicted with reasonable accuracy by both models; the difference between the two predicted cycles is negligible. The LuGre model adds apparently no extra frictional behaviour essential to the



hunting phenomenon. The LuGre closed-loop system has an extra state in comparison with the Switch closed-loop system and the numerical stiffness of the LuGre closed-loop system is considerably larger. To evaluate the Switch model, the integration process is halted on the transition between different phases of the system, the discontinuity is found by an iterative process and the integration is restarted. In our experience the Switch model is computationally more efficient.

## 8.4 Bifurcation Diagram

In this section, first the equilibria of the two different closed-loop systems will be determined and the local stability will be analysed. Secondly, periodic solutions will be sought and path-following techniques will be used to construct a bifurcation diagram. The system parameters used to perform these analyses are given in Table 8.1. The controller gain  $K$  is the closed-

$J = 0.026$ [kg·m <sup>2</sup> ]	$\sigma_2 = 0.1$ [N·m·s/rad]
$c_m = 16$ [N·m/V]	$\eta = 1e-6$ [rad/s]
$F_s = 0.53$ [N·m]	$\alpha = 10$ [1/s]
$F_c = 0.44$ [N·m]	$\sigma_0 = 2.2e+4$ [N·m/rad]
$v_s = 0.02$ [rad/s]	$\sigma_1 = 7.58$ [N·m·s/rad]

Table 8.1 - Closed-loop system parameters.

loop system parameter to be changed and is initialized corresponding to the Routh-Hurwitz stability criterion for the linear system without friction, i.e.,  $K > \frac{J}{c_m \tau_d (\tau_d + \tau_i)} = 0.0321$ . The hunting limit cycles will be characterized by the maximal angular displacement, i.e.,  $\max |x_1(t)| \forall 0 \leq t \leq T$  where  $T$  is the period time.

### 8.4.1 Equilibria and local stability

The equilibrium points of autonomous systems satisfy the condition  $\dot{\underline{x}} = f(\underline{x}) = 0$ . It is important to realize that the equilibrium points of interest are those for which the position error  $x_1$  and velocity error  $x_2$  are zero. The integral term  $x_3$  for either model and, additionally for the LuGre model, the bristle deflection  $x_4$  should not necessarily be zero, since it involves a regulator task. Hence, the local stability of the set of equilibrium points is of interest rather than the equilibrium points itself.

The equilibrium points of interest for the LuGre system are located on a line, i.e.,

$$\underline{x}_{LuGre}^* = \beta \left[ 0 \ 0 \ -\frac{\sigma_0}{K 2\pi c_m} \ 1 \right]^T,$$

where  $|\beta| \leq \frac{F_s}{\sigma_0}$  if the initial state  $|x_4(0)| \leq \frac{F_s}{\sigma_0}$  [24]. This invariant set means that the force produced from a non-zero bristle deflection is compensated by the integral action. Here, the

## 8.4 Bifurcation Diagram

local stability of the set of equilibrium points is tested by investigation of the eigenvalues of the corresponding Jacobian matrix. However due to the non-smoothness of the LuGre model, i.e., the absolute value  $|x_2|$  in the differential equations, the derivation of the corresponding Jacobian matrix needs special attention. The notion of *generalized differentials* [29] is essential and states that the *generalized derivative* of  $f$  at  $x$  is declared as *any* value  $f'_q(x)$  included between its left  $f'_-$  and right  $f'_+$  derivatives, where  $f'_q(x) = (1 - q)f'_- + qf'_+$ ,  $0 \leq q \leq 1$ . The closed convex hull of the derivative extremes is called the *generalized differential* of  $f$  at  $x$ . Now, the generalized differential of the vector field  $f_{LuGre}(\underline{x})$  with respect to  $\underline{x}$  can be regarded as the generalized Jacobian  $\tilde{J}_q = (1 - q)J_- + qJ_+$ ,  $0 \leq q \leq 1$ , where  $J_-$  and  $J_+$  are respectively the Jacobian matrices from left and right with respect to  $x_{2,LuGre}^* = 0$  at  $\underline{x}_{LuGre}^*$ . Hence, the generalized Jacobian in  $\underline{x}_{LuGre}^*$ , which is a 4 by 4 matrix where the system parameters from Table 8.1 are used, depends on controller gain  $K$ , convexity parameter  $q$  and  $\beta$ . For all  $\beta$ ,  $K > 0.0321$  and  $0 \leq q \leq 1$  one eigenvalue of the generalized Jacobian is equal to zero which corresponds to the invariant eigenvector. This invariant eigenvector is locally stable if the remaining three non-zero eigenvalues are in the open left-half plane and is satisfied for  $|\beta| \leq \frac{F_s}{\sigma_0}$  if (i) all system parameters are larger than zero and (ii) a sufficient condition  $\frac{\sigma_2}{J} > \pi$  holds. Both conditions, which can be constructed from the Routh-Hurwitz criterion, are satisfied as shown in Table 8.1 and indicates that the set of equilibrium points are locally stable for  $|\beta| \leq \frac{F_s}{\sigma_0}$ . This local stability analysis seems inconclusive for the boundary points of the equilibrium set, i.e.,  $\beta = \pm \frac{F_s}{\sigma_0}$ , since a perturbation along the eigenvector outside this set might enter locally unstable dynamics. However, due to the upper bound on the state  $x_4$  of the original nonlinear system, i.e.,  $|x_4(t)| \leq \frac{F_s}{\sigma_0} \forall t$ , these perturbations are impossible and therefore the set of equilibrium points are locally stable for all  $K > 0.0321$ .

The equilibrium points for the autonomous system concerning the Switch model are located on the line

$$\underline{x}_{Switch}^* = \gamma [0 \ 0 \ 1]^T, \quad \forall |\gamma| < \frac{F_s}{K c_m 2\pi}.$$

Again an invariant direction where the applied control effort  $u = K c_m 2\pi x_3^*$  is compensated by an equivalent portion of the static friction  $F_s$  and results in exactly the same equilibrium points as for the first three states of the LuGre closed-loop system. The local stability of such an invariant set is not trivial for this discontinuous system of Filippov-type [43]. However, the local stability of the equilibria for the Switch model will be investigated by examination of the bifurcation diagram in combination with numerical simulations.

### 8.4.2 Periodic solutions and Floquet multipliers

Hunting limit cycles, as given in Figure 8.2, can be regarded as a fixed point of a Poincaré map  $P$  on a Poincaré section. For the Switch closed-loop system, a Poincaré section might be the plane  $x_1 = 0$  in Figure 8.2. The stability of a periodic solution is determined by its *Floquet multipliers*  $\lambda_i$  ( $i = 1, \dots, n$ ), which are the eigenvalues of the fundamental solution matrix  $\Phi(t_0 + T, t_0)$  [53], where  $T$  is the period time of the solution. For the autonomous

systems considered here, a perturbation along the solution will give the same, however time-shifted, periodic solution. This means that one of the *Floquet multipliers* equals unity. If one or more *Floquet multipliers* lie outside the unit circle, then the periodic solution is unstable. The periodic solution, as well as its *Floquet multipliers*, changes as a parameter of the closed-loop system, e.g., the controller gain  $K$ , is altered. The limit cycle changes from stable to unstable or vice versa when a Floquet multiplier passes through the unit circle. For smooth systems, the fundamental solution matrix  $\underline{\Phi}(t_0 + T, t_0)$ , which is also known as the monodromy matrix  $\underline{\Phi}_T$  after one period time  $T$ , can be computed by solving the *variational equation* [100]. Here, the models used are non-smooth and the *variational equation* is not applicable as demonstrated by [84], [86]. Hence, the monodromy matrix is obtained by a sensitivity analysis [84] and either stable or unstable periodic solutions are found with a (single) shooting method [100]. The shooting method is used in a path-following algorithm [42] to investigate the influence of a parameter of the closed-loop system on the periodic solution.

For the LuGre closed-loop system, the path-following is started on the stable branch for  $K = 0.0321$  and terminated on the unstable branch at  $K = 0.615$ . The main interest is the bifurcation point that is given by the intersection of the stable and unstable branch at  $K = 0.620$  as depicted in the inset of the upper plot of Figure 8.3, where stable branches are depicted with solid lines (-) and unstable branches with dashed lines (- -). In the upper plot, the locally stable set of equilibrium points is shown by the solid line for the branch  $x_1 = 0$ . Investigation of this bifurcation diagram shows locally stable equilibrium points

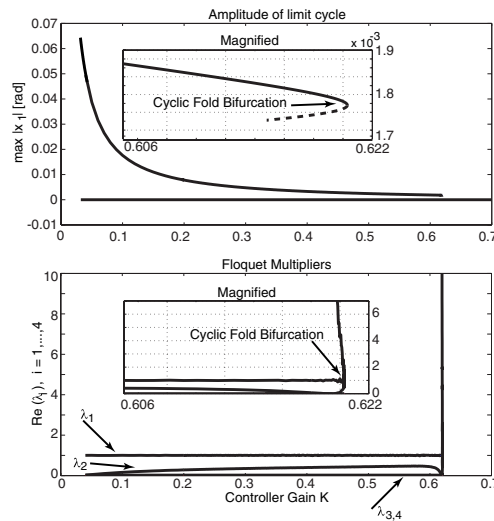


Figure 8.3 - Bifurcation diagram for the LuGre system as a function of the controller gain.

$|x_1| = 0$  together with locally stable periodic solutions for controller gains smaller than the bifurcation point. This might give raise to an expected unstable branch in between as

## 8.4 Bifurcation Diagram

initiated from the bifurcation point  $K = 0.620$  downwards to  $K = 0.615$  as depicted in the magnified inset of the bifurcation diagram with the dashed line. In the lower plot of Figure 8.3 the *Floquet multipliers*  $\lambda_i$ ,  $i = 1, \dots, 4$  are shown, where all multipliers are on the real axis. Floquet multiplier  $\lambda_1$  is equal to one due to the freedom to shift the phase of the limit cycles. Two multipliers are close to zero and one multiplier  $\lambda_2$  varies as the controller gain  $K$  changes. The Floquet multiplier  $\lambda_2$  predicts a bifurcation point since it passes the value  $+1$  at  $K = 0.620$ , which together with the fact that the stable branch folds into an unstable branch, results in a so-called cyclic fold bifurcation point [42]. To give an impression of the possible solutions for a fixed controller gain  $K$ , the equilibrium points, stable and unstable limit cycles for the LuGre system with  $K = 0.615$  are shown in Figure 8.4, where only the first three states are plotted to visualize the cycles.

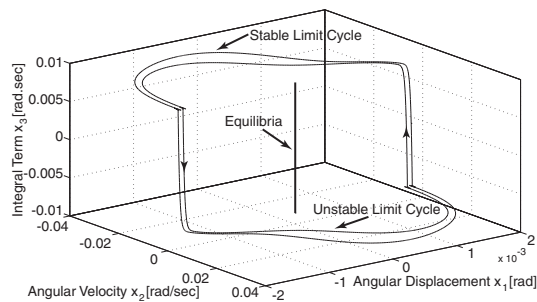


Figure 8.4 - Stable and unstable limit cycles for  $K = 0.615$ .

Secondly, the bifurcation diagram for the Switch closed-loop system is constructed. In the upper plot of Figure 8.5, the stable and unstable branches are shown for the amplitude of the periodic solutions. The path-following algorithm is again started on the stable branch at  $K = 0.0321$  and terminated at the unstable branch at  $K = 0.634$ . However, for  $K = \{0.0321, 0.2, 0.4, 0.6\}$  the unstable periodic solutions are computed by a single shooting method and depicted by circles. The autonomous system is of order  $n = 3$  and therefore the number of *Floquet multipliers* is 3 where one should be equal to unity corresponding the phase shift. The *Floquet multipliers*, which are all on the real axis, are depicted in the lower plot of Figure 8.5, where indeed one Floquet multiplier  $\lambda_1$  is equal to unity. One multiplier  $\lambda_3$  is equal to zero and  $\lambda_2$  varies as the gain is altered and passes through the value  $+1$  for  $K = 0.647$ , which again detects a cyclic fold continuous bifurcation. The equilibrium points, stable and unstable limit cycles for  $K = 0.634$  are depicted in Figure 8.6. The region of attraction of the equilibrium points in  $x_1$ -direction is bounded by the amplitude of the unstable periodic solution, i.e., in simulation all trajectories starting in the stick plane and  $|x_1| < \max |x_1^{unstable}(t)|$  appear to end up in the equilibrium set. Hence, the branch  $x_1 = 0$  in the bifurcation diagram of Figure 8.5 is expected to be locally stable for perturbations in  $x_1$ -direction.

## Part II - Friction Induced Limit Cycling

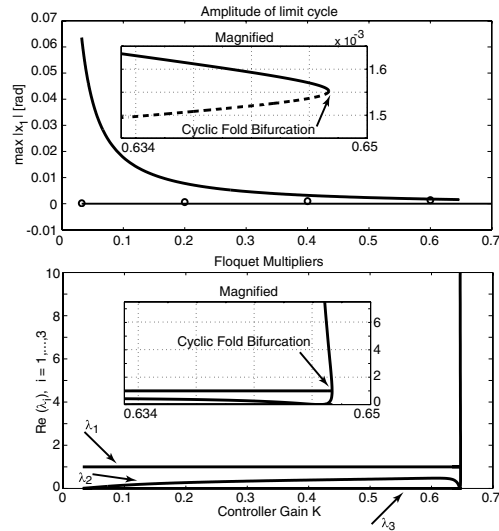


Figure 8.5 - Bifurcation diagram for the Switch system as a function of the controller gain.

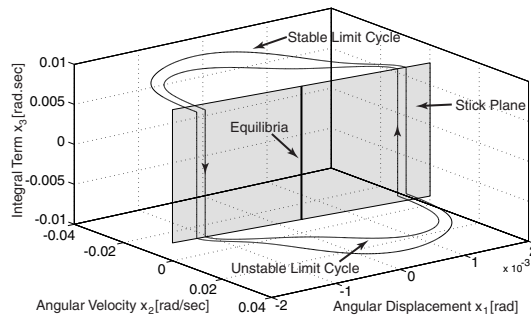


Figure 8.6 - Stable and unstable limit cycles for  $K = 0.634$ .

In the vicinity of the periodic solutions the nonlinear dynamics for both systems appear to depend only on the second *Floquet multiplier*, since this multiplier varies only its value for a varying controller gain  $K$ . For the Switch system, this is due to the fact that state perturbations  $\underline{x}(t) + \delta \underline{x}$  in the slip phase reduce in the stick phase to a  $x_1, x_3$  perturbation and *not* in  $x_2$ -direction. Furthermore, the perturbation in  $x_3$ -direction turns into a phase shift and is therefore not interesting for the dynamics. Moreover, this is not only locally valid around the periodic solutions but for all trajectories that enter the stick phase. Hence, the complex dynamics of this three-dimensional, autonomous, discontinuous Switch system might be described by means of an equivalent one-dimensional map as demonstrated in [104], [48].

## 8.5 Conclusions

The path-following techniques has been halted on the unstable branch due to the computationally expensive shooting method for unstable systems. For the Switch system, the unstable branch is extended by searching intermediate unstable periodic solutions, since only good initial estimates on the state  $x_1$  and period time  $T$  are needed. This is more difficult for the LuGre system due to the necessary good estimates on the entire state (dimension 4) and period time.

## 8.5 Conclusions

The numerical analysis of friction induced limit cycles presented in this chapter shows the disappearance of limit cycles for certain system parameters. The tools used enable us to follow branches of stable and unstable periodic solutions. Together with the stability analysis of the equilibrium points, bifurcation diagrams are constructed for both the static Switch friction model and the dynamic LuGre friction model. The resulting diagrams are both qualitatively and quantitatively very much alike, where for both systems cyclic fold bifurcation points are found for varying controller gain. The location of the bifurcation point is almost the same and the underlying dynamics of the two systems are comparable, since the *Floquet multipliers*  $\lambda_2^{Switch}$ ,  $\lambda_2^{LuGre}$  for the periodic solutions, show similar behaviour as a function of the control parameter  $K$ . With respect to the equilibrium points of the autonomous system, which include the desired position of the regulator task, it is noticed that for both models these are identical (for the first three states) even for varying model parameters. Furthermore, the differences in the limit cycles between the LuGre system and the Switch system, as depicted in Figures 8.2, 8.4, 8.5, are small and the cycles are approximately the same. The major difference between the two friction models is the extra state representing the averaged bristle deflection for the dynamic LuGre model. This extra state models the pure stick phase in the Switch model as a presliding regime with finite stiffness for the luGre model and describes frictional lag for small velocities, i.e.,  $|x_2| < v_s$ . The differences between the two friction models due to this extra state are not essential to describe the hunting behaviour properly. Hence, the Switch closed-loop system with its lower order and lower stiffness is favorable from a computational point of view and is more easy to visualize and interpret.

## Part II - Friction Induced Limit Cycling

## Chapter 9

# Friction Induced Hunting Limit Cycles: An Event Mapping Approach

### Abstract

This chapter studies the occurrence of limit cycles for a simple PID controlled motion system subjected to two different types of static frictional damping functions, i.e., (i) a Coulomb friction level plus a discontinuous rise to a larger maximum static friction level and (ii) Stribeck friction curves with a continuous drop from the maximum static friction level to the lower Coulomb friction level. The two types of friction characteristics are compared with respect to the so-called hunting phenomenon by means of an event mapping technique. The closed-loop nonlinear discontinuous dynamics are reduced to a numerically computed one-dimensional event map, which enables us to predict both stable and unstable limit cycles together with the local stability property of the equilibrium points. In addition, the set of the equilibrium points is studied analytically resulting in sufficient conditions on its local stability. For the different types of static frictional damping functions the combined numerical and analytic study results in a classification with respect to the ability to predict coexistence of stable and unstable hunting limit cycles, which shows that minor changes in the friction model might cause severe changes to the closed-loop nonlinear dynamics in terms of existing periodic solutions.

---

This chapter is in preparation for publication [69]. The developed Event Mapping Tool used in this chapter is documented in [93].



## 9.1 Introduction

In general, mechanical systems exhibit friction. A negative manifest of friction is a degeneration of performance in terms of increasing tracking errors and friction induced limit cycling, i.e., periodic solutions of a nonlinear autonomous system, for instance of a servo system. Due to its oscillatory and persistent behaviour, limit cycling is an undesirable phenomenon in controlled servo systems. Here, a friction induced phenomenon called hunting [7] is considered, which is mainly caused by the combination of a difference in the static friction level and the Coulomb friction and an integral action in the control loop for a simple regulator task. The friction induced hunting limit cycle results in a sequence of stick-slip oscillations around the desired position.

The research on friction induced stick-slip oscillations has been extensive over the past decades [7], [8], [46], [48], [49], [67], [86], [95], [104]. Friction induced limit cycles have been analysed in literature with different techniques and various results, e.g., the Describing Function Analysis (DFA) [7], [8], [46] was widely used but resulted only in qualitative prediction and even these were often found to be incorrect [8], [118]. Other important analysis tools are (i) Phase Plane Analysis (PPA) [48], [104], (ii) exact algebraic analysis [8], [95] and (iii) analysis tools originating from nonlinear dynamics [53], [67], [86]. The latter seems to be the most powerful due to the ability to deal with nonlinearities in the friction model, however are mainly based on expensive numerical investigation of the closed-loop system.

For the hunting phenomenon, Hensen et al. [67] compares two nonlinear friction models, i.e., the dynamic LuGre friction model [24] and the static Switch friction model [84], resulting in similar hunting behaviour of the nonlinear closed-loop dynamics. In [67], a numerically constructed bifurcation diagram predicts for both models a disappearance of the hunting limit cycles for certain controller settings which is conform the practically observed behaviour, where properly tuned industrial controllers indeed prevent stick-slip oscillations. In contrast to these results is the exact algebraic analysis by [8] for a PID controlled simple mass system in the presence of static friction and a lower Coulomb friction level. Using this friction model with a discontinuous jump in the friction level the authors state that the controlled system will exhibit a frictional limit cycle for all stabilizing controllers. The major difference between this idealized friction model and the static Switch friction model used in [67] is the shape of the friction curve for non-zero velocities, which expresses the so-called Stribeck friction. Radcliffe et al. [104] uses a Phase Plane Analysis tool to analyse and compare the hunting behaviour of the closed-loop dynamics for different frictional damping functions. For friction models with a larger static friction level than the Coulomb friction level only stable limit cycles are found for the investigated parameter set. The possibility of co-existing unstable limit cycles is not addressed and the performed stability analysis of the set of equilibrium points is far from complete.

## 9.2 The Closed-loop System

So, this chapter aims at improving these earlier results with respect to the following issues:

- come to a better understanding of the fundamental differences found between the exact algebraic results of [8] and the numerically computed results found by bifurcation analysis in [67].
- extend the exact algebraic results of [8] to study the local stability of the set of equilibrium points for more realistic friction models, i.e., nonlinear frictional damping functions which are capable of modeling Stribeck friction.

For this purpose, the focus in this chapter will be on the influence of the shape of the friction curve on the dynamic properties of the closed-loop system, i.e., stability of equilibrium points, types of periodic solutions and the possibility to predict the disappearance of the hunting phenomenon. Here, various friction characteristics, i.e., (i) a friction curve with a discontinuous drop in the friction level and (ii) friction curves with a continuous drop in the friction level, will be integrated in the Switch friction model [67], [86]. The resulting nonlinear closed-loop dynamics will be analysed by means of an *event mapping* technique [48], which is a Phase Plane Analysis similar to the one used in [104]. This one-dimensional mapping technique will be used to construct a so-called *event map* of the nonlinear closed-loop dynamics, which will give insight into the location, stability and attractor basin of periodic solutions and equilibrium set. However, analytic construction of this *event map* is not possible due to the use of nonlinear frictional damping functions and therefore numerical simulations will be used to construct the *event map*. Moreover, the numerical stability analysis of the equilibrium points will be supported by an exact algebraic analysis similar to the one presented in [8].

The outline of this chapter is as follows. A description of the closed-loop system, i.e., a simple PID controlled mass system subjected to friction, will be given in Section 9.2 together with the various friction characteristics under consideration and friction model used. For the various damping characteristics, a classification will be derived with respect to the local stability of the equilibrium set in Section 9.3. In Section 9.4, the construction of the equivalent one-dimensional map of the nonlinear discontinuous three-dimensional autonomous dynamic system will be discussed. The numerical results on the location of the limit cycles, both stable and unstable, together with their regimes of attraction will be given in Section 9.5 for the various friction curves. The chapter will be concluded in Section 9.6.

## 9.2 The Closed-loop System

For mechanical positioning systems, often modeled as a simple motor-driven mass system subjected to friction as shown in Figure 9.1, an important control problem is the regulator task, where due to a static friction level an integral action in the control loop is necessary to eliminate steady state errors. Hence, the simplest model of the closed-loop system reads as follows

$$m\ddot{q} + P(q + D\dot{q} + I \int_0^t q(\tau) d\tau) = -F$$

## Part II - Friction Induced Limit Cycling

where  $q$  is the position of the system,  $F$  the friction force,  $m$  the mass of the system to be controlled and  $P$ ,  $I$ ,  $D$  the controller parameters. For certain frictional damping functions

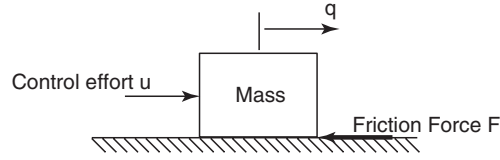


Figure 9.1 - Simple mass system subjected to friction.

and PID controller settings a limit cycle will exist around  $q = 0$ , which is called hunting [7].

To generate or simulate friction induced hunting limit cycles essential components in the closed-loop dynamics are:

- integral control,
- good stiction properties of the friction model, i.e., in the stick phase the sum of the external forces on the mass system are completely compensated for by an equivalent friction force and
- a frictional damping function with a larger static friction level than the Coulomb friction level [8], [67], [104], i.e., either a continuous or discontinuous drop in the friction force for non-zero velocity.

An applicable friction model to simulate stick-slip oscillations, like the hunting phenomenon, is the discontinuous Switch friction model as demonstrated in [67], [84]. The Switch model [84] is a static friction model that can be considered as a modified version of the Karnopp model [79]. The idea is to model the friction force as a set-valued function at  $\dot{q} = 0$ . The friction force is defined as

$$F(\dot{q}, u) = \begin{cases} g(\dot{q})\text{sgn}(\dot{q}) + b\dot{q}, & \forall \dot{q} \neq 0 \quad \text{Slip} \\ \min(|u|, F_s)\text{sgn}(u), & \forall \dot{q} = 0 \quad \text{Stick} \end{cases} \quad (9.1)$$

where  $u = -P(q + D\dot{q} + I \int_0^t q(\tau)d\tau)$  is the applied control effort,  $F_s$  is the maximum static friction at zero velocity,  $g(\dot{q})$  is the frictional damping curve for velocities unequal to zero and  $b$  is the viscous damping. The equation of motion for this model, describing the closed-loop system, reads

$$\begin{aligned} \dot{\underline{x}} &= f_{\text{Switch}}(\underline{x}) \\ &= \begin{bmatrix} x_2 \\ -\frac{P}{m}(x_1 + Dx_2 + Ix_3) - \frac{1}{m}F(x_2, u) \\ x_1 \end{bmatrix} \end{aligned} \quad (9.2)$$

where  $\underline{x} = [x_1 \ x_2 \ x_3]^T = [q \ \dot{q} \ \int_0^t q(\tau)d\tau]^T$  and the control effort  $u = -P(x_1 + Dx_2 + Ix_3)$ . The existence of solution of this Filippov-type of system [43] of Eq. (9.2) is not trivial and

## 9.2 The Closed-loop System

therefore the uniqueness of solution is also questionable. In [85] it is shown that for this system a solution of the differential inclusion, corresponding to the second state equation, i.e.,

$$m\dot{x}_2 \in F_{Switch}(\underline{x}) = \begin{cases} u - g(x_2) - bx_2, & x_2 > 0 \\ u + [-F_s, F_s], & x_2 = 0 \\ u + g(x_2) - bx_2, & x_2 < 0 \end{cases} \quad (9.3)$$

exists if the set-valued function  $F_{Switch}(\underline{x})$  is upper semi-continuous, closed, convex and bounded for all  $\underline{x} \in \mathbb{R}^3$ . To analyse the existence and the uniqueness of the solution of the differential inclusion Eq. (9.3), a choice for the frictional damping function  $g(x_2)$  has to be made. Here, two types of friction characteristics will be considered: (i) a frictional damping function with a discontinuous stick-slip transition and (ii) frictional damping functions with continuous stick-slip transitions. The frictional damping curves are described as follows:

- frictional damping functions with continuous stick-slip transitions, i.e.,  $g(x_2) = F_c + (F_s - F_c) \exp(-|x_2/v_s|^\beta)$  and
- a frictional damping function with discontinuous stick-slip transitions, i.e.,  $g(x_2) = F_c$ ,

where  $F_s$  is the static friction level,  $F_c$  the Coulomb friction level,  $v_s$  is the so-called Stribeck velocity and  $\beta$  determines the shape of the friction curve for velocities unequal to zero. Examples of these friction models are given in Figure 9.2. For the damping curves

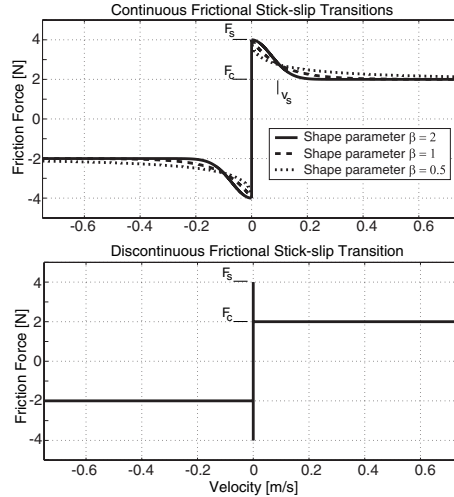


Figure 9.2 - Frictional damping characteristics with continuous and discontinuous stick-slip transitions.

with continuous transition from stick to slip the solution of the differential inclusion Eq. (9.3) exists since  $F_{Switch}(\underline{x})$  is upper semi-continuous, non-empty, closed, convex and bounded. The set  $[-F_s, F_s]$  at  $x_2 = 0$ , depicted by the solid black vertical line in the upper

plot of Figure 9.3, is the smallest closed convex set that contains the left and right limits of  $F_{Switch}(\underline{x})$  to  $x_2 = 0$ , which are shown by the arrows. Graphically this means that for the entire set  $[-F_s, F_s]$  at  $x_2 = 0$ , the left and right limits of  $F_{Switch}(\underline{x})$  to  $x_2 = 0$  should point towards this set, which is clearly satisfied. Hence, for these damping functions with

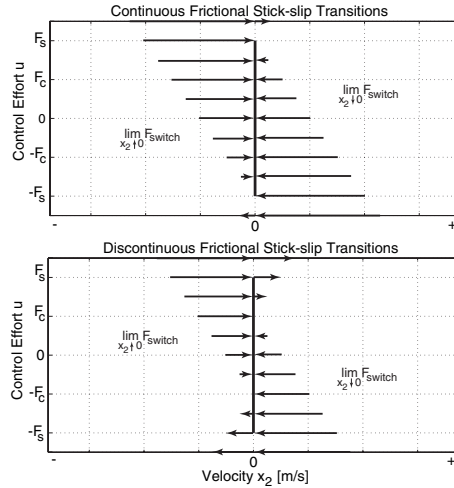


Figure 9.3 - Attraction and repulsion sliding modes for different frictional damping characteristics.

continuous stick-slip transitions, as shown in the figure, an attraction sliding mode [85] at  $x_2 = 0$  exists, since if  $-F_s \leq u \leq F_s$ , then  $\dot{x}_2 < 0$  for  $x_2 > 0$  and  $\dot{x}_2 > 0$  for  $x_2 < 0$ . Moreover, at  $x_2 = 0$  a transversal intersection exists if  $|u| > F_s$ . Therefore, a repulsion sliding mode [85] is not possible for these damping curves with continuous drop in the friction force and therefore uniqueness of the solution of the differential inclusion of Eq. (9.3) and the equation of motion of Eq. (9.2) is ensured. However, for the discontinuous stick-slip transition of the friction force with  $F_c < F_s$  there exist a repulsion sliding mode for  $F_c < |u| < F_s$ , as depicted in the lower plot of Figure 9.3, since the set  $[-F_s, F_s]$  at  $x_2 = 0$ , which is again shown by the solid black vertical line, is **not** the smallest closed convex set that contains the left and right limits of  $F_{Switch}(\underline{x})$  to  $x_2 = 0$ . Only on the smaller closed set  $[-F_c, F_c]$  at  $x_2 = 0$  the left and right limits of  $F_{Switch}(\underline{x})$  to  $x_2 = 0$ , which are shown again by the arrows, point both towards the set. For example, if  $F_c < u < F_s$ , then  $\dot{x}_2 > 0$  for  $x_2 \neq 0$  but  $m\dot{x}_2 = 0 \in u + [-F_s, F_s]$  and consequently with initial condition  $x_2(0) = 0$  has two possible solutions, i.e., one where the solution stays on the hyper-surface with  $x_2 = 0$  and one where the solution enters the slip phase immediately. Hence, if  $F_c < |u| < F_s$  the solutions for this model type are not unique.

Like the Karnopp friction model, a narrow band  $\eta \ll 1$  around zero velocity is introduced to numerically integrate the system of equations of the Switch model. Due to this narrow stick band the model distinguishes three situations: (i) the slip phase, (ii) the stick phase and (iii)

### 9.3 Local stability of equilibrium points

the transition phase, which all will be described by ordinary differential equations (ODEs). The transition phase describes the transition from stick to slip or velocity reversals without stiction. In contrast to the Karnopp model is the acceleration of the mass set to  $-\alpha x_2$  in the stick phase for the Switch model and forces the velocity  $x_2$  to zero for  $\alpha > 0$ . This acceleration term ensures that the ODE belonging to the stick phase does not suffer from numerical instabilities as in the Karnopp friction model. The three different ODEs for the different phases are implemented with the following pseudo code [84]:

**if**  $|x_2| > \eta$  **then**

$$\dot{\underline{x}} = \begin{bmatrix} x_2 \\ -\frac{P}{m}(x_1 + Dx_2 + Ix_3) - \frac{1}{m}(g(x_2)\text{sgn}(x_2) + bx_2) \\ x_1 \end{bmatrix}$$

**elseif**  $|u| > F_s$

$$\dot{\underline{x}} = \begin{bmatrix} x_2 \\ -\frac{P}{m}(x_1 + Dx_2 + Ix_3) - \frac{1}{m}F_s\text{sgn}(u) \\ x_1 \end{bmatrix}$$

**else**

$$\dot{\underline{x}} = \begin{bmatrix} 0 \\ -\alpha x_2 \\ x_1 \end{bmatrix}$$

**end**

where  $u = -P(x_1 + Dx_2 + Ix_3)$ . Due to this modification, even the friction curve with discontinuous stick-slip transition can be implemented without the problem of uniqueness of solution, since the solution in the stick phase can only leave the stick phase as  $|u| > F_s$ . From a mechanical point of view, this seems to be the desirable concept of friction.

### 9.3 Local stability of equilibrium points

The equilibrium points of the autonomous system, as described in Eq. (9.2), satisfy the condition  $\dot{\underline{x}} = f_{Switch}(\underline{x}) = 0$ . As a consequence of Eq. (9.2),  $x_1$  and  $x_2$  should be zero, which means that the closed-loop system is in the stick phase and therefore  $|x_3| \leq \frac{F_s}{PI}$ . Since it involves a regulator task, it is important to realize that the equilibrium points of interest are indeed those for which the position error  $x_1$  and velocity error  $x_2$  are zero. The integral term  $x_3$  should not necessarily be zero. Hence, the set of equilibrium points are located on the line

$$\underline{x}^* = \gamma [0 \ 0 \ 1]^T, \quad \forall |\gamma| \leq \frac{F_s}{PI}.$$

For the equilibrium points, the applied control effort  $u = -PIx_3^*$  is compensated by an equivalent portion of the static friction  $F_s$ . The local stability of such a set of equilibrium

## Part II - Friction Induced Limit Cycling

points on a line is not trivial. Here, the results presented by [8], which are obtained with an exact algebraic analysis of the same closed-loop system, are used to analyse the equilibrium set. With respect to the ability to promote hunting limit cycling [8] reports:

”By analysing the time-domain response of a servo with PID position control and Coulomb or Coulomb + static friction, it has been shown that no system with Coulomb friction alone will show a limit cycle in the neighbourhood of the origin, and that every system with minimal Coulomb friction and nonzero static friction has such a limit cycle as a possible motion.... when the Coulomb + static friction model is valid and the relative magnitudes of Coulomb and static friction lie in their normal range, there is no combination of PID control parameters that will eliminate stick-slip.”,

where the terms ”nonzero static friction” and ”normal range” express the range of the parameters  $F_s > F_c > 0$ .

The basic idea to analyse the local stability of the equilibrium points is to linearize the different nonlinear frictional damping characteristics about  $x_2 = 0$ , i.e., linearize the friction force in the slip phase of Eq. (9.1). If the resulting closed-loop system, with the linearized friction force embedded in Eq. (9.2), can locally be represented as a PID controlled system with Coulomb friction only, the equilibrium points are locally stable. The exact algebraic results from [8] show for such a closed-loop system that no hunting limit cycle exist on an open interval near the origin in  $x_1$  direction, i.e., solutions which start in the stick phase. Starting on this open interval the equilibrium set will be reached either with asymptotic convergence or with a contracting sequence of stick and slip transitions. A sufficient condition for these algebraic results is that the linear part of the closed-loop dynamics, i.e., the homogeneous part of Eq. (9.2), is asymptotically stable.

To perform the analysis on the local stability of the set of equilibrium points for damping functions with continuous stick-slip transitions, i.e.,

$$g(x_2) = F_c + (F_s - F_c) \exp\left(-\left|\frac{x_2}{v_s}\right|^\beta\right),$$

the following Taylor expansion at  $x_2 = 0$  for  $\beta > 1$  can be constructed:

$$\begin{aligned} g(x_2) &= g(0) + \left. \frac{\partial g(y)}{\partial y} \right|_{y=0} x_2 + R(x_2) \\ &\approx F_s, \end{aligned}$$

where  $R(x_2)$  is the rest term of this expansion with  $R(0) = 0$  and  $\left. \frac{\partial R(y)}{\partial y} \right|_{y=0} = 0$  and  $v_s$  is supposed to be positive.

### 9.3 Local stability of equilibrium points

For  $\beta = 1$  this damping function  $g(x_2)$  is not differentiable at  $x_2 = 0$ , but let us analyse this function for positive velocity  $x_2$  going to zero:

$$\begin{aligned} g(x_2) &= \lim_{y \downarrow 0} g(y) + \left. \frac{\partial g(y)}{\partial y} \right|_{y \downarrow 0} x_2 + R(x_2) \\ &\approx F_s + \frac{(F_c - F_s)}{v_s} x_2, \end{aligned}$$

where  $R(x_2)$  is again the rest term with  $\lim_{y \downarrow 0} R(y) = 0$  and  $\left. \frac{\partial R(y)}{\partial y} \right|_{y \downarrow 0} = 0$ . For negative velocity  $x_2$  going to zero the following approximation holds

$$\begin{aligned} g(x_2) &= \lim_{y \uparrow 0} g(y) + \left. \frac{\partial g(y)}{\partial y} \right|_{y \uparrow 0} x_2 + R(x_2) \\ &\approx F_s - \frac{(F_c - F_s)}{v_s} x_2, \end{aligned}$$

where once more  $R(x_2)$  is the rest term of this expansion with  $\lim_{y \uparrow 0} R(y) = 0$  and  $\left. \frac{\partial R(y)}{\partial y} \right|_{y \uparrow 0} = 0$ . Combining both results for  $\beta = 1$  the linearization can be written as:

$$g(x_2) \approx F_s + \frac{(F_c - F_s)}{v_s} |x_2|.$$

For the range  $0 < \beta < 1$  of the shaping parameter, the function  $g(x_2)$  is also not differentiable at  $x_2 = 0$  and moreover its first derivative with respect to  $x_2$  is undefined for both positive and negative velocity  $x_2$  approaching zero. Hence, the nonlinear frictional damping function in the slip phase can not be linearized for  $0 < \beta < 1$ .

Using the different linearizations of the nonlinear frictional damping characteristics in the slip of the friction force of Eq. (9.1), the following linearized friction forces are found about  $x_2 = 0$ :

$$F_{\text{slip}}(x_2) \approx \begin{cases} F_s \text{sgn}(x_2) + bx_2, & \forall x_2 \neq 0 \quad \forall \beta > 1 \\ F_s \text{sgn}(x_2) + \frac{(F_c - F_s)}{v_s} x_2 + bx_2, & \forall x_2 \neq 0 \quad \forall \beta = 1 \\ \text{undefined}, & \forall x_2 \neq 0 \quad \forall 0 < \beta < 1 \end{cases}$$

Substitution of either the first or second linearization in the slip phase of the state space representation of Eq. (9.2), the closed-loop system is locally reduced to a PID controlled simple mass system subjected to Coulomb friction only, where the Coulomb friction level is equal to the maximum static friction level of the original system. Moreover for  $\beta = 1$ , the linear dynamics in the slip phase of the closed-loop system is modified by the linearization. Hence, a sufficient condition for the local stability of the equilibrium set can be described as follows: if the linear part of the dynamics in the slip phase are asymptotically stable the equilibrium set is locally stable. For the first and second region of  $\beta$ , the characteristic



polynomial of the homogeneous part of the linearized closed-loop dynamics about  $x_2 = 0$  are:

$$s^3 + \frac{PD+b}{m}s^2 + \frac{P}{m}s + \frac{PI}{m} \quad \forall \quad \beta > 1$$

$$s^3 + \left(\frac{PD+b}{m} + \frac{F_c - F_s}{mv_s}\right)s^2 + \frac{P}{m}s + \frac{PI}{m} \quad \forall \quad \beta = 1.$$

For  $0 < \beta < 1$ , the linearization is undefined, which disables us to construct a characteristic polynomial for this region. Using the Routh Hurwitz stability criterion for the linear part of the linearized closed-loop dynamics, the following classification on the stability of the set of equilibria can be obtained (under the assumption that the linear part of dynamics of the original closed-loop system, i.e., represented by the characteristic polynomial corresponding to  $\beta > 1$ , are asymptotically stable):

- Stable for damping functions with continuous stick-slip transitions and  $\beta > 1$ , since the linear part of the dynamics of the linearized closed-loop system are the same as for the original system.
- Stable for damping functions with continuous stick-slip transition with  $\beta = 1$  if  $\left(\frac{PD+b}{m} - I\right) > \frac{F_s - F_c}{mv_s}$ , which is a sufficient condition.
- For damping functions with continuous stick-slip transitions where  $0 < \beta < 1$ , no sufficient condition on the local stability of the set of equilibrium points can be obtained, since the linearization is undefined.

For the frictional damping function with discontinuous stick-slip transition this analysis is not valid due to the discontinuous jump in the friction level. However, [8] shows for this system that in the neighbourhood of the origin the sequence of stick and slip transitions is diverging. Hence, the equilibrium set is locally unstable.

## 9.4 Event Mapping: a Phase Plane Analysis

To study the global three-dimensional nonlinear dynamics of the closed-loop system for the various damping functions, a technique similar to a Phase Plane Analysis [7] is used. With respect to the friction induced hunting limit cycles the system might be described by a one-dimensional iterated mapping as shown by [104]. Such a reduction of dimension can only take place for a system with sufficiently strong dissipation in the phase space [48]. For the hunting stick-slip oscillations, an infinite dissipation occurs when the closed-loop system enters the stick phase, i.e., a finite volume in the slip phase is reduced to zero volume within finite time in the stick phase.

To illustrate the *event mapping* technique, as presented in [48], the closed-loop system of Eq. (9.2) is considered for a damping function with continuous stick-slip transition. The system is initialized in the stick phase with  $\underline{x}(0) = [0.1 \ 0 \ 0]^T$  and the closed-loop parameters used

### 9.4 Event Mapping: a Phase Plane Analysis

Mass	$m = 1$	[kg]
Static friction level	$F_s = 4$	[N]
Coulomb friction level	$F_c = 2$	[N]
Stribeck velocity	$v_s = 0.1$	[m/s]
Shape parameter	$\beta = 2$	[-]
Viscous damping	$b = 1$	[N.s/m]
Controller gain	$P = 10$	[N/m]
Derivative action	$D = 1$	[s]
Integral action	$I = 10$	[1/s]
Narrow stick width	$\eta = 1e-8$	[m/s]
Acceleration coefficient	$\alpha = 10$	[1/s]

Table 9.1 - Closed-loop system parameters.

in this simulation study are given in Table 9.1 and the phase portrait and time responses are shown in Figure 9.4.

The equilibrium points, as described in the previous section where  $x_1 = x_2 = 0$ , define a continuous line E with an upper and a lower bound for  $x_3$ , as depicted in the phase portrait of the three states of Figure 9.4a). The corresponding time responses, as depicted

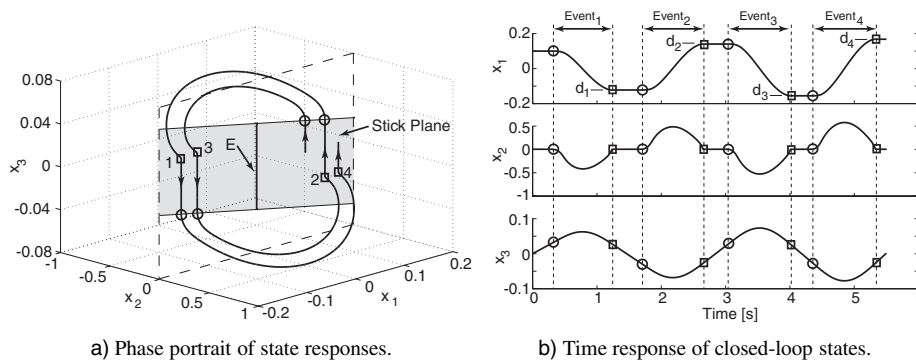


Figure 9.4 - Closed-loop state responses.

in Figure 9.4b), show a diverging sequence of stick-slip oscillations. The stick plane in Figure 9.4a) defines the phase where (i) the mass has zero velocity and (ii) the control effort  $u$  is smaller or equal to the maximum static friction level  $F_s$ . Depending on the actual state  $x_1$  the integral term  $x_3 = \int_{t_0}^{t_e} x_1 d\tau$  will increase in either positive or negative direction in the stick plane. The integral term builds up and eventually the control effort will overcome the maximum static friction level. Hence, the system enters the slip phase, which transition is defined as the beginning of an *event* and depicted as a circle in Figure

9.4. The return transition into the stick phase, depicted as a square, defines the end of an *event*. Two successive events are separated by one stick phase that can be characterized by the state  $x_1 = d$  which is constant during the stick phase. The consecutive values of the state  $x_1$  in stick phase can be represented by a one-dimensional map  $d^{n+1} = \mathcal{P}(d^n)$  in the  $(d^n, d^{n+1})$  plane. Such a map is the so-called *event map* and its graphical interpretation is in general much simpler than that of the global motion. Moreover, the map is a single valued function  $\mathcal{P}(d^n)$  due to the uniqueness of the solution for the motion system subjected to the Switch friction model as discussed in Section 9.2. For the motion presented in Figure

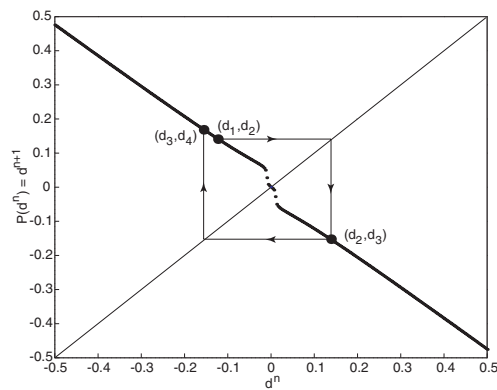


Figure 9.5 - Numerically constructed *event map* of the closed-loop system for a frictional damping function with continuous stick-slip transition.

9.4 the equivalent one-dimensional map is given in Figure 9.5, which can graphically be interpret as follows: one starts with the initial state in the stick phase, characterized by  $d^1$ , on the horizontal axis and reads off  $d^2 = \mathcal{P}(d^1)$  on the vertical axis. The horizontal line with right arrow intersecting the  $45^\circ$  line corresponds to the iterative process of replacing  $d^1$  on the horizontal axis by  $d^2$ . The iteration now continues by progressively reading off  $d^{n+1}$  on the vertical axis and using the horizontal line through  $d^{n+1}$  with the  $45^\circ$  line to reflect  $d^{n+1}$  onto the horizontal axis. Hence, the combination  $(d^1, d^2)$  is iterated to  $(d^2, d^3)$  and successively  $(d^2, d^3)$  to  $(d^3, d^4)$ . These three points, depicted by big dots, are part of the *event map* and describe only a very small part of the global dynamics of the system.

To investigate the global dynamics of the closed-loop system, the function  $\mathcal{P}(d^n)$  has to be computed, which will be constructed numerically since it is impossible to derive an analytic expression for the *event map* of the closed-loop systems with nonlinear damping functions. To construct the *event map*, the system is initialized in the stick phase for different initial positions  $x_1 = d^1$  and integrated numerically until the system enters the stick phase again. Hence, on a grid  $d^1 = [0, \Delta d, \dots, \bar{d} - \Delta d, \bar{d}]$  the next iterated points  $d^2$  of the map are computed. These points are elements of the single valued function  $\mathcal{P}(d^n)$  defining the global dynamics of the closed-loop system. Due to the fact that the closed-loop system is odd with respect to the origin the function  $\mathcal{P}(d^n)$  will also be odd, i.e.,  $\mathcal{P}(d^n) = -\mathcal{P}(-d^n)$  and

## 9.5 Numerical Results

therefore the numerical integration is limited to positive initial positions. The elements of the function  $\mathcal{P}([\underline{d}, \underline{d} + \Delta d, \dots, \bar{d} - \Delta d, \bar{d}])$  with  $\Delta d = 0.001$  and  $\bar{d} = -\underline{d} = 0.5$ , as depicted with small dots in Figure 9.5, give an impression of the global dynamics. To locate a limit cycle, i.e., a closed trajectory, the second iterated *event map* is of interest, since the first iterated map  $\mathcal{P}(d^n)$ , as shown in the figure, maps an initial state  $d^n$  to a state  $d^{n+1}$  which has an opposite sign after one *event* and will not close the trajectory immediately, as can be seen Figure 9.4. However, the map describing an initial state  $d^n$  to a state  $d^{n+2}$  which has possibly the same sign after two events might close the trajectory at once when  $d^n = d^{n+2}$ . This second iterated map is defined by

$$d^{n+2} = \mathcal{P}(d^{n+1}) = \mathcal{P}(\mathcal{P}(d^n)) = \mathcal{P}^2(d^n)$$

and the fixed points of the map  $\mathcal{P}^2$  locate both (i) the equilibrium points of the system and (ii) the limit cycles. The fixed points of the map are located at

$$d^* = \{d^n | d^{n+2} = \mathcal{P}^2(d^n) = d^n\}$$

and the local stability of the fixed points of the map can be determined by the contraction theorem [120]. A fixed point of the map is locally stable if the response is locally contracting to this point, i.e., the slope of the map  $\mathcal{P}^2$  in the fixed point of interest has an absolute value smaller than 1. A fixed point is locally unstable if the response is locally diverging from this point, i.e., the slope of the map  $\mathcal{P}^2$  in the fixed point of interest has an absolute value larger than 1.

In Figure 9.6, the second iterative *event map*  $\mathcal{P}^2(d^n)$  is shown together with its fixed points  $d^* \in \{d_1^*, d_2^*, d_3^*\}$ . The exact location of the limit cycles are computed by approximating the single value function  $\mathcal{P}^2(d^n)$  in their vicinity with a third order polynomial through four neighbouring data points. Through the origin, defining the equilibrium set, the function  $\mathcal{P}^2(d^n)$  is approximated with a line through three data points including the origin. These approximations are used to locate the fixed points of the map and to determine their local stability. In Table 9.2, the occurring types of solution together with their location and local stability are given. The equilibria of the closed-loop system, for a damping function with continuous stick-slip transition and shaping factor  $\beta = 2$ , are indeed locally stable as predicted analytically in the previous section. Moreover, there exist for this system two limit cycles, where one is stable and one is unstable. Another interesting feature of the one-dimensional *event map* is the ability to describe the attractor basins for the different solutions, i.e.,  $d^n \in (-d_2^*, d_2^*)$  will eventually end up in the origin and therefore in the equilibrium set and starting  $d^n \in [-0.5, -d_2^*), (d_2^*, 0.5]$  will end up in the stable limit cycle with amplitude  $d_3^*$ .

## 9.5 Numerical Results

In this section, the location of the equilibrium points and limit cycles together with their local stability, are determined for two other damping functions with continuous stick-slip

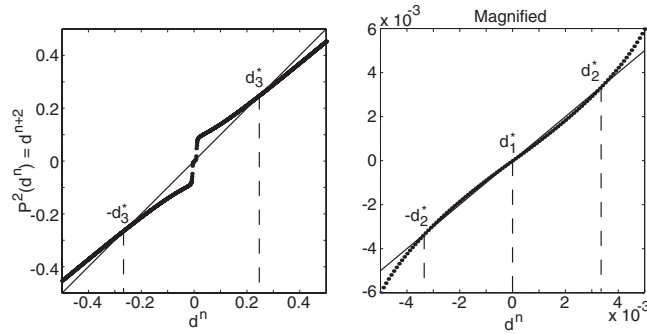


Figure 9.6 - Second iterated *event map* locating the equilibrium set and limit cycles.

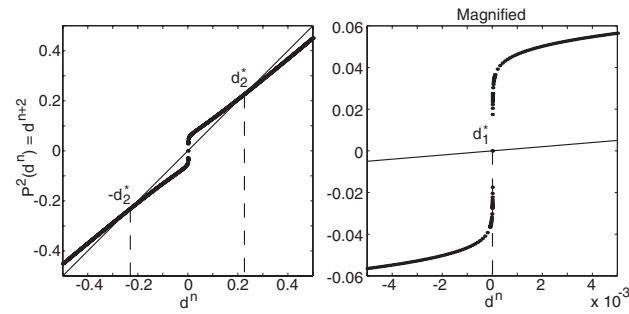
Fixed point	Type of solution	Local stability
$d_1^* = 0$	Equilibrium set	Stable
$d_2^* = 0.0034$	Limit cycle	Unstable
$d_3^* = 0.2523$	Limit cycle	Stable

Table 9.2 - Fixed points of the second iterated *event map*  $\mathcal{P}^2(d^n)$ .

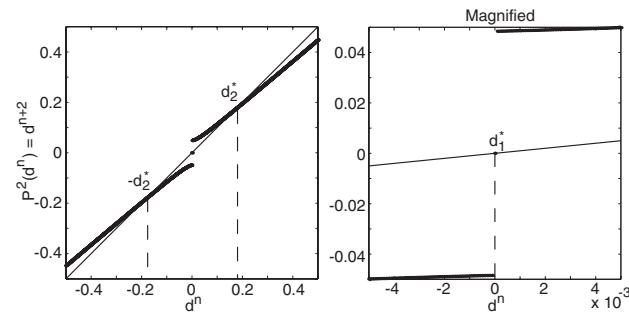
transitions, i.e., with shaping parameter  $\beta = 1$  and  $\beta = 0.5$ , and the damping function with a discontinuous stick-slip transition. Again the corresponding *event map*  $\mathcal{P}^2(d^n)$  is used to analyse the various stick systems where the closed-loop system parameters are chosen equal to the parameters in Table 9.1 except for the shaping parameter  $\beta$ . In Figure 9.7 the various second iterated *event maps* are given and for the various damping functions the closed-loop system shows only one limit cycle, which are depicted with  $d_2^*$ , which is clearly different from the two limit cycles found for the damping function with  $\beta = 2$  in Section 9.4. For  $\beta = 1$  the equilibrium set  $d_1^*$  is unstable as shown in the magnified part of Figure 9.7a), since the slope through the origin is larger than 1. As expected the sufficient condition for the stability of the equilibrium set as derived in Section 9.3 is not satisfied, i.e., for  $(\frac{PD+b}{m} - I) = 1$  [1/s] is smaller than  $\frac{(F_s - F_c)}{m v_s} = 20$  [1/s]. The details about the fixed points for the *event map* for  $\beta = 1$  are given in Table 9.3. For the damping function with a discontinuous stick-slip transition and the damping function with a continuous stick-slip transition where  $\beta = 0.5$  an interesting phenomenon appears for the equilibrium set, i.e., in the neighbourhood of the origin. The *event maps*, as depicted in Figures 9.7b)-9.7c), seem to be both discontinuous around the origin predicting unstable sets of equilibrium points. Moreover, the attractor basin for the stable limit cycle is the entire domain excluded the origin. The details on these two damping functions are also given in Table 9.3.

An interesting question is what will happen when for instance the controller gain  $P$  is altered. Moreover, it is of interest to know how the system characteristics change for

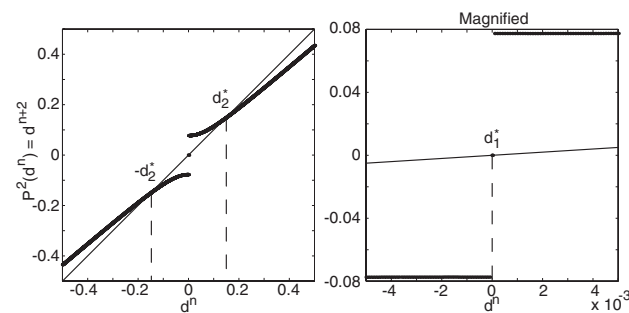
## 9.5 Numerical Results



a) Second iterated *event map* for the system where the damping function has a continuous stick-slip transition and  $\beta = 1$ .



b) Second iterated *event map* for the system where the damping function has a continuous stick-slip transition and  $\beta = 0.5$ .



c) Second iterated *event map* for the system where the damping function has a discontinuous stick-slip transition.

Figure 9.7 - Second iterated *event map* locating the equilibrium set and limit cycles for various damping functions.

## Part II - Friction Induced Limit Cycling

Continuous damping function with $\beta = 1$		
Fixed point	Type of solution	Local stability
$d_1^* = 0$	Equilibrium set	Unstable
$d_2^* = 0.2314$	Limit cycle	Stable

Continuous damping function with $\beta = 0.5$		
Fixed point	Type of solution	Local stability
$d_1^* = 0$	Equilibrium set	Unstable
$d_2^* = 0.1786$	Limit cycle	Stable

Discontinuous damping function		
Fixed point	Type of solution	Local stability
$d_1^* = 0$	Equilibrium set	Unstable
$d_2^* = 0.1485$	Limit cycle	Stable

Table 9.3 - Fixed points of  $\mathcal{P}^2(d^n)$  for the various damping functions.

the different damping functions. Hence, the fixed points of the second iterated *event maps* together with their local stability for the various damping functions, on a grid  $P = \{10, \dots, 31\}$  [N/m] with step-size 1, are computed and shown in Figure 9.8. The so-called bifurcation diagram of Figure 9.8a), predicts for the frictional damping function, with a continuous stick-slip transition and  $\beta = 2$ , a disappearance of the hunting limit cycles for controller gains larger than approximately  $P = 21$  [N/m]. The equilibrium set is for all computed controller gains locally stable as expected by the analytic results presented in Section 9.3. Figure 9.8b) presents the changing dynamics for the system with the continuous stick-slip transition and  $\beta = 1$ , where the unstable equilibrium set becomes stable and intersects with the stable limit cycles for controller gain  $P \approx 27$  [N/m]. Larger controller gains predict only stable equilibrium points and no limit cycles. The sufficient condition derived for this closed-loop system predicts locally stable equilibrium points for  $P > \frac{F_s - F_c}{Dv_s} + \frac{mI}{D} - \frac{b}{D} = 29$  [N/m]. This bound can be considered as an analytic upper bound due to the fact that this condition is only sufficient and not necessary.

The equilibria of the closed-loop systems with (i) the continuous frictional stick-slip transition where  $\beta = 0.5$  and (ii) the discontinuous frictional stick-slip transition, as depicted in Figure 9.8c)-9.8d), are locally unstable for all computed controller gains. Stable limit cycles are present for all values of  $P$  for the damping function with a discontinuous stick-slip transition which is conform the exact algebraic results obtained in [8].

From the bifurcation diagrams it can be seen that a small change in the shaping parameter  $\beta$ , the closed-loop dynamics completely changes with respect to the existing periodic solutions and stability property of the equilibrium points. Let us return to the analytic sufficient condi-

## 9.5 Numerical Results

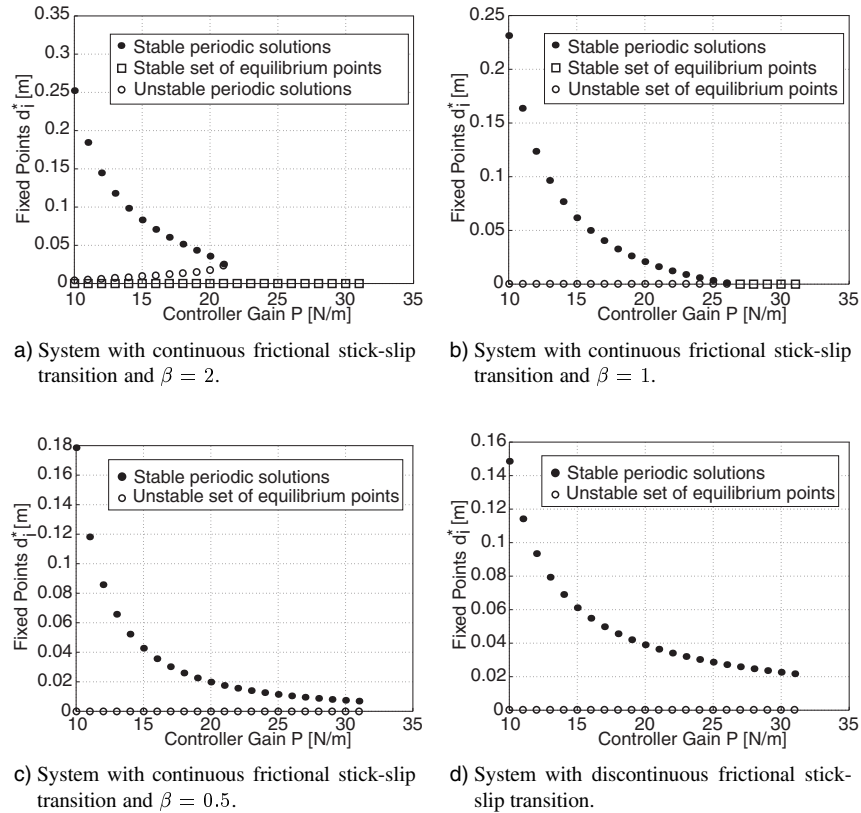


Figure 9.8 - Bifurcation diagram with varying controller gain  $P$ .

tion for  $\beta = 1$ , since for this frictional damping curve the closed-loop characteristics change apparently dramatically. The condition can be rewritten as  $PD > \frac{F_s - F_c}{v_s} + mI - b$  and can be interpreted as the minimal derivative control  $PD$  which suffices to stabilize the equilibrium points and even eliminate hunting limit cycles. However, in case where there is no drop in the friction force, i.e., the static friction level  $F_s$  is equal to the Coulomb friction level  $F_c$ , this condition reduces to  $PD > mI - b$ . This difference is introduced due to the negative slope in the Stribeck curve for velocities unequal to zero. Hence, the extra derivative control, expressed by  $\frac{F_s - F_c}{v_s}$ , is necessary to eliminate this negative slope in the vicinity of velocities equal to zero. Moreover, this extra derivative control manipulates the Stribeck curve such that there does no longer exist a drop in the friction force for all velocities unequal to zero. This explains the way hunting limit cycles are induced, since along the velocities for which the slope of the friction force is negative the closed-loop dynamics are unstable if the controller adds not enough damping to the system. The same idea might be applied to the other



friction curves, where for the damping curves with continuous stick-slip transition and  $\beta > 1$  a sufficient condition to eliminate hunting limit cycles might be constructed and could read

$$PD > |\min_y(\frac{\partial g(y)}{\partial y} |y)| + mI - b, \quad \forall y > 0.$$

For the friction curves with continuous frictional stick-slip transition and  $0 < \beta < 1$  this is not applicable due to the fact that the minimal slope is undefined. The same conclusion holds for friction curve with the discontinuous frictional stick-slip transition and elimination of the hunting phenomenon seems not to be possible for these two friction types by adding extra damping to the system.

## 9.6 Conclusions

In this chapter, the closed-loop dynamics of a PID controlled mass system subjected to friction is represented with an equivalent one-dimensional map. This one-dimensional map reveals all the nonlinear dynamical properties such as (i) stability of the equilibrium set and (ii) the existence of limit cycles with their stability properties. The so-called *event map* is used to examine the differences in the nonlinear closed-loop dynamics for various frictional damping functions. As presented in the previous section it is essential to consider the different possible solutions for the different frictional damping functions. A classification on the

Continuous damping function with $\beta > 1$	
Equilibrium set	Stable
Limit cycles	Possible - both stable and unstable
Elimination of hunting	Possible
Continuous damping function with $\beta = 1$	
Equilibrium set	Stable or unstable
Limit cycles	Possible - only stable
Elimination of hunting	Possible
Continuous damping function with $0 < \beta < 1$	
Equilibrium set	Unstable
Limit cycles	Always - stable
Elimination of hunting	Never

Table 9.4 - Classification for frictional damping functions with continuous stick-slip transitions.

various friction curves with a continuous transition of the friction force from the stick phase to the slip phase is given in Table 9.4 with respect to the following dynamical properties: (i) possible existence of stable and unstable limit cycles, (ii) possible disappearance of the

## 9.6 Conclusions

hunting phenomenon and (iii) stability property of the equilibrium set. This classification is based on analytic observations presented in Section 9.3 together with the numerical results in Section 9.4 and 9.5. From this table can be concluded that practically identified friction curves with continuous stick-slip transitions where  $\beta$  lies between zero and one are not able to describe the experimentally observed phenomenon that hunting limit cycles can be eliminated by properly chosen PID settings. The results for the frictional damping function with discontinuous stick-slip transition are equal to the observations for the friction curves with continuous stick-slip transitions where  $0 < \beta < 1$ . Moreover, the results are conform the exact algebraic results performed by [8].

Overall, it can be concluded that minor changes in the friction model might cause severe changes to the closed-loop nonlinear dynamics in terms of existing periodic solutions.

## Part II - Friction Induced Limit Cycling

## Chapter 10

# Analysis of Friction Induced Limit Cycles on an Experimental Linear Motor Motion System

### 10.1 Introduction

In this chapter friction induced limit cycles are studied for an experimental Linear Motor Motion System (LiMMS). To this end some of the identification techniques as proposed in Part I and the described analysis tools of Part II are utilized to perform an identification of the system and to analyse the closed-loop dynamics for both the experimental setup and the estimated model. Therefore, this chapter finalizes the thesis with the synthesis of the obtained knowledge for both the identification and the analysis of controlled mechanical systems with friction.

As for the described closed-loop systems in the previous two chapters, the LiMMS system shows friction induced limit cycles for a PID controlled regulator task with certain controller settings. However, the LiMMS dynamics show an additional nonlinearity due to the working principle of the linear motor itself, which introduces a position dependent nonlinear force, the so-called cogging force. Here, it will be illustrated that for this more general and more complex dynamic system the previously gained insight and already used analysis tools for friction induced limit cycles are still applicable. Moreover, the practically observed limit cycles are compared to the ones predicted by the identified model and bifurcation diagrams for both the experimental LiMMS setup and the identified model are constructed.

---

This chapter is in preparation for publication.

The outline of this chapter is as follows. In Section 10.2 the working principle of the experimental LiMMS setup will be explained in detail, which results in a description of the main dynamical phenomena present in the system. This knowledge will be used in Section 10.3 to model and identify the system. As for the previous chapters, two different friction models will be identified, i.e., the static Switch friction model [84] and the dynamic LuGre friction model [24]. In Section 10.4 the experimentally observed closed-loop behaviour of the LiMMS setup will be compared to the models predicted closed-loop behaviour in terms of stability of the set of equilibrium points and time responses (and their phase portraits) of existing stable periodic solutions. For the LiMMS model with the Switch friction model event maps will be constructed and compared with an experimentally constructed event map for the LiMMS setup. The construction of bifurcation diagrams for both the LiMMS setup and the LiMMS model with the Switch friction model will conclude this section. This chapter will be closed with conclusions in Section 10.5.

## 10.2 Experimental Setup

In this chapter a Linear Motor Motion System is considered to analyse experimental friction induced limit cycles, which are mainly due to its highly reproducible dynamics. In practice, this means that observed system behaviour is time invariant, since changes in the dynamic properties, for instance due to temperature fluctuations or wear, are minimal by construction. A schematic picture of the experimental LiMMS setup with the additional real-time hardware is shown in Figure 10.1.

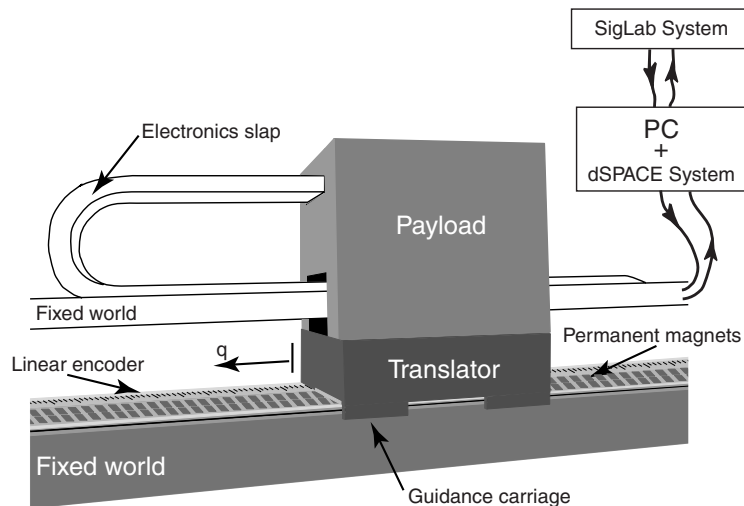


Figure 10.1 - Schematic representation of the LiMMS apparatus.

## 10.2 Experimental Setup

The working principle of the LiMMS is in analogy with a rotational electromotor and consists of two main parts as depicted in Figure 10.2:

- a stator, which is formed by a number of base-mounted permanent magnets.
- a translator, the analogon of the rotor in a rotational electromotor, which consists of a number of iron-core coils and which moves the attached payload mass.

When a three-phase current is applied to the coils, a series of attraction and repellent forces between the poles of the coils and the permanent magnets will be generated and results in a thrust force  $F$  acting on the freely movable translator with the payload mass.

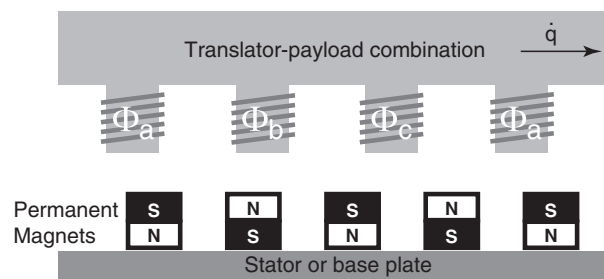


Figure 10.2 - Schematic representation of the working principle of a three-phase synchronous permanent magnet linear motor.

Besides the induced thrust force  $F$ , three extra forces are acting on the mass of the translator-payload combination  $m$ , that is:

- cogging force. Due to the iron-core coils used in the translator an additional attraction force is caused between the permanent magnets and the iron cores even when no current is flowing through the coils. This cogging force is position dependent and is often modeled as a sinusoidal function with (i) a spatial frequency that depends on the pitch of the magnets and (ii) an amplitude that depends on the magnetic force generated,
- reluctance force. As the translator moves the self-inductance of the coil windings changes, which is only present as current flows through the coils. This effect is mainly generated by errors in the commutation, which is the changing of the phase angle of the three-phase current according to the actual position of the translator. The present commutation process assumes an ideal equidistantly spaced array of magnets, whereas in the real LiMMS the magnets are not alligned with high accuracy and have large magnetic tolerance due to cost considerations,
- friction force, which is introduced by a number of ball bearings guiding the translator-payload combination carriage.

The combination of the position dependent cogging and reluctance force is often called the force ripple in the thrust force [99]. Here, the position dependent part of the reluctance force will be lumped into the cogging force due to the lack of an accurate motor model. The combined ripple force will be referred to as cogging force. For more detailed information on linear motors and their modeling, the reader is referred to [11], [90]. Overall, it can be concluded that the mass combination of the LiMMS is driven by the thrust force  $F$  and subjected to two nonlinear forces, of which one, the cogging force  $F_c$ , is a function of position and the other, the friction force  $F_f$ , depends on velocity.

The displacement of the translator-payload combination is measured with an incremental linear encoder with a resolution of 1 [ $\mu\text{m}$ ]. The LiMMS is supplied by a current-controlled sinusoidal commutation, which produces the three-phase current for the coils. The current-controlled commutation is commanded by a voltage, which expresses the desired effective current through the coils. The thrust force  $F$  is considered to be linear with the commanded voltage  $u$ , i.e.,  $F = c_m u$  where  $c_m$  is the motor constant. The current-controlled commutation together with software safety layers are running on a dSPACE system [37]. During the experiments the sampling frequency of the dSPACE system is set to 5 [kHz]. To perform on-line frequency domain measurements, a SigLab system [113] is used to conduct and process the measurements. The brand of the separate hardware devices is given in Table 10.1.

Device	Brand	Model-type
Encoder	Heidenhain	LIDA 201
LiMMS	PHILIPS	Unknown
dSPACE	dSPACE	DS1103
SigLab	DSP Technology	20-42

Table 10.1 - Inventory of the experimental LiMMS setup.

### 10.3 Modeling and Identification

The LiMMS as described in the previous section is modeled as a double integrator system subjected to the two nonlinear forces, which can mathematically be represented as:

$$m\ddot{q} = -F_f(\dot{q}) - F_c(q) + c_m u, \quad (10.1)$$

where

$m$	[kg]	Mass of translator-payload combination
$q$	[m]	Position of translator-payload combination
$F_f$	[N]	Friction force
$F_c(q)$	[N]	Position dependent cogging force
$c_m$	[N/V]	Motor gain
$u$	[V]	Commanded voltage

### 10.3 Modeling and Identification

Before this model of the LiMMS can be identified assumptions have to be made for the modeling of (i) the velocity dependent friction force  $F_f(\dot{q})$  and (ii) the position dependent cogging force  $F_c(q)$ . For this system, two friction models will be identified, i.e., the dynamic LuGre friction model [24] and the static Switch friction model [84], whereas the cogging force will be modeled by a look-up table that performs a 1-D linear interpolation of input values using the identified table. The identification procedure issues three estimation stages, one for the double integrator behaviour, one for the cogging force and one for the friction force. By performing appropriate experiments each phenomenon can be isolated from the (nonlinear) dynamics. In the following three subsections each stage will be explained and applied for the identification of the LiMMS.

#### 10.3.1 Double integrator behaviour

To exclude the nonlinear friction and cogging forces from an experiment in order to isolate the double integrator behaviour, the LiMMS is controlled with a weak PD controller as proposed in Section 5.2.1 and a Pseudo Random Binary Signal (PRBS) is injected in the closed-loop system as  $v$ , as depicted in Figure 10.3. The measured Frequency Response Function (FRF)  $S(j\omega) = W(j\omega)/V(j\omega)$  is equal to the closed-loop sensitivity if an appropriate reference signal  $r$  is used, where by definition  $W(j\omega) = \mathcal{F}\{w(t)\}$  and  $V(j\omega) = \mathcal{F}\{v(t)\}$ . Here, a reference trajectory is used which moves the mass forth and back over 90 % of the allowable working range, i.e., 0.5 [m], at a constant velocity. For constant velocity the friction force is assumed to be constant and the cogging force is affecting the measurement at only one frequency equal to  $\pm v_r/0.015$  [Hz], where  $v_r$  is the velocity of the reference trajectory and 0.015 [m] is the average pitch of the permanent magnets. During the identification procedure, the reference velocity is set to 0.1 [m/s] to avoid stick-slip oscillations artifacts. A PRBS

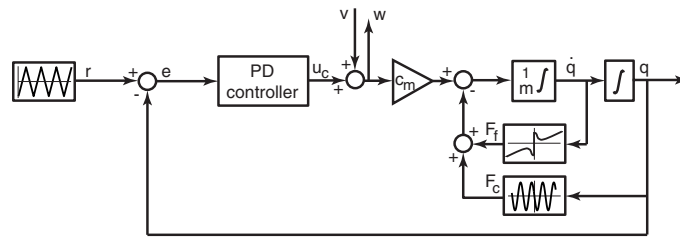


Figure 10.3 - Closed-loop configuration.

signal of a bandwidth up to 500 [Hz] with a RMS level of 0.1 [V] is applied for  $v$  and the measured FRF  $S(j\omega)$  is obtained by averaging 50 different time series of 8192 samples at a sampling frequency of 10 [kHz] with a Hanning window and 50% overlap. Fragments of the time series that contain the velocity reversal of the reference trajectory have been removed from the data. Using the measured sensitivity FRF and the knowledge of the PD controller, the linear dynamics of the system, i.e.,  $P(j\omega)$ , can be reconstructed as depicted in Figure 10.4. The reconstructed LiMMS FRF shows a double integrator behaviour up to 140



[Hz] which locates the first eigenfrequency of the system. The cogging force is influencing the measurement at  $\pm 6.6$  [Hz], which is below the range of interest and therefore not an impediment. The quotient of the motor gain  $c_m$  and the mass  $m$  can be determined by fitting

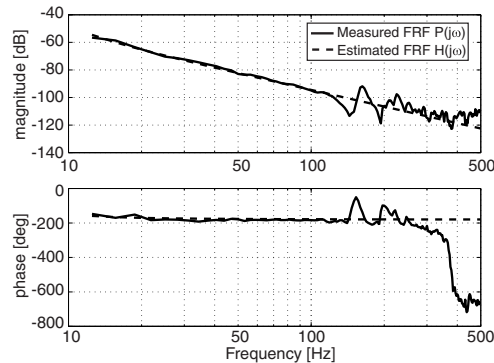


Figure 10.4 - Measured FRF  $P(j\omega)$  and estimated model FRF  $H(j\omega)$  of the LiMMS.

a double integrator model on the measured dynamics up to 140 [Hz] as depicted by the dashed line in Figure 10.4 and estimated as  $m/c_m = 0.12$  [kg·V/N]. The motor gain is more difficult to obtain and is described in [59] where a motor gain equal to  $c_m = 74.4$  [N/V] was measured. From this it follows that the mass of the translator-payload combination is equal to 8.93 [kg].

### 10.3.2 Cogging force

Next, the cogging force is recorded by moving the mass with a low constant velocity controlled tracking task. In such experiment, the inertia will not play a role and the Coulomb plus viscous friction will be nearly constant. In order to keep the payload moving the control effort will be equal to the cogging force, apart from an offset due to the constant friction part. Again, the closed-loop setting as presented in Figure 10.3 is utilized, however for this purpose a PID controller, accounting for the reconstructed FRF of the linear dynamics  $P(j\omega)$  as shown in Figure 10.4, is used with a as high as possible open-loop bandwidth, a gain margin of at least 6 [dB] and a phase margin of at least 30 [deg]. The tuned PID controller, which for this LiMMS has been discussed in more detail in [59] and [22], has an open-loop bandwidth of approximately 74 [Hz] and sufficient stability margins. This 'strong' controller is necessary to track the low velocity with a as high as possible accuracy, since then the controller effort  $c_m u_c$  will be close to the real position dependent cogging force apart from the offset due to the constant friction part. The reference trajectory  $r$  defines one forth and back movement of the mass with a desired velocity of 0.05 [m/s] over a stroke of 0.45 [m]. The control effort, which is approximately equal to the cogging force since the tracking error  $e = r - q$  is in the order of  $\pm 50$  [ $\mu\text{m}$ ], is depicted in Figure 10.5a) with respect to the measured position  $q$  where a clear offset from zero is recorded for both directions. This is of course due to fric-

### 10.3 Modeling and Identification

tion, which for constant velocities can be considered to be constant. These frictional offsets

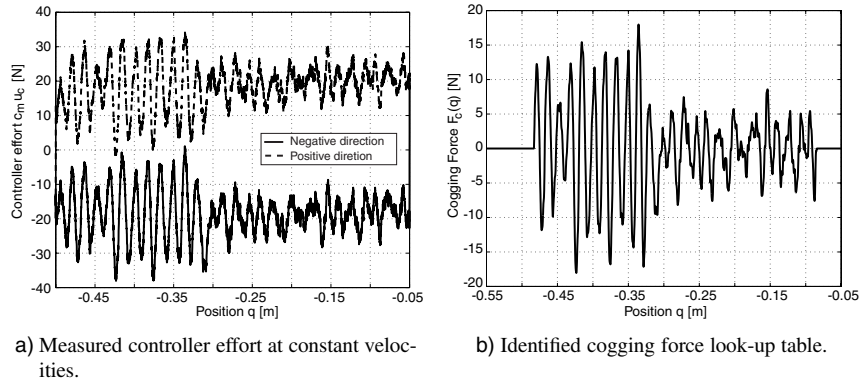


Figure 10.5 - Estimation and construction of cogging force.

are removed from the data, since the cogging force is expected to have an average value (with respect to position) equal to zero. It appears that the differences in the controller forces for the separate directions are negligible and one cogging force look-up table, which suffice for both directions, can be constructed by passing the measured controller forces through a fifth order Butterworth filter with a cut-off frequency of 35 [Hz]. This spatial cut-off frequency is based on the averaged pitch of the permanent magnets. The filter is applied once forward and once backward to avoid phase shifts and the resulting position dependent cogging force look-up table is shown in Figure 10.5b). From both pictures in Figure 10.5 it is clearly visible that for positions from -0.05 [m] down to -0.3 [m] a different cogging pattern is present than for positions from -0.3 [m] down to -0.5 [m]. This is in correspondence with the construction of the permanent magnet array itself, since due to assembly the magnet stroke is divided into two parts with apparently different cogging properties.

#### 10.3.3 Friction force

The third estimation stage consists of the modeling and estimation of the friction force. As stated earlier, two friction models will be used to identify the friction force: (i) the dynamic LuGre friction model [24] and (ii) the static Switch friction model [84]. As discussed in Chapter 8 the difference with respect to friction induced hunting limit cycles between these two friction models is small, but from a computational and analysis point of view is the Switch friction model preferable. Here, these observations are tested for this more general system with the additional nonlinear cogging force and in particular model predicted limit cycles are compared to experimental limit cycles observed on the LiMMS.

The Stribeck curve, as discussed in the Chapters 5, 8 and 9, defines for the static Switch model the frictional damping function for velocities unequal to zero and for the dynamic

LuGre model this curve represents the friction force at constant velocities. Let us recall the commonly used mathematical model of the Stribeck curve

$$g(\dot{q}) = F_C + (F_s - F_C) \exp\left(-\left(\frac{\dot{q}}{v_s}\right)^2\right),$$

where  $F_C$  is the Coulomb friction level,  $F_s$  the static friction level and  $v_s$  the Stribeck velocity. Here, the Stribeck model parameters are estimated by constructing a velocity-friction map as discussed in Section 5.3.2. For this purpose the closed-loop setting as given in Figure 10.3 is used once more with the tuned 'strong' PID controller, where the identified cogging look-up table is added to the controller effort in a feedforward manner. The reference trajectory consists of movements of the mass at different constant velocities in both directions covering the complete stroke. For every constant velocity, the averaged controller feedback effort, i.e.,  $c_m u_c$ , is a measure for the friction force, since the cogging force has already been compensated for and the inertial term is absent for constant velocities. The averaged controller feedback efforts at different velocities in both directions are shown in Figure 10.6 with circles and the estimated Stribeck curve plus viscous friction term, where for positive and negative velocities the model parameters are allowed to be different, is depicted with the solid line. In Table 10.2, the estimated direction dependent parameters together with their

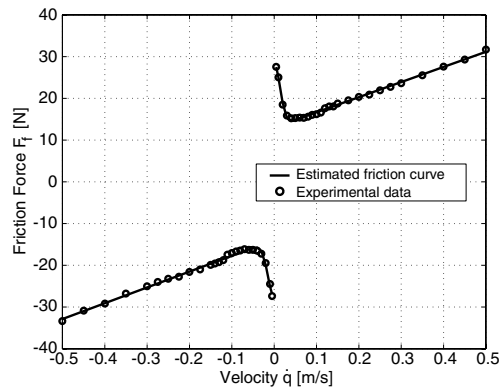


Figure 10.6 - Experimental velocity-friction map and estimated friction curve.

averaged values are given. The differences between negative and positive velocities are so small that in the sequel of this chapter the averaged values are used, which is beneficial for the implementation and evaluation of the Stribeck curve in the two models.

At this point, the estimated Stribeck curve completes the identification of the LiMMS model for the static Switch friction model. Here, the corresponding set-valued function of the friction force at  $\dot{q} = 0$ , as discussed in Section 9.2, is also a function of the position dependent cogging force  $F_c(q)$  and is defined as

$$F_f(\dot{q}, u, F_c(q)) = \begin{cases} g(\dot{q})\text{sgn}(\dot{q}) + b\dot{q}, & \forall \dot{q} \neq 0 \quad \text{Slip} \\ \min(|c_m u - F_c(q)|, F_s)\text{sgn}(c_m u - F_c(q)), & \forall \dot{q} = 0 \quad \text{Stick} \end{cases}$$

### 10.3 Modeling and Identification

Parameter	Unit	$\dot{q} > 0$	$\dot{q} < 0$	Averaged value
$F_s$	[N]	28.3	27.5	27.9
$F_C$	[N]	13.35	13.45	13.4
$v_s$	[m/s]	0.019	0.020	0.0195
$b$	[N·s/m]	36.45	37.95	37.20

Table 10.2 - Stribeck model parameters together with the viscous damping parameter.

where  $c_m u$  is the applied force,  $F_s$  the static friction at zero velocity,  $g(\dot{q})$  the frictional damping curve for velocities unequal to zero and  $b$  the viscous damping.

To complete the identification of the dynamic LuGre friction model, the remaining unidentified dynamic friction model parameters, i.e., the average bristle stiffness  $\sigma_0$  and the average bristle damping  $\sigma_1$ , are estimated with the frequency domain approach as proposed in Chapter 4. The model of the LiMMS with the LuGre friction model results in

$$m\ddot{q} = -F_c(q) - \sigma_0 z - \sigma_1 \dot{z} - b\dot{q} + c_m u \quad (10.2)$$

$$\dot{z} = \dot{q} - \sigma_0 \frac{|\dot{q}|}{g(\dot{q})} z, \quad (10.3)$$

where  $z$  is the internal friction state representing the average bristle deflection. The idea is to use the second order model description of the linearization of Eqs. (10.2-10.3) about zero velocity and zero state  $z$  by measuring a FRF in this locally valid regime to obtain estimates for  $\sigma_0$  and  $\sigma_1$  as discussed in Section 4. The linearization of this system can be obtained. However, the linearization is performed at positions  $q = q^*$  where the additional position dependent cogging force is zero, i.e.,  $F_c(q^*) = 0$ , which reduces the linearization into the following second order dynamics

$$m\ddot{q} = -(\alpha + \sigma_0)q - (\sigma_1 + b)\dot{q} + c_m u$$

where  $\alpha = \partial F_c / \partial q$  is the slope of the cogging force  $F_c(q)$  at  $q = q^*$ . So, the presence of cogging is locally felt as an additional stiffness between mass and fixed world. An estimate of this second order behaviour is obtained by performing an open-loop experiment, where a FRF  $F(j\omega)$  is measured by excitation of the system with a PRBS signal of a bandwidth up to 200 [Hz] and a RMS level below the static friction  $F_s$ . The measured FRF  $F(j\omega)$  is obtained by averaging 50 different time series of 8192 samples at a sampling frequency of 10 [kHz] with a Hanning window and 50% overlap and is depicted in Figure 10.7a) with a solid line. For low frequencies the system behaves like a spring with finite stiffness attached to the fixed world. A second order transfer function is estimated on this measured FRF represented by the dashed line in Figure 10.7a), where the following estimates for the dynamic friction model parameters are found: (i)  $\sigma_0 + \alpha = 1.3e6$  [N/m] and (ii)  $\sigma_1 + b = 3.65e3$  [N·s/m]. The contribution of  $\alpha$ , which is in the range of [-1e4, 1e4] [N/m], is very small compared to  $\sigma_0$ , so approximately  $\sigma_0 \approx 1.3e6$  [N/m]. As  $b = 37.2$  [N·s/m] it follows that  $\sigma_1 =$

## Part II - Friction Induced Limit Cycling

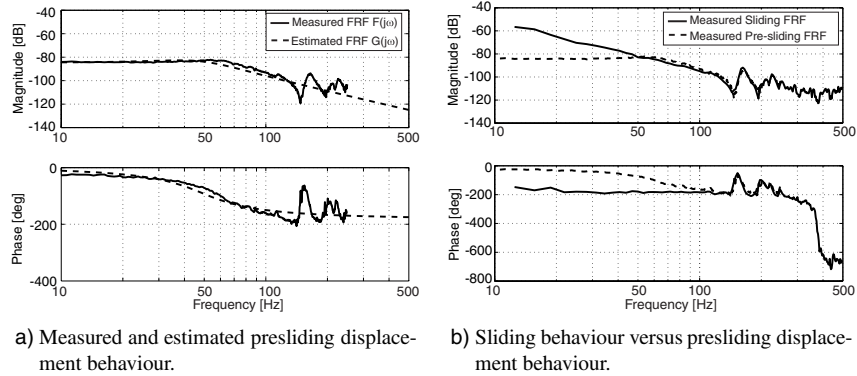


Figure 10.7 - Identification of the dynamic friction model parameters.

3.61e3 [N.s/m]. This measurement is repeated at different positions with zero crossings of the cogging force and the measurement varies with respect to the low frequent behaviour up to a factor 4, which implies that the stiffness  $\sigma_0$  ranges from 0.5e6 to 2e6 [N/m]. This variation can be due to different properties of the surface contacts between the ball bearings and the guidance carriage and/or due to the reluctance force which is not included in the model and might influence the motor gain. In Figure 10.7b) the measured double integrator behaviour or sliding dynamics is shown together with the second order behaviour in the presliding displacement regime to visualize the essential differences. Up to 100 [Hz] a clear distinction between the two regimes is visible, i.e., -2 slope versus 0 slope and damping behaviour in the presliding displacement regime from 50 [Hz] to 100 [Hz], where for higher frequencies both regimes have similar dynamics and for instance the first eigenfrequency is measured at exactly the same location with the same (anti-)resonance peaks. The major difference between the LuGre friction model and the Switch friction model is the modeling of this presliding displacement regime with a finite stiffness for the LuGre friction model. In this way, the dynamic LuGre model is capable of modeling a number of practically observed dynamic friction phenomena such as varying break-away and frictional lag.

## 10.4 Experimental Observations versus Model Predictions

To validate and compare the identified models with the experimental LiMMS setup, both the models and the system are controlled with a weak PID controller and subjected to a regulator task, which might result in a hunting limit cycle. As reported in the previous chapters essential properties for a system to promote hunting limit cycles are: (i) integral control and (ii) a drop in the friction level from a higher static friction level to a lower Coulomb friction level. The second characteristic is satisfied for this LiMMS, since the identified Stribeck

## 10.4 Experimental Observations versus Model Predictions

curve shows such a drop in the friction force and the first property can of course be satisfied by including integral control in the controller design.

Here, a similar PID controller is used as for the system in Chapter 8, where the frequency-domain shape of the controller is fixed, i.e.,

$$u_c = -K\left[\left(1 + \frac{\tau_d}{\tau_i}\right)(q - q_d) + \tau_d \dot{q} + \frac{1}{\tau_i} \int_0^t (q - q_d) d\tau\right], \quad (10.4)$$

where  $\tau_i$  determines the integral part and  $\tau_d$  the derivative controller part. A fixed controller shape will be utilized, i.e.,  $\tau_i = \tau_d = \frac{1}{2\pi}$  [s/rad], and the desired position for the regulator task is chosen to be in the vicinity of a zero crossing of the cogging force, i.e.,  $q_d = -0.38$  [m] and  $F_c(q_d) = 4.866$  [N], which is an arbitrary choice. The states of the closed-loop system are defined as the error  $e_1 = q - q_d$ , its time derivative  $e_2 = \dot{e}_1 = \dot{q}$  and its time integral  $e_3 = \int_0^t e_1 d\tau$ .

In this section, the closed-loop behaviour of both the LiMMS setup and the two models will be compared to one another for varying controller gain. First, the time responses will be studied to get an impression of the accuracy of both the identified LiMMS models. Second, the set of equilibrium points will be considered together with its local stability property. Third, the dynamics of the LiMMS setup and LiMMS model with the Switch friction model will be represented by an event map as discussed in Chapter 9 and additionally bifurcation diagrams are constructed.

### 10.4.1 Time Responses

First the PID controlled regulator task is applied to the LiMMS where the controller gain  $K$  is altered in search of a period solution or limit cycle which is reproducible and stable. For  $K = 10$  [V/m] a stable limit cycle is found with consecutive stick and slip phases, which is depicted with the solid line in Figure 10.8a), where in the upper plot the error  $e_1$  is shown and in the lower plot the controller force  $c_m u_c$ . The highly reproducible dynamics of the experimental LiMMS setup is clearly visible, since the periodic solution is time invariant after the transient behaviour of the first 5 seconds. The dashed line depicts the time response of the identified model with the Switch friction model and shows very similar behaviour of both the error and the controller effort except for the period time, which seems to be slightly larger for the model. The corresponding phase portrait of the closed-loop states of one period time for both the experimental and the model limit cycle are given in Figure 10.8b). The model response corresponds extremely well with the experimental periodic solution and the identification procedure appears to have resulted in an accurate model for the LiMMS. For the LuGre friction model similar results of the time responses are recorded as depicted in Figures 10.8c) and 10.8d) and little difference with respect to the Switch friction model can be seen. This is in line with the earlier observation in Chapter 8 that the presliding behaviour is not a dominant effect in the limit cycle response. It should be emphasized that the internal friction state  $z$  is not visualized in Figure 10.8d).

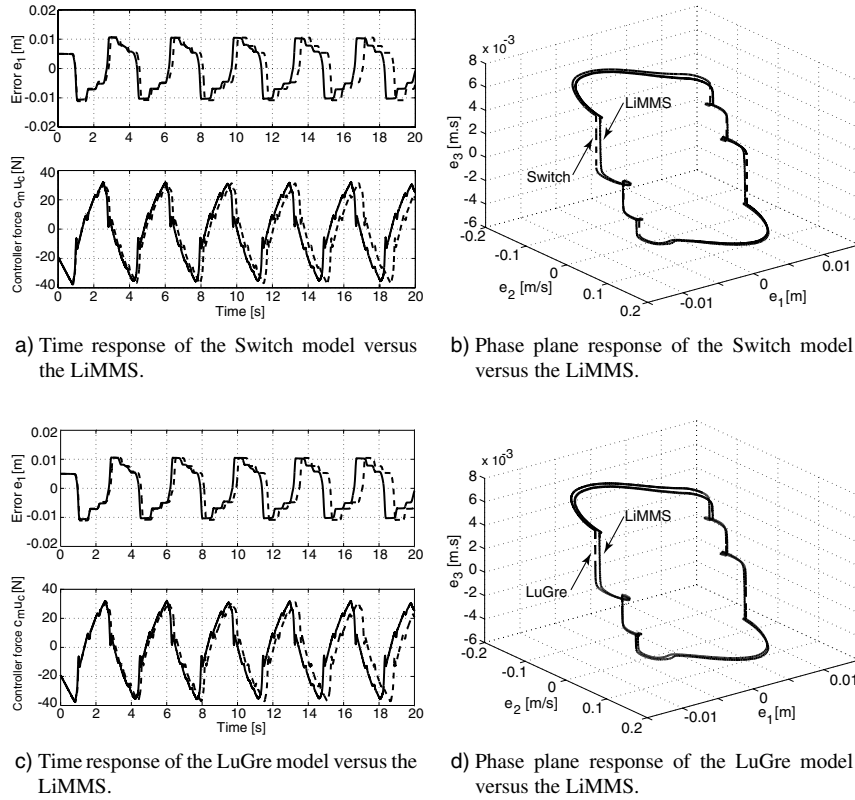


Figure 10.8 - Hunting limit cycle for  $K = 10$  [V/m] for both models and LiMMS setup.

### 10.4.2 Set of Equilibrium Points

An essential aspect of the closed-loop dynamics is the set of equilibrium points with its local stability property. First of all, it is important to realize that the equilibrium points of interest are those for which the position error  $e_1$  and velocity error  $e_2$  are zero. The integral term  $e_3$  does not need to be zero for either the LiMMS setup and both friction models, since a regulator task is being performed. Hence, the local stability of the set of equilibrium points is of interest rather than the stability of the separate equilibrium points.

In Figure 10.9 the experimental LiMMS setup is initialized twice with different initial conditions in the vicinity of the set of equilibrium points and the measured time responses indicate that for the two examined initial conditions the set of equilibrium points is locally attracting. Also, Figure 10.9 shows that - as  $e_1$  and  $e_2$  become zero - the control effort, and thus  $e_3$ , does not become zero and is different for the two cases. Moreover, Figure 10.9

## 10.4 Experimental Observations versus Model Predictions

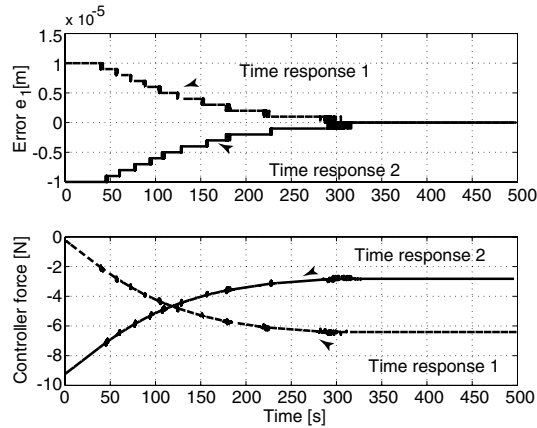


Figure 10.9 - Local stability of two equilibrium points for  $K = 10$  [V/m].

clearly illustrates that the closed-loop dynamics is in the presliding displacement regime, since a non-zero controller force, smaller than the static friction level minus the locally present cogging force, slowly moves the system on a microscopic scale. Experimentally, the local stability of the entire set of equilibrium points is hard to determine due to the infinite number of initial conditions necessary to perform this analysis. Hence, both LiMMS models will be used to analyse the local stability property of the set of equilibrium points for varying controller gain, where the stability analyses as presented in Chapters 8 and 9 will be utilized. However, the observation that the time responses of Figure 10.9 show presliding displacements stimulates the use of the LuGre friction model for the analysis of the local stability of the set of equilibrium points, since this friction model is capable of modeling this friction phenomenon whereas the Switch friction model lacks this property. However, to be able to perform a comparison between the two models both models are tested for this property.

Let us start with the analysis for LiMMS model with the Switch friction model. This model lacks the presliding displacement dynamics, which can be illustrated with the following train of thoughts. If the LiMMS model with the Switch friction model is initialized in the stick phase with the same conditions as used in Figure 10.9, the friction force will completely compensate the applied non-zero controller force in the stick phase. Consequently, the system will not move until it reaches the slip phase due to an increasing integral term in either positive or negative direction. Then the dynamics in the slip phase determines whether the system will enter the stick phase in a contracting or diverging manner as discussed in Chapter 9. Hence, the dynamics in the slip phase are essential for the local stability property of the equilibrium set. Let us take a closer look at this property of the equilibrium set for the Switch



friction model, where the equilibrium points are located on the line

$$\underline{e}_{eq} = \gamma [0 \ 0 \ 1]^T, \quad \forall \frac{-F_s - F_c(-0.38)}{2\pi K c_m} \leq \gamma \leq \frac{F_s - F_c(-0.38)}{2\pi K c_m},$$

where  $\underline{e}^T = [e_1, e_2, e_3]^T$ . The equilibrium points define a continuous line with an upper and a lower bound for  $e_3$ . For the equilibrium points, the controller force  $c_m u_c = -K 2\pi c_m e_3^*$  is compensated by an equivalent portion of the static friction  $F_s$  minus the cogging force in the desired position, i.e.,  $F_c(-0.38)$ . In Section 9.3 the local stability of a similar set of equilibrium points has been discussed and for a Stribeck curve comparable with the one used in this chapter it was shown that a sufficient condition for the local stability of such a set can be derived. Performing an algebraic analysis for the identified model with the Switch friction model, along the same line as presented in Section 9.3, results again in a sufficient condition, which states that the set of equilibrium points is locally stable if the homogeneous part of the linearized dynamics, represented by characteristic polynomial

$$s^3 + \left(\frac{K c_m}{2\pi m} + \frac{b}{m}\right)s^2 + \frac{K 2c_m + \alpha}{m}s + \frac{K 2\pi c_m}{m}, \quad \alpha = \left.\frac{\partial F_c(q)}{\partial q}\right|_{q=q_d},$$

is asymptotically stable, where  $\alpha$  is the derivative with respect to position of the cogging force in  $e_1 = 0$ . Using the Routh Hurwitz stability criterion, these dynamics are asymptotically stable if (i) the coefficients of the characteristic polynomial are all positive, which is only in question for the third coefficient  $\frac{K 2c_m + \alpha}{m}$ , since the others are all positive due to positive values of the system parameters as given in the previous section and (ii) the following inequality holds

$$\left(\frac{K c_m}{2\pi m} + \frac{b}{m}\right)\left(\frac{K 2c_m + \alpha}{m}\right) - \frac{K 2\pi c_m}{m} > 0.$$

For the identified cogging force  $\alpha$  is equal to  $-7.1586e3$  [N/m], which can be interpreted as a locally negative stiffness. Now, a sufficient condition with respect to the controller gain  $K$  for the local stability of the set of equilibrium points can be derived and is equal to  $K > 50.3389$  [V/m]. For the controller gain  $K = 10$  [V/m] used throughout this section no conclusion can be drawn for the local stability due to the possible conservatism of this criterion.

In contrast to the Switch friction model the presliding displacement regime is also incorporated in the LuGre friction model and the question arises whether the set of equilibrium points for this model type are locally stable as they seem to be for the real LiMMS setup. For the closed-loop dynamics with the LuGre friction model the set of equilibrium points lie on the following line

$$\underline{e}_{eq} = \left[ 0 \ 0 \ -\frac{(F_c(-0.38) + \beta \sigma_0)}{K 2\pi c_m} \ \beta \right]^T,$$

where  $\underline{e} = [e_1, e_2, e_3, z]^T$  with  $z$  representing the average bristle deflection and  $|\beta| \leq \frac{F_s}{\sigma_0}$  if the initial state  $|z(0)| \leq \frac{F_s}{\sigma_0}$  [24]. This invariant set implies that the force produced from a

## 10.4 Experimental Observations versus Model Predictions

non-zero bristle deflection together with the non-zero cogging force for  $e_1 = 0$  is compensated by the integral action. Hence, one eigenvalue of the Jacobian matrix in  $\underline{e}_{eq}$  should be zero with an eigenvector equal to  $[0 \ 0 \ -\frac{\sigma_0}{K2\pi c_m} \ 1]^T$ . However, due to the non-smoothness of the LuGre model, i.e., the absolute value  $|e_2| = |\dot{q}|$  in the differential equations, the derivation of this Jacobian matrix needs special attention as discussed earlier in the Chapters 4 and 8. The notion of *generalized differentials* [29] states that the *generalized derivative* of a vector field at a certain state is declared as *any* value included between its left and right derivatives. The generalized differential of the vector field belonging to the closed-loop dynamics with respect to the states  $\underline{e} = [e_1, e_2, e_3, z]^T$  can be regarded as the generalized Jacobian  $\tilde{J}$ . The generalized Jacobian in  $\underline{e}_{eq}$  is

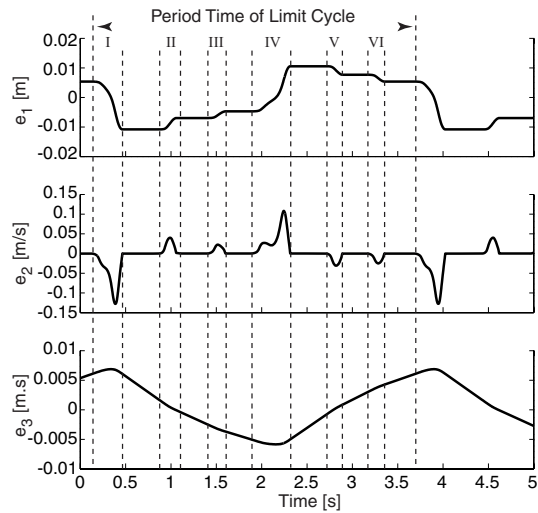
$$\tilde{J}_s(\underline{e}_{eq}) = \begin{bmatrix} 0 & 1 & 0 & 0 \\ -\frac{(2Kc_m + \alpha)}{m} & -\left(\frac{Kc_m}{2\pi m} + \frac{b + \sigma_1}{m}\right) + \frac{\sigma_1 \sigma_0 \beta (2q - 1)}{m F_s} & -\frac{K2\pi c_m}{m} & -\frac{\sigma_0}{m} \\ 1 & 0 & 0 & 0 \\ 0 & 1 - \frac{\sigma_0 \beta (2q - 1)}{F_s} & 0 & 0 \end{bmatrix},$$

$\forall 0 \leq s \leq 1, |\beta| \leq F_s/\sigma_0$ , where  $\alpha$  is again the derivative with respect to position of the cogging force in  $e_1 = 0$ . The three non-zero eigenvalues have to be in the open left-half plane for all  $0 \leq s \leq 1$  and  $|\beta| \leq \frac{F_s}{\sigma_0}$  to guarantee the local stability of the set of equilibrium points, since as for the equilibrium set the internal friction state  $z(t)$  is bounded within  $[-F_s/\sigma_0, F_s/\sigma_0] \ \forall t$ . In Chapter 8 an equivalent set of equilibrium points has been considered with the only difference that here the additional nonlinear cogging force is present, which is expressed in the Jacobian by the  $\alpha$  coefficient. The characteristic equation  $\det(\tilde{J}_s(\underline{e}_{eq}) - \lambda I) = 0$  belonging to this eigenvalue problem has one eigenvalue equal to zero and for the remaining polynomial the same conditions as derived for the set of equilibrium points for the Switch friction model should hold, which results in a lower bound on the controller gain  $K > 50.3389$  [V/m]. However, due to the possible conservatism of the analysis and consequently of this condition nothing can be concluded for the stability property of the set of equilibrium points for the controller gain  $K = 10$  [V/m] as used in this section.

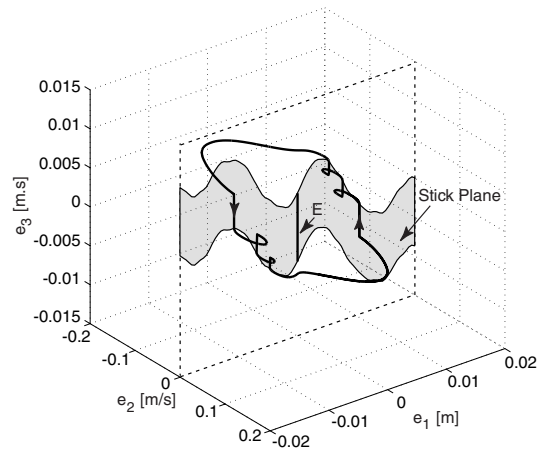
### 10.4.3 Event map

To give a more complete picture of the accuracy of the identified model it is possible to construct an event map, as described in Section 9.4, for the closed-loop dynamics of the model with the Switch friction model, since the dynamics for this controlled system only differs from the one presented in the previous chapter with respect to the additional cogging force. This cogging force changes only the dynamics in the slip phase and alters the set-valued friction function for  $e_2 = \dot{q} = 0$ , which shows in (i) a shifted line of equilibrium points  $E$  and (ii) a different shape of the stick plane, as depicted in the phase portrait of Figure 10.10b). In other words, the effective break-away force is equal to the static friction force minus the position dependent cogging force and therefore this break-away force becomes also position dependent. The event mapping technique reduces the nonlinear third order closed-loop dynamics into a one-dimensional iterated map on a predefined interval. To illustrate the event mapping technique once more, the time responses of the three closed-loop

## Part II - Friction Induced Limit Cycling



a) Time response for the model with Switch friction model.



b) Phase plane response for the model with Switch friction model.

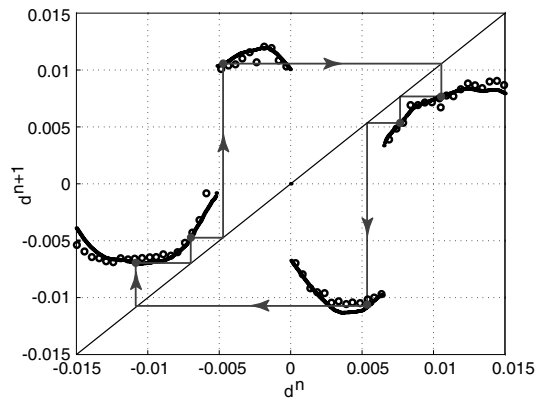
Figure 10.10 - Events occurring in the limit cycle for  $K = 10$  [V/m].

states for the observed model limit cycle are given in Figure 10.10a), where the stick and slip phases are separated by the vertical dashed lines. Each start of a slip phase is called an event and for this specific limit cycle there occur 6 events in one period time, represented by roman numbers. By definition every event is succeeded by a stick phase, which can be

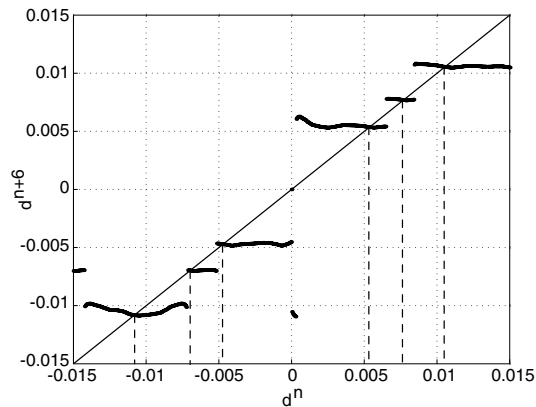
## 10.4 Experimental Observations versus Model Predictions

characterized by the corresponding error  $d = e_1$  since this state remains constant during the stick phase as can be seen in Figures 10.10a) and 10.10b).

By constructing a one-dimensional map of the errors in succeeding stick phases, i.e.,  $(d^n, d^{n+1})$ , the so-called first iterated event map  $\mathcal{P}(d^n)$  will be obtained. Here, the event map for the model is constructed by initializing the system in the stick phase on the interval  $d^1 = [-0.015, 0.015]$  with 500 intermediate points. When the system enters the next time the stick phase, the corresponding error  $d^2$  is recorded and mapped in Figure 10.11a) with the dots. To compare this event map with the closed-loop dynamics of the experimental setup



a) First iterated event map for both the LiMMS setup and the model.



b) Sixth iterated event map for the model.

Figure 10.11 - Event maps of the closed-loop dynamics for  $K = 10$  [V/m].

a similar idea is exploited. The LiMMS is first controlled with the 'strong' PID controller, as explained in the Section 10.3.2, to a point on a predefined grid around the desired position  $q_d = -0.38$  [m]. Due to this 'strong' PID controller every position can be reached and maintained. If the point has been reached the 'strong' controller is switched off and the 'weak' PID controller, as described in this section, is switched on with a desired regulator position of  $q_d = -0.38$  [m]. Then the system starts in the stick phase, where the integral control will build up and finally the system will start moving. When the system 'sticks' again the corresponding error is recorded and a point in the experimental event map is found. The word 'sticks' is placed between quotes, since for this experimental setup with the presliding displacement regime pure stiction can not occur and this returning in the stick phase is determined by visual inspection of the time responses. In Figure 10.11a) the experimental event map is shown with the circle points and due to the time-consuming nature of these experiments the number of points is limited to 60 on the interval  $d^1 = [-0.015, 0.015]$ . On this interval the LiMMS and the model with the Switch friction model show strong correspondence with respect to their closed-loop dynamics expressed by the constructed event maps. The limit cycle predicted by the model is also shown graphically in the event map by the lines with the arrows. By moving along these lines in a clock-wise manner, i.e., in forward time, the consecutive errors in the stick phases belonging to the period solution are found. The exact locations of the error in each stick phase together with the stability property of this limit cycle can be obtained by looking at the six times iterated event map  $\mathcal{P}^6(d^n)$ , since one period of the limit cycle consists of six stick phase and is depicted for the model in Figure 10.11b). The fixed points of this map, i.e.,  $d^n = \mathcal{P}^6(d^n)$ , give the error in each stick phase and if the map in these points is locally contracting the points are locally stable and otherwise locally unstable. The fixed points for the observed limit cycle are visualized with the 6 vertical dashed lines and in each of these fixed points the event map is locally contracting. Hence, the limit cycle is stable, which is conform the experimental and simulation results since unstable periodic solutions are hard to find for an experimental setup or through numerical integration in general. With the constructed event maps we should also be able to predict the presence of unstable periodic solutions as demonstrated in Chapter 9. However, due to the fast changes of the first iterated event map  $\mathcal{P}(d^n)$  on some intervals, which are caused by the nonlinear position dependent cogging force, the resolution of the (next) iterated event maps is too low to clearly distinguish the location and number of unstable periodic solutions. Increasing the number of points in the constructed event maps might resolve this problem, but needs additional computational effort and a very fine grid due to the locally high stiffness of the cogging force, i.e.,  $[-1e-4, 1e-4]$  [N/m] as described in Section 10.3.3. The unstable periodic solutions are believed to be extremely unstable, since the sixth iterated map shows for the found stable periodic solution fast contracting maps, i.e., approximately horizontal function  $\mathcal{P}^6(d^n)$ , at the corresponding fixed points.

For the identified model with the LuGre friction model such a construction of an event map is not possible. However as for the experimentally obtained event map, it would be possible to construct an approximate event map by using the consecutive errors in the succeeding presliding displacement regimes when the LuGre friction model approximates pure stiction. This is mainly due to the fact that the time scale in this presliding displacement regime

## 10.4 Experimental Observations versus Model Predictions

is much longer than it is in the 'slip' phase, which enables us to distinguish the different dynamic regimes. Here, the construction of this approximate event map is omitted, since little difference is expected with respect to the Switch friction model for the hunting limit cycles as illustrated in Chapter 8 and this is moreover motivated by the small discrepancies between the time responses of both models and the experimental LiMMS setup as shown in the Figures 10.8a)-10.8d).

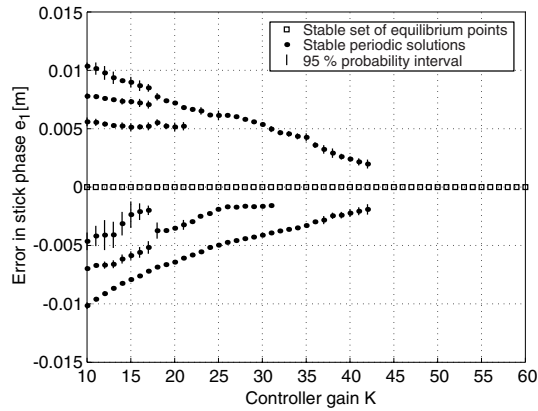
### 10.4.4 Bifurcation diagram

In the Chapters 8 and 9, it has been shown that an increase of the controller gain  $K$  can eliminate a similar type of friction induced limit cycle. Hence, the next interesting step is the construction of a bifurcation diagram, which shows the structural change in closed-loop behaviour with respect to the controller gain. Here, two bifurcation diagrams are constructed: one for the experimental LiMMS setup and one for the LiMMS model with the Switch friction model. Due to the asymmetric structure of the limit cycles for the LiMMS setup the periodic solutions will be characterized with the different values of the first state variable, i.e., the controller error  $e_1$ , during the various stick phases that are present in one cycle of the solution. For the experimental LiMMS setup, data is recorded for a fixed controller gain after some transient behaviour and through visual inspection of the found stable limit cycle the periodic solution is characterized. For the LiMMS model and the same fixed controller gain, an event map is constructed and stable fixed points of its iterated event maps are sought. To make a comparison between the experimentally constructed bifurcation diagram and the model predicted diagram, the controller gain  $K$  is increased with steps of 1 [V/m] starting from the previously chosen value  $K = 10$  [V/m].

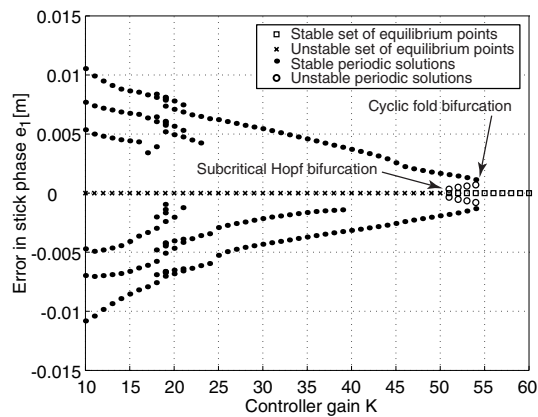
In Figure 10.12a) the experimentally obtained bifurcation diagram is shown, where for an increasing gain the amplitude of the limit cycle decreases and finally at approximately  $K = 42$  [V/m] the friction induced limit cycles disappear. Due to an increasing controller gain the stiffness in the closed-loop dynamics will increase and therefore the amplitude of the limit cycles will decrease as measured. However, the practically observed hunting phenomenon seemingly disappears at once, since the amplitude of the limit cycles at  $K = 42$  [V/m] is non-zero. This experimental result supports the closed-loop analysis presented in the previous two chapters, where the disappearance of the friction induced hunting limit cycle were predicted via a cyclic fold bifurcation. At  $K = 10$  [V/m] the previously found stable periodic solution with 6 stick phases is depicted by six dots and as the gain increases the number of stick phases present in the limit cycles decrease. The vertical lines through the dots give the 95 % probability interval of the measurements which are obtained by visual inspection of the different stick phases of the limit cycles for an approximately periodic data record of 100 [sec]. As discussed earlier the set of equilibrium points seems to be locally stable for the experimental LiMMS setup and are depicted for the varying controller gain with squares in the bifurcation diagram.

The constructed bifurcation diagram for the LiMMS model with the Switch friction model is shown in Figure 10.12b). The number of dots at each controller gain indicates again the

## Part II - Friction Induced Limit Cycling



a) Experimental bifurcation diagram for the LiMMS setup.



b) Predicted bifurcation diagram for LiMMS model with the Switch friction model.

Figure 10.12 - Bifurcation diagram of closed-loop dynamics for a varying controller gain  $K$ .

number of stick phases found in the stable periodic solution. Moreover, this number is equal to the number of event map iterations needed to find locally contracting fixed points at this controller gain, e.g., for  $K = 10$  [V/m] 6 stick phases are recorded for each period time and consequently for the sixth iterated event map the first contracting fixed points (in total six) are found as given in Figure 10.11b). The same tendency of decreasing amplitudes of the limit cycles for increasing controller gains as for the experimental bifurcation diagram is shown. For this LiMMS model, the friction induced limit cycles disappear at a somewhat larger value of the controller gain, i.e.,  $K \approx 54$  [V/m], than measured for the experimental

## 10.5 Conclusions

setup. However, the overall picture of both bifurcation diagrams is very similar and clearly shows a close correspondence of the closed-loop model with the experimental LiMMS setup. The set of equilibrium points are locally unstable up to  $K \approx 50$  [V/m] and become locally stable for larger values. At this structural change or bifurcation point an unstable periodic solution is born, which might indicate the occurrence of a subcritical Hopf bifurcation [108]. At this controller gain, which closely corresponds to the analytic sufficient condition for the local stability of the set of equilibrium points derived previously, the negative stiffness due to the cogging force is compensated for and the linear part of the closed-loop dynamics has become locally stable. From this point on the closed-loop dynamics behaves similar to the closed-loop system as described in the Chapters 8 and 9, since the amplitude of the limit cycles are so small that the cogging force can be approximated with a linear function, i.e.,  $F_c(q) \approx \alpha e_1 + F_c(-0.38)$ . As expected from the obtained insight for this type of hunting limit cycles from the previous two chapters a cyclic fold bifurcation seems to change the structural behaviour in such a manner that for controller gains larger than this bifurcation point, here at approximately  $K \approx 54$  [V/m], no periodic solutions exist anymore.

For controller gains larger than  $K = 40$  [V/m], the constructed event maps have enough resolution to predict unstable periodic solutions besides the stable periodic solution, which is due to the increased controller stiffness for these high gains. Hence, for  $K \in [40, 50]$  [V/m] only one stable limit cycle with two stick phases is expected for the closed-loop dynamics and no unstable periodic solution as can be seen from the bifurcation diagram in Figure 10.11b). For controller gains lower than  $K = 40$  [V/m] a cascade of doubling of the number of stick phases occurs and especially for the interval  $K \in [17, 22]$  [V/m] the number of stick phases increases very fast for decreasing gains, which might be a route to chaotic behaviour. For these controller gains it is believed that the number of unstable periodic solutions is infinite.

## 10.5 Conclusions

The ideas developed for the identification and analysis of controlled mechanical systems with friction have shown to be also applicable for the more general dynamics of the experimental LiMMS setup. Especially, the reduction of the closed-loop dynamics for the PID controlled regulator task with the event mapping technique is illustrated to be an extremely powerful analysis tool for both the model and the practical setup. Moreover, it has been shown that the LiMMS setup, due to its highly time-invariant and reproducible dynamics, can be modeled with high accuracy, where the closed-loop behaviour indicates a quantitative and qualitative close correspondence between the model and the experimental setup. Moreover, the expected cyclic fold bifurcation for the disappearance of the friction induced hunting limit cycles is indeed observed in the experimental setup, which strongly supports the supposed mechanism behind this structural change of the closed-loop dynamics.



## Part II - Friction Induced Limit Cycling

# Chapter 11

## In Retrospect

In this final chapter, the main contributions with respect to friction induced limit cycles are summarized and ideas for future research are unfolded. However, the origin of the examined hunting phenomenon is not yet fully understood and therefore this closing chapter will start with a discussion on the mechanism behind this form of limit cycles.

### 11.1 The Origin of Hunting Limit Cycles

In the previous three chapters the hunting phenomenon is described with different friction models, various frictional damping functions and even for an experimental setup the friction induced limit cycles are recorded, but the main mechanism behind the phenomenon is not yet fully explained. Let us try to give a glimpse of the origin of this problem, where we will first return to the local stability issue of the set of equilibrium points as discussed in Chapter 9.

#### 11.1.1 Set of equilibrium points

In Chapter 9 exact algebraic results [8] were used to perform a local stability analysis of the equilibrium set for various frictional damping functions, which are used in the Switch friction model. The proposed idea is to locally represent the nonlinear closed-loop dynamics as a PID controlled mass system with Coulomb friction only and to use the known exact algebraic results for the analysis of this closed-loop system. However, the obtained conditions are only sufficient as illustrated by the results for the continuous frictional damping function with shaping parameter  $\beta = 1$  in Section 9.5, where the equilibrium set was stabilized for a lower controller gain  $P$  than the analytically derived sufficient lower bound indicates. Hence, it is of interest to understand the sufficient nature of these algebraic analytic results and to extend these to necessary conditions if possible.

Let us recall the closed-loop system as described in Section 9.2 once more, where the idea was to model the friction force as a set-valued function for zero velocity, which is defined as

$$F(\dot{q}, u) = \begin{cases} g(\dot{q})\text{sgn}(\dot{q}) + b\dot{q}, & \forall \dot{q} \neq 0 \quad \text{Slip} \\ \min(|u|, F_s)\text{sgn}(u), & \forall \dot{q} = 0 \quad \text{Stick} \end{cases}$$

## Part II - Friction Induced Limit Cycling

where  $u = -P(q + D\dot{q} + I \int_0^t q(\tau)d\tau)$  is the applied control effort,  $F_s$  is the maximum static friction at zero velocity,  $g(\dot{q})$  is the frictional damping curve for velocities unequal to zero and  $b$  is the viscous damping. The equation of motion for this model, describing the closed-loop system, reads

$$\begin{aligned}\dot{\underline{x}} &= f_{Switch}(\underline{x}) \\ &= \begin{bmatrix} x_2 \\ -\frac{P}{m}(x_1 + Dx_2 + Ix_3) - \frac{1}{m}F(x_2, u) \\ x_1 \end{bmatrix}\end{aligned}$$

where  $\underline{x} = [x_1 \ x_2 \ x_3]^T = [q \ \dot{q} \ \int_0^t q(\tau)d\tau]^T$  and the control effort  $u = -P(x_1 + Dx_2 + Ix_3)$ . However the same system parameters are used as given in Table 9.1, for the moment no Stribeck curve is applied by setting the Coulomb friction level equal to the static friction level, i.e.,  $F_c = F_s = 4$  [N]. The exact algebraic results for such a closed-loop system, as presented in [8], states that for assumed *asymptotically stable dynamics of the linear part* and a non-zero positive Coulomb friction level no limit cycles can occur and the set of equilibrium points is locally stable. The assumption that only *asymptotically stable dynamics of the linear part*, in combination with non-zero Coulomb friction, results in locally stable equilibria causes the sufficiency property of the derived stability conditions in Section 9.3. To explain this we will numerically simulate this system, which differs from the original non-linear closed-loop system only with respect to the velocity dependent Stribeck characteristics or better the lack of it, for a decreasing viscous damping coefficient. The sufficient condition on the local stability of the set of equilibrium points for such a system is determined by the stability of the linear dynamics and for this particular system it can be shown that

- the terms  $\frac{PD+b}{m}$ ,  $\frac{P}{m}$  and  $\frac{PI}{m}$  need to be positive, which is satisfied if all system parameters are positive and
- the following inequality holds

$$\frac{(PD + b) P}{m} > \frac{PI}{m}.$$

For the system parameters as given in Table 9.1 with a fixed controller gain  $P = 10$  [N/m] these two conditions are satisfied. For a varying viscous damping coefficient the stability property of this linear dynamics changes at  $b = 0$  [N·s/m], since then  $\frac{(PD+b)P}{m}$  becomes equal to  $\frac{PI}{m}$ . Hence, let us look at the time responses of the closed-loop dynamics, where  $F_c = F_s = 4$  [N], for decreasing viscous damping coefficients starting with the original damping  $b = 1$  [N·s/m]. In Figure 11.1a) the time responses of the first state  $x_1$  are depicted for (i)  $b = 1$  [N·s/m] in the upper plot, (ii)  $b = 0$  [N·s/m] in the middle plot and  $b = -1.253$  [N·s/m] in the lower plot, where the upper two responses for infinite time converge to zero. When the linear part of the system becomes marginally stable, i.e.,  $b = 0$  [N·s/m], the stability of the closed-loop dynamics undergoes no change. Even for a range of negative viscous damping coefficients the closed-loop dynamics is stable and first changes for approximately  $b \approx -1.253$  [N·s/m]. In Figure 11.1b) the closed-loop system

## 11.1 The Origin of Hunting Limit Cycles

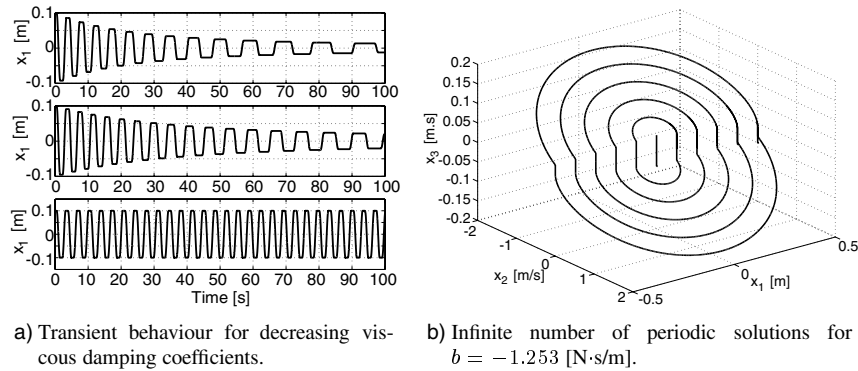


Figure 11.1 - Structural change of the closed-loop dynamics.

for this particular value is initialized at various states in the stick phase, where each of the resulting trajectories shows a limit cycle around the equilibrium set. Apparently, in the stick phase the system is able to stabilize the unstable linear dynamics in the slip phase, resulting in a contracting sequence of the first state  $x_1$  for consecutive stick phases even for the negative parameter interval  $b = (-1.253, 0]$  [N·s/m]. For values below this critical value  $b^* = -1.253$  [N·s/m] the closed-loop dynamics are unstable and the sequence of stick events is diverging. This numerical example illustrates the sufficiency property of the used exact algebraic stability conditions in the previous chapters.

Imagine that necessary conditions for the local stability of the set of equilibrium points for such a system with only Coulomb friction would be available, what would it tell about the closed-loop dynamics in the presence of the nonlinear velocity dependent Stribeck curve? It would enable us to construct necessary conditions for the local stability of the set of equilibrium points for the nonlinear case and would possibly in addition locate the creation or disappearance of stable or unstable periodic solutions. Returning to the question what causes the nonlinear closed-loop dynamics to enter a limit cycle, the numerically computed necessary condition for this specific parameter setting will be used to illustrate the idea behind this phenomenon.

### 11.1.2 Passivity property

The computed necessary condition with respect to the viscous damping coefficient for the local stability of the set of equilibrium points can be used to divide the original closed-loop dynamics with the nonlinear velocity dependent Stribeck curve into two blocks, i.e., one consisting of the oscillatory closed-loop behaviour of the PID controlled regulator task with Coulomb friction only and one with the remaining nonlinear velocity dependent function which is strongly related to the Stribeck curve as depicted in Figure 11.2. In other words, the

## Part II - Friction Induced Limit Cycling

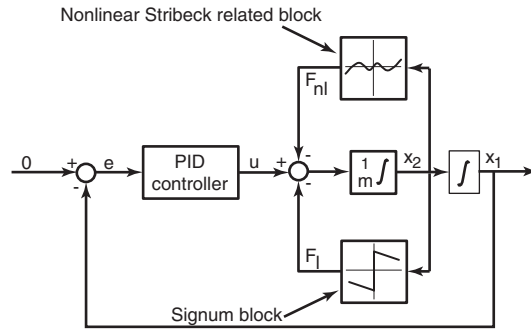


Figure 11.2 - Decomposition of the nonlinear friction force.

frictional damping characteristic of the system can be decomposed in

$$g(x_2)\text{sgn}(x_2) + bx_2 = \underbrace{g(x_2)\text{sgn}(x_2) - F_s\text{sgn}(x_2) + bx_2 - b^*x_2}_{\text{Nonlinear Stribeck related block}} + \underbrace{F_s\text{sgn}(x_2) + b^*x_2}_{\text{Signum block}},$$

where  $g(x_2)$  is the velocity dependent Stribeck curve,  $b$  is the viscous damping coefficient of the original system as given in Table 9.1, that is  $b = 1$  [N·s/m], and  $b^*$  is the critical value of the viscous damping coefficient for which the closed-loop system with Coulomb friction only becomes oscillatory, i.e.,  $b^* = -1.253$  [N·s/m]. The nonlinear Stribeck related block will stabilize or destabilize the marginally stable closed-loop dynamics of the system with Coulomb friction only. Intuitively, from this decomposition a sufficient condition for the elimination of limit cycles can be constructed, i.e., if the map  $x_2 \mapsto F_{nl}$  is passive then the closed-loop dynamics will be stable. Due to non-passive elements in the closed-loop dynamics such as integral control this is only a sufficient condition and not a necessity. In Figure 11.3 the nonlinear Stribeck related friction force  $F_{nl}$  is shown for the various frictional damping curves as used throughout Chapter 9 for these specific system parameters. For  $\beta = 2$  in the upper left plot, small excursions of velocities unequal to zero will encounter a passive map, which illustrates the local stability of the set of equilibrium points, but the map is not passive for all velocities unequal to zero, which destabilizes the system. However for large velocities the map shows again a passive stabilizing behaviour and in combination with the locally non-passive map this will result the system to enter a stable limit cycle. This mechanism supports the numerical results from Table 9.2 that predict the coexistence of a locally stable equilibrium set, an unstable limit cycle and a stable limit cycle. For the other frictional damping characteristics none of the maps is passive for small excursions of the velocity indicating unstable equilibrium points. Again in combination with the passive stabilizing behaviour for large velocities forces the closed-loop system is forced into a stable limit cycle and shows the mechanism for the coexisting locally unstable set of equilibrium points and the stable limit cycle.

## 11.2 Summary of Contributions

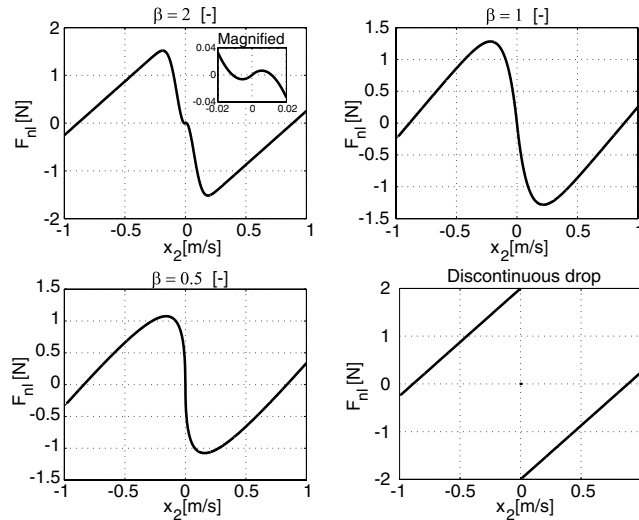


Figure 11.3 - Nonlinear Stribeck related friction force  $F_{nl}$  as a function of velocity  $x_2$ .

## 11.2 Summary of Contributions

The contributions of this part have been obtained by the analysis of the controlled mechanical system as being a general nonlinear dynamical system using tools from this particular research field, but more important by asking the central question what the complete picture of the closed-loop dynamics looks like. From the results presented in this part it can be concluded that the combination of nonlinear dynamics and control theory can be extremely powerful and even necessary to understand complicated nonlinear phenomena in controlled mechanical systems, such as the discussed friction-related problem of hunting limit cycles.

### 11.2.1 Friction induced hunting limit cycles

Hunting limit cycles, which might exist for a PID controlled single mass system with friction and a regulator task, have been investigated in this second part of the thesis for different types of friction models, various frictional damping functions, and moreover numerical results have been compared to experimental results. The performed studies have resulted in a clear understanding of this specific friction induced phenomenon and the gap between experimentally observed behaviour and model predictions has to some degree been closed.

An important research item, as pointed out in Chapter 1, is the search for the minimal model complexity that describes a certain phenomenon to its full extend. To this end two friction models have been compared with respect to the hunting phenomenon in Chapter 8, where for (i) the dynamic LuGre friction model and (ii) the alternate static Switch friction model the disappearance of the hunting limit cycles has been predicted with a cyclic fold bifurcation.

At this structural change of the closed-loop behaviour, which was found for an increasing controller gain, a stable and an unstable periodic solution fuse and consequently shows the extinction of the limit cycles. This numerical result is in line with the practical observation that hand-tuned PID controllers eliminate hunting, which has successfully been verified on an experimental setup in Chapter 10. With respect to this friction-related problem the two investigated friction models show little difference, both in a quantitative and qualitative sense, for the closed-loop dynamics, which have been illustrated by numerically constructed bifurcation diagrams. This observation indicates that the additional frictional dynamics for the LuGre friction model is not essential to the hunting phenomenon, which makes the Switch friction model beneficial from a computational and complexity point of view.

As for general dynamical systems, the important aspects of location and stability property of the equilibrium point(s) has been addressed to complete the dynamical picture for these closed-loop systems. In Chapter 8 and 9, for both used friction models the location and the stability property of the set of equilibrium points appeared to be very much alike. For a Gaussian frictional damping function, i.e., the Stribeck curve with  $\beta = 2$ , sufficient conditions have been derived analytically indicating locally stable sets of equilibrium points for the examined parameter settings.

In Chapter 9, the analysis of the stability property of the equilibrium points together with the constructed bifurcation diagrams have resulted for varying frictional damping curve in a characterization of the closed-loop properties, such as the number of coexisting limit cycles. Moreover, it has been shown why the limiting case of a discontinuous drop in the friction level can not predict the experimentally observed disappearance of the hunting limit cycles as presented in Chapter 8.

The ideas developed in Chapters 8 and 9 have been validated for a more general dynamical setting of an experimental Linear Motor Motion System, where besides the nonlinear velocity dependent friction force also a nonlinear position dependent cogging force is present. The expected cyclic fold bifurcation for the hunting limit cycles has been measured on this experimental setup for an increasing controller gain. Moreover, the computed bifurcation diagram, based on an identified model of the system, showed a close resemblance, both qualitatively and quantitatively, to the experimentally constructed bifurcation diagram and has indicated that the used modeling and identification procedures have resulted in an accurate model.

### 11.2.2 Analysis tools

The tools from the field of nonlinear dynamics, which have been used throughout this second part, have made an enormous contribution to the understanding and analysis of the hunting phenomenon. Two types of analysis tools have been used to numerically construct the bifurcation diagrams, which together with their drawbacks and merits are:

- The path-following technique, which is able of following branches of stable and unstable periodic solutions to numerically construct a bifurcation diagram. Especially the abil-

## 11.2 Summary of Contributions

ity to compute unstable periodic solutions makes the applied tool so powerful, since it can reveal important properties of the nonlinear dynamics as has been demonstrated in Chapter 8 with the prediction of a cyclic fold bifurcation. Moreover, the path-following tools are applicable for general nonlinear dynamical systems, as has been illustrated for the fourth order non-smooth closed-loop dynamics with the LuGre friction model. However, the found branches give only a local, i.e., in the vicinity of the periodic solutions, picture of the closed-loop dynamics, since for example existing unstable branches are likely to be missed by this technique, because the required initial conditions are part of the unstable solution itself, which is unknown beforehand. Moreover, for very unstable periodic solutions, which is expressed by large Floquet multipliers, it is shown to be numerically difficult to follow these unstable branches.

- The event mapping technique, as presented in Chapter 9, is able to reduce the third order discontinuous closed-loop dynamics with the Switch friction model to a one-dimensional map. This addresses immediately the major drawback of this technique, in that it can not be applied to a general class of nonlinear dynamical systems. However, as for many techniques with limited applicability, the event mapping technique has demonstrated to be very powerful for the analysis of the closed-loop dynamics under consideration. In Chapter 9 and 10 this technique has been used to numerically investigate the closed-loop dynamics on a predefined interval. The constructed event maps have revealed all the interesting closed-loop features, such as location and stability properties of existing limit cycles and equilibrium set. To construct bifurcation diagrams, as in Chapter 9 and 10 for a varying controller gain, a large number of event maps have to be computed, which might be a drawback from a computational point of view.

For the analysis of the controlled mechanical system as a nonlinear dynamical system the above tools have shown to be indispensable.

For the analytic derivation of the stability conditions for the set of equilibrium points with the dynamic LuGre friction model, the notion of *generalized differentials* [29] had to be exploited due to the non-smoothness introduced by this friction model, which appeared to be necessary and useful for the analysis in Chapter 8 and 10.

### 11.2.3 Controller design

Throughout this second part the shape of the used PID controller has been fixed and the structural properties of the closed-loop dynamics have been studied only for varying controller gain. Due to this specific controller structure an increase of the controller gain will lead to a simultaneous increase of the proportional, derivative and integral control. Hence, it is difficult to conclude what part of the controller causes the closed-loop system to eliminate the hunting limit cycles for increasing controller gains. However, using the ideas developed in Section 11.1.2 it can be concluded that the added damping due to the increasing derivative control should be large enough to ensure a passive map from velocity



to the nonlinear Stribeck related force  $F_{nl}$ .

One way to satisfy that condition is by incorporating the negatively-sloped Stribeck curve in the controller design, i.e., not only the linear closed-loop dynamics without friction has to be stable but also the linear closed-loop dynamics with the largest negative damping of the Stribeck curve should be stable. Returning to part one of this thesis, a controller synthesis with this property has been developed in Chapter 5, where based on a Polytopic Linear Model the negative damping of the Stribeck curve is incorporated in the controller design. This gain-scheduled PD controller synthesis can easily be extended with integral control and the resulting static or gain-scheduled PID controller will avoid hunting limit cycles.

### 11.3 Recommendations for Future Research

The analysis of the hunting limit cycles have resulted in a clear picture of the phenomenon, but have also introduced some new and open problems. In combination with the present work the following research directions are advisable.

#### 11.3.1 Analysis of non-smooth systems

The models used throughout this part were either non-smooth (for the LuGre friction model) or discontinuous (for the Switch friction model), which resulted for the closed-loop dynamics in non-smooth or discontinuous nonlinear system descriptions. However, the analysis of these non-smooth systems is far from complete and the majority of the used analysis techniques in Chapter 8-10 are in some sense based on simulations, which can be interpreted as just doing experiments as stated in Chapter 1. For instance, the constructed event maps in Chapter 9 and 10 give only information of the closed-loop dynamics on the predefined grid through simulations and at intermediate points no strong conclusions on the closed-loop dynamics can be drawn. In addition, it is desirable to know whether there exist more periodic solutions outside the examined domain. Moreover, some of the analysis tools, such as *Floquet theory* and bifurcation theory, have been developed and yet only fully understood for smooth nonlinear systems. Hence, the development of analysis tools for bifurcations of non-smooth dynamical systems is strongly advised to be able to understand and give a more complete picture of the nonlinear phenomena present in these systems.

#### 11.3.2 Necessary conditions

As indicated in Section 11.1.1, the derived conditions for local stability of the set of equilibrium points, as discussed in Chapter 9, are only sufficient. Construction of necessary conditions will enable us to predict exactly the local stability property of the equilibrium set for a given set of system parameters. Moreover, such necessary conditions will locate structural changes of the closed-loop behaviour and therefore indicate the creation or disappearance of periodic solutions, such as the predicted subcritical Hopf bifurcation in Section 10.4.4. For the closed-loop system a similar exact algebraic synthesis as presented

### 11.3 Recommendations for Future Research

in [8] might be performed to obtain necessary conditions. However, due to the large number of system parameters it is recommended first to non-dimensionalize the closed-loop system in order to reduce the number of parameters, which has been demonstrated for an equivalent closed-loop system in [6] and [8].

These desirable necessary conditions for the local stability of the set of equilibrium points can also be used to construct necessary conditions for the elimination of the hunting phenomenon. To this end the idea of dividing the closed-loop dynamics in a marginally stable closed-loop system and a nonlinear Stribeck related block as introduced in Section 11.1.2 might be exploited. However the interaction between the nonlinear Stribeck related force and the marginally stable closed-loop dynamics with Coulomb friction only is far from trivial due to the third order dynamics with non-passive elements like integral control. Therefore, necessary conditions for the disappearance of hunting limit cycles will be hard to derive, but remains the ultimate goal.

#### 11.3.3 Dynamic friction models

For dynamic friction models, such as the LuGre model, it might be of interest to follow an equivalent research path as presented for the discontinuous Switch friction model. For a varying frictional damping function  $g(x_2)$  in the LuGre model the set of equilibrium points might also change its local stability and consequently alter the closed-loop properties dramatically, for example the number of coexisting periodic solutions might change suddenly. If such analysis would show, in comparison with the results for the Switch friction model, no structural changes for a varying shape of the frictional damping function the conclusions drawn from the study performed in Chapter 8 might have to be reconsidered. In addition, it might be of interest to study whether the closed-loop dynamics for the standard parameterization of the LuGre friction model collapses into the same closed-loop dynamics as for the Switch friction model when for instance the presliding stiffness  $\sigma_0$  approaches infinity. Moreover, Altpeter [1] has constructed sufficient conditions for the disappearance of the hunting phenomenon for the closed-loop dynamics of the LuGre friction model, which indicated a strong dependency on the relative difference between the static friction level  $F_s$  and the Coulomb friction level  $F_c$  rather than a dependency on the negative slope of the frictional Stribeck curve as presented here. Hence, it is of future interest to construct necessary conditions to understand the differences between the two insights, which might reveal the origin of this friction induced phenomenon.

The difference between the practically observed locally stable set of equilibrium points for the LiMMS and the predicted unstable equilibrium set for the LuGre model in Section 10.4.2 is not yet fully understood. However, in our opinion the additional presliding stiffness in the LiMMS, which is also modeled by the LuGre friction model and not by the Switch friction model, is responsible for the measured stable set of equilibria. For the analysis of the LiMMS model with the LuGre friction model, it seems to be too restrictive to consider the set of equilibrium points only to be locally stable if all points on the equilibrium line are locally stable.

### **11.3.4 General control engineering rules**

The present work intended to be useful for the analysis and understanding of friction induced hunting limit cycles. However, the developed ideas and the used analysis tools can, in combination with known results from other friction induced phenomena such as the stick-slip oscillations for PD controlled mechanical systems at low velocities, be valuable for the synthesis of general design rules for the widely used PID or PD controllers. It would be desirable to be able to tune the controller for a specific task with as little as possible knowledge of the system and still be sure that the negative side effect of friction induced limit cycling can not occur. Hence, it is advisable to express the design rules in as few as possible number of necessary parameters, such as mass, difference between static and Coulomb friction level and largest negative slope of the Stribeck curve.

### **11.3.5 More general controlled mechanical systems with friction**

In a broader context, the question arises whether the developed ideas can contribute to a more general class of controlled mechanical system with friction, where for instance several contact surfaces introduce friction to a higher dimensional controlled mechanical system with additional flexibility and inertia. Although this is a difficult and open topic, the important question which follows from this second part and which can be used as a starting point for the analysis of such complex systems is the following:

What kind of periodic solutions and equilibria with what kind of local stability property exist for the closed-loop (nonlinear) dynamics of the controlled mechanical system with friction?

# Appendix A

## Terminology

In this appendix, some frequently used terminology with respect to nonlinear dynamical systems throughout the second part of this thesis will be discussed briefly. For a more detailed synthesis on nonlinear dynamical systems and its properties the reader is referred to Guckenheimer et al. [53], Khalil [80], Parker et al. [100] and Sastry [108].

### A.1 Nonlinear Autonomous System

Consider a  $n$ th-order autonomous smooth nonlinear dynamical system represented by the differential equation

$$\dot{x}(t) = f(x(t), \mu), \quad x(t_0) = x_0 \quad (\text{A.1})$$

where  $\dot{x} \equiv dx/dt$ ,  $x$  is the state vector with  $n$  state variables,  $t$  is time,  $\mu$  is a system parameter and  $f$  is a column of nonlinear functions of the state vector  $x$  and parameter  $\mu$ . Due to the fact that the vectorfield  $f$  does not explicitly depend on time  $t$  the system is called autonomous. Due to the nonlinear nature of the differential equation the following phenomena might occur:

- Multiple isolated equilibria. In contrast to linear time invariant systems, autonomous smooth nonlinear systems can have more than one isolated equilibrium point. The state may converge to one of the several steady-state operating points, depending on the initial state of the system.
- Limit Cycles. For a linear time invariant system to oscillate, it must have a pair of eigenvalues on the imaginary axis. The amplitude of the oscillation will be dependent on the initial state. However, there are nonlinear systems which can go into an oscillation irrespective of the initial state. This type of oscillation, which describes a closed-orbit in the state space, is known as a limit cycle.
- Bifurcations. Nonlinear dynamical systems might possess the property that qualitative features, such as the number of equilibrium points, the number of limit cycles, and stability of these phenomena, change with parametric variation in the model. Linear

---

The derivations and definitions presented in this appendix are taken from Khalil [80], Leine [85] and Sastry [108].

systems with parameters have behaviour that is considerably less subtle. As parameters of the linear system change, the system can change from stable to unstable and the number of equilibria can go through infinity if any of the eigenvalues go through the origin.

### A.1.1 Equilibrium points and stability

A point  $x = x^*$  in the state space is said to be an equilibrium point of Eq. (A.1) if it has the property that whenever the state of the system starts at  $x^*$  it will remain at  $x^*$  for all future time.

**Definition A.1 Equilibrium Point.**  $x^*$  is said to be an equilibrium point of Eq. (A.1) if  $f(x^*(t), \mu) \equiv 0$  for all  $t \geq 0$ .

**Definition A.2 Stability in the sense of Lyapunov.** The equilibrium point  $x = x^*$  is called a stable equilibrium point of Eq. (A.1) if for all  $t_0 \geq 0$  and  $\epsilon > 0$ , there exists  $\delta(t_0, \epsilon)$  such that

$$|x_0 - x^*| < \delta(t_0, \epsilon) \Rightarrow |x(t) - x^*| < \epsilon \quad \forall t \geq t_0$$

where  $x(t)$  is the solution of Eq. (A.1) starting from  $x_0$  at  $t_0$ .

### A.1.2 Limit cycles and stability

Oscillation is one of the most important phenomena that can occur in nonlinear dynamical systems. A system corresponding to Eq. (A.1) oscillates when it has a nontrivial periodic solution or limit cycle

$$x(t + T) = x(t), \quad \forall t \geq 0 \tag{A.2}$$

for some  $T > 0$ , where  $T$  is the minimal period time of the limit cycle. The word “nontrivial” is used to exclude constant solutions corresponding to equilibrium points. A constant solution satisfied the above equation, but it is not what we have in mind when we talk of limit cycles or periodic solutions. The image of a periodic solution in the phase portrait is a closed trajectory, that is usually called a period orbit or a closed orbit.

The stability of a limit cycle can be determined with the *Floquet theory*. We assume that Eq. (A.1) has a known periodic solution denoted by  $x_p(t)$ , which satisfies Eq. (A.2). A disturbance  $y(t)$  is superimposed on the periodic solution  $x_p(t)$  resulting in the solution

$$x(t) = x_p(t) + y(t). \tag{A.3}$$

Substituting Eq. (A.3) in Eq. (A.1), assuming that  $f(x(t), \mu)$  is at least twice differentiable with respect to  $x(t)$ , expanding the results in a Taylor series around  $x_p$ , and collecting the linear terms in the disturbance, the following differential equation is obtained

$$\dot{y}(t) = \frac{\partial f(x(t), \mu)}{\partial x} y(t) + \mathcal{O}(\|y(t)\|^2) \tag{A.4}$$

## A.1 Nonlinear Autonomous System

or

$$\dot{y}(t) \cong J(x_p(t), \mu)y(t) \quad (\text{A.5})$$

where  $J(x_p(t), \mu)$  is the Jacobian matrix of  $f(x_p(t), \mu)$ . The n-dimensional linear system of Eq. (A.5) has n linearly independent solutions  $y_i(t)$ , where  $i = 1, 2, \dots, n$ . These solutions are usually called a fundamental set of solutions. This fundamental set can be expressed in the form of a square matrix called *fundamental solution matrix* as

$$\underline{\Phi}(t) = [ y_1(t) \quad y_2(t) \quad \cdots \quad y_n(t) ]. \quad (\text{A.6})$$

The fundamental solution matrix after a period time  $T$  is called the monodromy matrix  $\underline{\Phi}(T)$  and its eigenvalue are called *Floquet Multipliers* [53], [100]. Each Floquet multiplier provides a measure of the local divergence or convergence along a particular direction over one period of the periodic solution. The Floquet multipliers determine therefore the stability of the periodic solution. The fundamental solution matrix can be regarded as a set of fundamental solutions of the linearization in the disturbance of the nonlinear system. The concept of a fundamental solution matrix is therefore important in the stability analysis of periodic solutions of nonlinear dynamical systems.

### A.1.3 Bifurcation (diagrams)

It is often desirable to know how the equilibrium points and the periodic solutions of a nonlinear dynamical system as represented by Eq. (A.1) change when a parameter of the system  $\mu$  is altered. The number and type of equilibrium points and periodic solutions - being stable or unstable - can change at a certain parameter value  $\mu = \mu^*$ . The qualitative change in the structural behaviour of the system is called a *bifurcation* [101].

**Definition A.3 Bifurcation Point.** (Seydel [111]) A bifurcation point (with respect to system parameter  $\mu$ ) is a solution  $(x^*, \mu^*)$ , where the number of equilibrium points or (quasi-)periodic solutions changes when  $\mu$  passes  $\mu^*$ .

In order to illustrate graphically the dependence of the equilibrium points and the periodic solutions of Eq. (A.1) on  $\mu$ , we require a scalar measure of the n-dimensional state vector  $x(t)$ . Examples of such a measure, denoted by  $[x]$ , are  $[x] = \max(x_1)$  or  $[x] = \|x\|$  and a diagram depicting the measures  $[x]$ , corresponding to all equilibrium points  $x^*$  and periodic solutions  $x_p$ , versus  $\mu$  is called a *bifurcation diagram*. The continuous curves of the measures corresponding to the equilibrium points  $x^*$  and periodic solutions  $x_p$  under variation of  $\mu$  are called *branches*. The branches of smooth systems are continuous and smooth but can split into one or more other branches.

Appendix

# Bibliography

- [1] Altpeter, F., “Friction Modeling, Identification and Compensation”, Ph.D. Thesis, École Polytechnique Fédérale de Lausanne, Switzerland, (1999).
- [2] Amontons, G., “De le résistance causée dans les machines”, *Mémoires de l'Academie des Sciences*, 203-222, (1699).
- [3] Angelis, G.Z., van de Molengraft van de, M.J.G., van der Linden, R.J.P., and Kok, J.J., “Robust controller design and performance for polytopic models”, In *Proceedings of the European Control Conference.*, Karlsruhe, (1999).
- [4] Angelis, G.Z., “System Analysis, Modelling and Control with Polytopic Linear Models”, Ph.D. Thesis, Eindhoven University of Technology, The Netherlands, (2001).
- [5] Armstrong-Hélouvry, B., “Control of machines with friction”, *Kluwer Academic Publishers.*, (1991).
- [6] Armstrong-Hélouvry, B., “Stick-slip and control in low-speed motion”, *IEEE Trans. on Automatic Control*, **38**(10), 1483-1496, (1993).
- [7] Armstrong-Hélouvry, B., Dupont, P., and Canudas de Wit, C., “A survey of models, analysis tools and compensation methods for the control of machines with friction”, *Automatica*, **30**, 1083-1138, (1994).
- [8] Armstrong-Hélouvry, B., and Amin, B., PID Control in the Presence of Static Friction: A Comparison of Algebraic and Describing Function Analysis, *Automatica*, **32**, 679-692, (1996).
- [9] Bai, E., and Sastry, S.S., “Parameter identification utilizing prior information”, *International Journal of Control*, **44**, 455-473, (1986).
- [10] Barabanov, N., and Ortega, R., “Necessary and sufficient conditions for passivity of the LuGre friction model”, *IEEE Trans. on Automatic Control*, **45**(4), 830 -832, (2000).
- [11] Basak, A., “Permamnet-Magnet DC Linear Motors”, Oxford, UK:Clarendon, (1996).
- [12] Bellman, R., “Dynamic Programming”, *Princeton University Press*, New Jersey, (1957).
- [13] Bernard, J.E., “The simulation of Coulomb friction in mechanical systems”, *Simulation*, **34**(1), 11-16, (1980).



- [14] Bifano, T., Dow, T., and Scattergood, R., "Ductile-Regime Grinding: A New Technology for Machine Brittle Materials", *ASME J. of Engineering for Industry*, Vol. 113, 184-189, (1991).
- [15] Blackwell, C.C., Sirlin, S.W. and Laskin, R.A., "Precision pointing of scientific instruments on space station: The LFGGREG perspective", *Proc. IEEE National Aerospace and Electronics Conf. NAECON 1988*, IEEE, Dayton, 566-573, (1988).
- [16] Bliman, P.-A., and Sorine, M., "Easy-to-use Realistic Dry Friction Models for Automatic Control", In *Proc. of 3rd European Control Conference*, Rome, Italy, 3788-3794, (1995).
- [17] Bohlin, T., "A case study of grey box identification", *Automatica*, **30**(2), 307-318, (1994).
- [18] Bonsignore, A., Ferretti, G. and Magnani, G., "Coulomb Friction Limit Cycles in Elastic Positioning Systems", *ASME J. of Dyn. Systems, Measurement and Control*, Vol. 121, 298-301, (1999).
- [19] Bosgra, O.K. and Kwakernaak, H., "Design Methods for Control Systems", *Notes for a course of the Dutch Institute of Systems and Control*, (1997).
- [20] Boyd, S., El Ghaoui, L., Feron, E. and Balakrishnan, V., "Linear Matrix Inequalities in System and Control Theory", *SIAM*, (1994).
- [21] Brandenburg, G., and Schäfer, U., "Influence and partial compensation of simultaneously acting backlash and Coulomb friction in a position- and speed-controlled elastic two-mass system", *Proc 2nd European Conf. on Power Electronics and Applications*, EPE, Grenoble, 1041-1047, (1987).
- [22] Bukkems, B.H.M., "Friction Induced Limit Cycling: An Experimental Case Study", Internal DCT-report No. 2001-35, Eindhoven University of Technology, Department of Mechanical Engineering, Dynamics and Control Technology Group, (July 2001).
- [23] Callafon de, R., "Feedback Oriented Identification for Enhanced and Robust Control", Phd. Thesis, Delft University Press, (October 1998).
- [24] Canudas de Wit, C., Olsson, H., Åström, K.J., and Lischinsky, P., "A New Model for Control of Systems with Friction", *IEEE Trans. on Automatic Control*, **40**(3), 419-425, (1995).
- [25] Canudas de Wit, C., and Lischinsky, P., "Adaptive friction compensation with partially known dynamic friction model", *Int. Journal of Adaptive Control and Signal Processing*, **11**, 65-80, (1997).
- [26] Canudas de Wit, C., "Control of Friction-driven Systems", In *Proceedings of the European Control Conference*, Karlsruhe, (1999).

- [27] Carlson, J.M., and Langer, J.S., “Mechanical model of an earthquake fault”, *Physical Review A*, **40**, 6470-6484, (1989).
- [28] Cebuhar, W.A., “Smoothing and approximate linearization of discontinuous control systems”, Ph.D. Thesis, Dept. of Applied Mathematics, Harvard University, (1988).
- [29] Clarke, F.H., Ledyaev Yu., S., Stern, R.J., and Wolenski, P.R., “Nonsmooth Analysis and Control Theory”, Graduate Texts in Mathematics, New York, (1998).
- [30] Coulomb, C.A., “Théorie des machines simples”, *Mémoires de Mathématique et de Physique de l'Académie des Sciences*, 161-331, (1785).
- [31] Courtney-Pratt, J., and Eisner, E., “The effect of a tangential force on the contact of metallic bodies”, In *Proc. Royal Society*, vol. A238, 529-550, (1957).
- [32] Czichos, Z., “Tribology”, Elsevier, Amsterdam, (1978).
- [33] Dahl, P., “A solid friction model”, Aerospace Corp., El Segundo, CA, Tech. Rep. TOR-0158(3107-18)-1, (1968).
- [34] Dahl, P., “Solid friction damping of mechanical vibrations”, *AIAA Journal*, **14**(12), 1675-1682, (1976).
- [35] Dankowicz, H., and Nordmark, A., On the Origin and Bifurcations of Stick-slip Oscillations. *Physica D*, **136**, 280-302, (2000).
- [36] Dasgupta, S., Anderson, B.D.O., and Kaye, R.J., “Output-error identification methods for partially known systems”, *International Journal of Control*, **43**, 177-191, (1986).
- [37] dSPACE digital signal processing and control engineering GmbH, “DS1102 User’s Guide”, Paderborn, Germany.
- [38] Dupont, P.E., “Avoiding stick-slip through PD control”, *IEEE Trans. on Automatic Control*, **39**(5), 1059-1097, (1994).
- [39] Dupont, P.E., and Dunlap, E.P., “Friction modeling and PD compensation at very low velocities”, *ASME Journal of Dynamic Systems, Measurement and Control*, Vol. 117, 9-14, (1995).
- [40] Dupont, P.E., Armstrong, B., and Hayward, V., “Elasto-plastic friction model: contact compliance and stiction”, In *Proc. of American Control Conference*, Vol. 2, 1072 - 1077, (2000).
- [41] Eborn, J., and Olsson, M., “Modelling and simulation of an industrial control loop with friction”, *Proc. of the 4th IEEE Conference on Control Applications*, 312-322, Albany, New York, (1995).
- [42] Fey, R.H.B., Steady-state behaviour of reduced dynamic systems with local nonlinearities. Ph.D. Thesis, Eindhoven University of Technology, The Netherlands, (1992).

- [43] Filippov, A.F., *Differential equations with discontinuous right-hand sides*, Mathematics and Its Applications, Kluwer Academic, Dordrecht, The Netherlands, (1998).
- [44] Futami, S., Furutani, A., and Yoshida, S., "Nanometer positioning and its microdynamics", *Nanotechnology*, **1**(1), 31-37, (1990).
- [45] Gäfvert, M., "Comparison of two friction models", Master's thesis, LUTFD2/TFRT-5561-SE, Lund Institute of Technology, (1996).
- [46] Gäfvert, M., "Comparisons of Two Dynamic Friction Models", *Proc. of the 6th IEEE Conference on Control Applications*, Hartford, (1997).
- [47] Gäfvert, M., Svensson J., and Åström K.J., "Friction and Friction Compensation in the Furuta Pendulum", In *Proceedings of the European Control Conference.*, Karlsruhe, (1999).
- [48] Galvanetto, U., and Knudsen, C., Event Maps in a Stick-Slip System. *Nonlinear Dynamics*, **13**, 99-115, (1997).
- [49] Galvanetto, U., and Bishop, S.R., Dynamics of a Simple Damped Oscillator Undergoing Stick-Slip Vibrations. *Meccanica*, **34**, 337-347, (1999).
- [50] Gawthrop P.J., Jezek J., Jones R.W., and Sroka I., "Grey-box model identification", *Control-Theory and Advanced Technology*, **9**(1), 139-157, (1993).
- [51] Gelb, A., "Applied optimal estimation", *M.I.T. Press*, (1978).
- [52] Goto, F., and Kudo, S., "Measurement of the plastically deformed domain caused by microdrilling in CdS single crystal", *Precision Engineering*, Vol. 14 (**4**), 243-245, (1992).
- [53] Guckenheimer, J., and Holmes, P., *Nonlinear Oscillations, Dynamic Systems, and Bifurcations of Vector Fields*. *Applied Mathematical Sciences 42*, New York, (1983).
- [54] Hashimoto, M., Koreyeda, K., Shimono, T., Tanaka, H., Kiyosawa, Y., and Hirabatashi, H., "Experimental study on torque control using harmonic drive built-in torque sensors", *Proc. Inter. Conf. on Robotics and Automation IEEE*, 2026-2031, (1992).
- [55] Haessig, Jr. D.A., and Friedland, B., "On the Modeling and Simulation of Friction", *Journal of Dynamic Systems, Measurements, and Control*, **113**, 354-362, (1991).
- [56] Haessig, D., and Friedland, B., "A Method for Simultaneous State and Parameter Estimation in Nonlinear Systems", In *Proc. of the American Control Conference*, Albuquerque, New Mexico, 947-951, (1997).
- [57] Harnoy, A., Friedland, B., Semenock, R., Rachoor, H., and Aly, A., "Apparatus for Empirical Determination of Dynamic Friction", In *Proc. of the American Control Conference*, Baltimore, Maryland, 546-550, (1994).

- [58] Held, D., and Maron, C., “Estimation of friction characteristics, inertial and coupling coefficients in robotic joints based on current and speed measurements”, *Robot Control 1988, Selected Papers from the 2nd IFAC Symp.*, 207-212, (1988).
- [59] Hendriks, S.G.M., “Iterative Learning Control on the H-drive”, Internal DCT-report No. 2000-37, Master’s Thesis, Eindhoven University of Technology, Department of Mechanical Engineering, Dynamics and Control Technology Group, (2000).
- [60] Hensen, R.H.A., Angelis, G.Z., Molengraft v.d., M.J.G., Jager de, A.G., and Kok, J.J., “Grey-box modeling of friction: An experimental case-study”, In *Proceedings of the European Control Conference.*, Karlsruhe, (1999).
- [61] Hensen, R.H.A., “Extended Kalman Filter based System Identification Tool”, Internal report No. 99.003, Eindhoven University of Technology, Department of Mechanical Engineering, Dynamics and Control Technology Group, (1999).
- [62] Hensen, R.H.A., Angelis, G.Z., Molengraft v.d., M.J.G., Jager de, A.G., and Kok, J.J., “Grey-box modeling of friction: An experimental case-study”, *European Journal of Control.*, Vol. 6, 3, pages 258-267, (2000).
- [63] Hensen, R.H.A., Angelis, G.Z., and Molengraft v.d., M.J.G., “Adaptive optimal friction control based on a polytopic linear model”, In *Proceedings of the Fourteenth Mathematical Theory of Networks and Systems Symposium.*, Proceedings CD-ROM, Perpignan, France, (2000).
- [64] Hensen, R.H.A., Molengraft v.d., M.J.G., and Steinbuch, M., “Frequency domain identification of dynamic friction model parameters”, to appear in *IEEE Trans. on Control Systems Technology*.
- [65] Hensen, R.H.A., Molengraft v.d., M.J.G., and Steinbuch, M., “High Performance Regulator Control for Mechanical Systems Subjected to Friction”, submitted to *IEEE Trans. on Robotics and Automation*.
- [66] Hensen, R.H.A., Molengraft v.d., M.J.G., and Steinbuch, M., “High Performance Regulator Control for Mechanical Systems Subjected to Friction”, In *Proc. of the IEEE Conference on Control Applications*, Mexico City, Mexico, (2001).
- [67] Hensen, R.H.A., Molengraft v.d., M.J.G., and Steinbuch, M., “Friction Induced Hunting Limit Cycles: A Comparison between the LuGre and Switch Friction Model”, submitted for publication in *Automatica*.
- [68] Hensen, R.H.A., “Friction Induced Limit Cycles: Hunting”, Internal report No. DCT 2001-21, Eindhoven University of Technology, Department of Mechanical Engineering, Dynamics and Control Technology Group, (2001).
- [69] Hensen, R.H.A., Molengraft v.d., M.J.G., and Leine, R.I., “Friction Induced Hunting Limit Cycles: An Event Mapping Approach”, in preparation for publication.

- [70] Hess, D.P., and Soom, A., "Friction at a lubricated line contact operating at oscillating sliding velocities", *J. Tribology*, Vol. 112, 147-152, (1990).
- [71] Hojjat, Y., and Higuchi, T., "Application of electromagnetic impulsive force to precise positioning", *J. Japan Soc. Precision Engineering*, **25**(1), 39-44, (1991).
- [72] Hornik, K., Stinchcombe, M., and White H., "Multilayer feedforward networks are universal approximators", *Neural Networks*, **2**, 359-366, (1989).
- [73] Horowitz, I., Oldak, S., and Shapiro, A., "Extensions of Dithered Feedback Systems", *Int. J. of Control*, **54**(1), 83-109, (1991).
- [74] Jansen, J.D., "Nonlinear Dynamics of Oilwell Drillstrings", Ph.D. Thesis, Delft University Press, The Netherlands, (1993).
- [75] Johansen, T.A., and Foss, B.A., "Nonlinear local model representation for adaptive systems", *Int. Conf. on Intelligent Control and Instrumentation*, **2**, 677-682, (1992).
- [76] Johansen, T.A., and Foss, B.A., "State-space modeling using operating regime decomposition and local models", *Preprints 12th IFAC World Congress*, **1**, 431-434, (1993).
- [77] Johnson, C.T., and Lorenz, R.D., "Experimental identification of friction and its compensation in precise, position controlled mechanisms", *Proc. of the Indus. App. Soc. Annual Meeting*, 1400-1406, (1991).
- [78] Kato, S., Sato, N. and Matsubayashi, T., Some considerations of characteristics of static friction of machine tool slideway. *J. of Lubrication Technology*, **94**(3), 234-247, (1972).
- [79] Karnopp, D., "Computer Simulation of Stick-Slip Friction in Mechanical Dynamic Systems". *ASME Journal of Dynamic Systems, Measurement and Control*, Vol. 107, 100-103, (1985).
- [80] Khalil, H.K., *Nonlinear Systems*, Prentice Hall, Upper Saddle River, New Jersey, (1996).
- [81] Knudsen, C., Slivsgaard, E., Rose, M., True, E., and Feldberg, R., "Dynamics of a model of a railway wheelset". *Nonlinear Dynamics*, **6**, 215-236, (1994).
- [82] Kobayashi, A., "Ultra-precision machining of plastics", In *Proc. SPIE Production Aspects of Point Machined Optics*, San Diego, CA, SPIE Vol. **508**, 31-36, (1984).
- [83] Lee, H.S., and Tomizuka, M., "Robust Motion Controller Design for High-Accuracy Positioning Systems", *IEEE Trans. on Industrial Electronics*, **43**, No. 1, (February 1996).
- [84] Leine, R.I., van Campen, D.H., de Kraker, A., and van den Steen, L., Stick-Slip Vibrations Induced by Alternate Friction Models. *Nonlinear Dynamics* **16**, 41-54, (1998).

- [85] Leine, R.I., “Bifurcations in Discontinuous Mechanical Systems of Filippov-Type”, Ph.D. Thesis, Eindhoven University of Technology, The Netherlands, (2000).
- [86] Leine, R.I., van Campen, D.H., and van de Vrande, B.L., Bifurcations in Nonlinear Discontinuous Systems. *Nonlinear Dynamics*, Vol. 23, 2, 105-164, (2000).
- [87] Leith, D., and Leithead, W., “Survey of Gain-scheduling Analysis and Design”, *Int. Journal of Control*, 73, 1001-1025, (2000).
- [88] Murray-Smith, R., and Johansen, T.A., “Multiple Model Approaches to Modelling and Control”, *Taylor and Francis*, London (1997).
- [89] Narendra, K.S., Parthasarathy, K., “Identification and Control of Dynamical Systems Using Neural Networks”, *IEEE Transactions on Neural Networks*, 1, 4-27, (1990).
- [90] Nasar, S.A. and Boldea, I., “Linear Electric Motors: Theory, Design and Practical Applications”, Englewood Cliffs, NJ:Prentice-Hall, (1987).
- [91] Nijmeijer, H., and van der Schaft, A.J., “Nonlinear Dynamical Control Systems”, *Springer*, (1990).
- [92] Nitsche, R., and Gaul, L., “Vibration Control Using Semi-Active Friction Damping”, In *Proceedings of the European Control Conference.*, Karlsruhe, (1999).
- [93] Nooijens, J.C.J., “Event Mapping Tool”, Internal DCT-report No. 2001-06, Eindhoven University of Technology, Department of Mechanical Engineering, Dynamics and Control Technology Group, (2001).
- [94] Nussbaum, J., and Ruina, A., “A two degree-of-freedom earthquake model with static/dynamic friction”, *PAGEOPH* 125, 629-656, (1987).
- [95] Olsson, H., and Åström, K.J., “Friction generated limit cycles”, In *Proc. of the 1996 IEEE Conference on Control Applications*, Dearborn, MI, 798-803, (1996).
- [96] Olsson, H., and Åström, K.J., “Observer-Based Friction Compensation”, *Proc. of the 35th Conference on Decision and Control*, Kobe, Vol. 4, 4345-4350, (1996).
- [97] Olsson, H., Åström, K.J., Canudas de Wit, C., Gäfvert, M., and Lischinsky, P., “Friction Models and Friction Compensation”, *European Journal of Control*, 4(3), 176-195, (1998).
- [98] Olsson, H., and Åström, K.J., “Friction generated limit cycles”, *IEEE Trans. on Control Systems Technology*, 9(4), 629-636, (2001).
- [99] Otten, G., de Vries, T.J.A., van Amerongen, J. and Rankers, A.M., “Linear Motor Motion Control Using a Learning Feedforward Controller”, *IEEE/ASME Trans. on Mechatronics*, Vol.2 (3), 179-186, (1997).

- [100] Parker, T.S., and Chua, L.O., *Practical Numerical Algorithms for Chaotic Systems*. New York: Springer-Verlag, (1989).
- [101] Poincaré, H., *Les Méthodes Nouvelles de la Mécanique Céleste*, Gautier-Villars, Paris, (1899).
- [102] Rabinowicz, E., The intrinsic variables affecting the stick-slip process. *Proc. Physical Society London*, **71**(4), 668-675, (1958).
- [103] Rabinowicz, E., *Friction and Wear of Materials*. New York: John Wiley and Sons, (1965).
- [104] Radcliffe, C.J., and Southward, S.C., "A property of stick-slip friction models which promotes limit cycle generation". *Proc. 1990 American Control Conference.*, ACC, San Diego, CA, 1198-1203, (1990).
- [105] Rice, J.R., and Ruina, A.L., "Stability of steady-state frictional slipping". *J. of Applied Mechanics*, **50**, 343-349, (1983).
- [106] Ruina, A.L., "Friction Laws and Instabilities: A Quasistatic Analysis of Some Dry Frictional Behaviour". Ph.D. Dissertation, Division of Engineering, Brown University, (1980).
- [107] Rugh, W., and Shamma, J., "Research on Gain Scheduling", *Automatica*, **36**, 1401-1425, (2000).
- [108] Sastry, S., *Nonlinear Systems Analysis, Stability and Control*. New York: Springer-Verlag, (1999).
- [109] Selmic R., and Lewis F.L., "Neural network approximation of piecewise continuous functions: application to friction compensation", *Proc. Int. Symp. on Intelligent Control*, 227-232, (1997).
- [110] Sepehri, N., Sassini, F., Lawrence, P.D., and Ghasempoor, A., "Simulation and experimental studies of gear backlash and stick-slip friction in hydraulic excavator swing motion", *ASME J. of Dyn. Systems, Measurement and Control*, Vol. 118, 463-467, (1996).
- [111] Seydel, R., *Practical Bifurcation and Stability Analysis; From Equilibrium to Chaos*, Interdisciplinary Applied Mathematics 5. New York: Springer-Verlag, (1994).
- [112] Shorten R., and Murray-Smith R., "On Normalising Radial Basis Function Networks", *Irish Neural Networks Conf.*, University College Dublin, (1994),
- [113] SigLab Model 20-42, DSP Technology Inc., "User Guide", Fremont, CA.
- [114] Stribeck, R., "Die Wesentlichen Eigenschaften der Gleit- und Rollenlager - the key qualities of sliding and roller bearings", *Zeitschrift des Vereines Seutscher Ingenieure*, **46**(38), 1342-1348, **46**(39), 1432-1437, (1902).

- [115] Sugeno, M., and Kang, G.T., "Structure identification of fuzzy model", *Fuzzy Sets and Systems*, **26**, 15-33, (1988).
- [116] Swevers, J., Al-Bender, F., Ganseman, C.G., and Prajogo, T., "An Integrated Friction Model Structure with Improved Presliding Behavior for Accurate Friction Compensation", *IEEE Trans. on Automatic Control*, Vol. 45 (4), 675-686, (2000).
- [117] Tafazoli, F., de Silva, C.W., and Lawrence, P.D., "Tracking Control of an Electrohydraulic Manipulator in the Presence of Friction", *IEEE Trans. on Control Systems Technology*, **6**(3), 401-411, (1998).
- [118] Townsend, W.T., and Salisbury, J.K., "The effect of Coulomb friction and stiktion on force control", *Proc. 1987 Inter. Conf. on Robotics and Automation*, IEEE, Rayleigh, 883-889, (1987).
- [119] Van den Steen, L., "Suppressing stick-slip-induced drillstring oscillations: a hyperstability approach", Ph.D. Thesis, University of Twente, The Netherlands, (1997).
- [120] Vidyasagar, M., "Nonlinear Systems Analysis", Prentice-Hall, Englewood Cliffs, New Jersey, (1978).
- [121] Wang, L.X., and Mendel, J.M., "Fuzzy Basis Functions, Universal Approximators and Orthogonal Least-Squares Learning", *IEEE Transactions on Neural networks*, **3**, 807-814, (1992).





# Samenvatting

Wrijving kan de prestatie van geregelde mechanische systemen, zoals nauwkeurige plaatsingsmachines, behoorlijk verslechteren en negatieve effecten zoals volgfouten, langdurige inschakelverschijnselen of limiet-cycli introduceren. Naar verwachting zullen veel van de hedendaagse geregelde mechanische systemen profiteren in termen van snelheid en nauwkeurigheid wanneer de wrijving wordt meegenomen in het regelaarontwerp. Voor dit doel lijkt het zinvol om de wrijving te modelleren met geschikte wrijvingsmodellen, waarvan vervolgens de corresponderende modelparameters geïdentificeerd worden. Het resulterende model kan enerzijds gebruikt worden voor het ontwerp van een regelaar en anderzijds voor de analyse van wrijvingsgeïnduceerde fenomenen zoals limiet-cycli.

De inhoud van dit proefschrift is driedelig en richt zich op (i) de ontwikkeling van identificatie procedures voor mechanische systemen met wrijving, (ii) regelaarontwerp voor mechanische systemen met wrijving en (iii) de analyse van wrijvingsgeïnduceerde ‘hunting’ limiet-cycli. Dit laatste is een wrijvingsgeïnduceerd fenomeen voor een één-massa systeem met wrijving in combinatie met een PID-geregelde positioneer-taak.

Twee grijze modelstructuren, i.e. modelstructuren die voor handen zijnde fysische ‘witte’ kennis van het systeem combineren met ‘zwarte’ deelstructuren, worden voorgesteld en gebruikt om wrijving te modelleren in mechanische systemen. De twee zwarte deelstructuren, i.c. een Neuraal Netwerk model en een Polytopisch Linear Model (PLM), zijn beide in staat wrijvingskarakteristieken te modelleren die niet verklaard kunnen worden met de fysische ‘witte’ kennis van het systeem. In een experimentele studie zijn beide grijze modellen gebruikt om een roterende-arm-systeem met wrijving te identificeren. Een Extended Kalman Filter is op een iteratieve, off-line manier gebruikt voor het schatten van de onbekende modelparameters.

In tegenstelling tot deze statische grijze modellen zijn dynamische wrijvingsmodellen, zoals het LuGre-wrijvingsmodel, in staat om meerdere in de praktijk waargenomen wrijvingsfenomenen te modelleren. Zo wordt bijvoorbeeld het zogenaamde ‘presliding’ verplaatsingsgebied, i.e. veerachtig gedrag voor snelheden rond nul, wel beschreven door het LuGre model terwijl de genoemde grijze modellen deze eigenschap niet hebben. Voor de identificatie van het ‘presliding’ verplaatsingsgebied wordt een efficiënte frequentiedomein identificatie methode gepresenteerd. De identificatie procedure van de dynamische modelparameters in het LuGre model, i.e., (i) de stijfheid en (ii) de damping van het ‘presliding’ fenomeen, is hierbij gereduceerd tot één enkel experiment. Voor een servomechanisme zijn tijd-domein validatie experimenten uitgevoerd die laten zien dat de verkregen parameterschattingen leiden tot een goede beschrijving van het gelineariseerde

‘presliding’-gedrag.

Met betrekking tot het eerste doel van dit werk kan geconcludeerd worden dat zowel tijd-domein als frequentie-domein identificatie procedures belangrijk zijn om alle dynamische eigenschappen in een mechanisch systeem met wrijving te modelleren en te begrijpen. Deze combinatie is vooral krachtig als beide domeinen op een aanvullende manier gebruikt worden.

Het dynamische LuGre-wrijvingsmodel en het statische PLM-wrijvingsmodel zijn vergeleken met betrekking tot de prestatie voor positioneer-taken van mechanische systemen met wrijving. Een klassieke PID-regelaar gecombineerd met voorwaartse sturing van een massa- en wrijvingsterm is vergeleken met (i) een PID-regelaar gecombineerd met een LuGre model-gebaseerde wrijvingscompensatie en (ii) een ‘gain-scheduled’ optimale PD-regelaar gebaseerd op de PLM. Deze laatste bestaat uit een voorwaartse sturing waarin alle voor handen zijnde systeemkennis op basis van de PLM is verwerkt en een niet-lineaire terugkoppeling die in optimale zin ontworpen is. De regelaars zijn vergeleken met de klassieke PID-regelaar door middel van experimenten op een roterende-arm-systeem met wrijving. De prestaties voor derde-orde servo-opzetfuncties tonen dat de ‘gain-scheduled’ optimale PD-regelaar resulteert in betere prestaties met betrekking tot inschakeltijden en maximale volgfout na het einde van de opzetfunctie. Het volgedrag van de LuGre-gebaseerde regelaar en de klassieke PID regelaar zijn vergelijkbaar terwijl het volgedrag van de ‘gain-scheduled’ PD-regelaar slechter is.

Het matige inschakelgedrag van de klassieke PID-regelaar wordt veroorzaakt door een verandering in de dominante dynamica waarbij van een dubbele integrator gedrag in de slip-fase naar een massa-veer gedrag in het ‘presliding’ verplaatsingsgebied overgeschakeld wordt. Dit heeft tot gevolg dat de eigenschappen van de gesloten-lus dynamica zullen verslechteren doordat de bandbreedte afneemt en tevens dat de stabiliteitsmarges verslechteren in het ‘presliding’ verplaatsingsgebied. De onderdrukking van statische fouten is beperkt bij gebruik van een eenvoudige PID-regelaar vanwege de additionele stijfheid in het ‘presliding’ verplaatsingsgebied.

Het derde doel van dit proefschrift, dat bestaat uit de analyse van wrijvingsgeïnduceerde ‘hunting’ limiet-cycli, is uitgevoerd door analyse van het niet-lineaire gesloten-lus systeem. De ‘hunting’ limiet-cycli zijn voorspeld voor een eenvoudig mechanisch systeem bestaande uit één massa onder invloed van wrijving en een PID-geregelde positioneer-taak. De twee gebruikte wrijvingsmodellen, i.e., (i) het dynamische LuGre-wrijvingsmodel en (ii) het statische Switch-wrijvingsmodel, zijn vergeleken met betrekking tot dit ‘hunting’ fenomeen. Analyse technieken die hun oorsprong vinden in de theorie van de niet-lineaire dynamica, zijn gebruikt om de wrijvingsgeïnduceerde limiet cycli te onderzoeken. Voor een variërende versterking van de regelaar zijn stabiele en instabiele periodieke oplossingen numeriek berekend met een eenvoudige ‘shooting’ methode. De stabiele en instabiele takken zijn berekend met ‘path-following’ technieken, die samen met de stabiliteits-analyse van de gesloten-lus evenwichtspunten resulteert in een bifurcatie diagram. Voor beide wrij-

vingsmodellen voorspelt de bifurcatie-analyse de verdwijning van het ‘hunting’ gedrag voor regelaar versterkingen groter dan de versterking behorend bij het ‘cyclic fold’ bifurcatie-punt.

In tegenstelling tot deze numeriek intensieve bifurcatie-analyse is het ‘hunting’ fenomeen ook bestudeerd met een efficiëntere ‘event mapping’ techniek. Twee verschillende typen statische wrijvingsfuncties, i.c., (i) een Coulombs wrijvingsniveau gecombineerd met een discontinue stap naar een hoger maximaal statisch wrijvingsniveau en (ii) wrijvingscurves met een continu verloop van het maximale statische wrijvingsniveau naar het lagere Coulombse wrijvingsniveau, zijn gebruikt om het ‘hunting’ fenomeen te onderzoeken en te voorspellen. In het bijzonder is een classificatie verkregen met betrekking tot de mogelijkheid om zowel stabiele als instabiele limiet cycli te voorspellen. Verder wordt de lokale stabiliteit van de evenwichtspunten besproken en worden attractie-gebieden aangegeven.

Het verkregen inzicht in de ‘hunting’ limiet cycli is gebruikt in een experimentele studie waar een lineair motor systeem wordt beschouwd. Naast de snelheidsafhankelijke wrijvingskracht bezit dit systeem ook een niet-lineaire positie afhankelijke ‘cogging’ kracht. De door de niet-lineaire krachten en PID geregelde positioneer-taak geïnduceerde limiet cycli zijn zowel experimenteel als numeriek geanalyseerd met de ‘event mapping’ aanpak.

De gebruikte analyse technieken, i.e. de ‘path-following’ en ‘event mapping’ techniek, die beide hun oorsprong vinden in de analyse van niet-lineaire dynamische systemen, leveren een belangrijke bijdrage tot het begrip en analyse van het ‘hunting’ fenomeen. In de beschouwing van het geregelde mechanische systeem met wrijving als een algemeen niet-lineair dynamisch systeem blijken beide analysetechnieken onontbeerlijk te zijn.



# List of Publications

## Chapter 3

Hensen, R.H.A., Angelis, G.Z., Molengraft v.d., M.J.G., Jager de, A.G., and Kok, J.J., “Grey-box modeling of friction: An experimental case-study”, *European Journal of Control*, Vol. 6, 3, 258-267, (2000).

## Chapter 4

Hensen, R.H.A., Molengraft v.d., M.J.G. and Steinbuch, M., “Frequency domain identification of dynamic friction model parameters”, to appear in *IEEE Trans. on Control Systems Technology*.

## Chapter 5

Hensen, R.H.A., Molengraft v.d., M.J.G. and Steinbuch, M., “High Performance Regulator Control for Mechanical Systems Subjected to Friction”, submitted to *IEEE Trans. on Robotics and Automation* (under review).

## Chapter 8

Hensen, R.H.A., Molengraft v.d., M.J.G. and Steinbuch, M., “Friction Induced Hunting Limit Cycles: A Comparison between the LuGre and Switch Friction Model”, submitted for publication in *Automatica* (under review).

## Chapter 9

Hensen, R.H.A., Molengraft v.d., M.J.G. and Leine, R.I., “Friction Induced Hunting Limit Cycles: An Event Mapping Approach”, in preparation for publication.

## Other

Hensen, R.H.A., Angelis, G.Z. and Molengraft v.d., M.J.G., “Adaptive optimal friction control based on a polytopic linear model”, In *Proceedings of the Fourteenth Mathematical Theory of Networks and Systems Symposium.*, Proceedings CD-ROM, Perpignan, France, (2000).

Kostić, D., Hensen, R.H.A., Jager de, A.G., and Steinbuch, M., “Modeling and Identification of a RRR-robot”, In *Proceedings of the 40th IEEE Conference on Decision and Control.*, Proceedings CD-ROM, Orlando, (2001).

Kostić, D., Hensen, R.H.A., Jager de, A.G., and Steinbuch, M., “Closed-form Kinematic and Dynamic Models of an Industrial-like RRR-Robot”, submitted to *2002 IEEE International Conference on Robotics and Automation*.



# Dankwoord

Vier jaar na het behalen van mijn ingenieursdiploma loopt er met dit proefschrift weer een hoofdstuk op z'n eind. Echter is dit proefschrift een schamele afspiegeling van de ontwikkeling die ik heb mogen doormaken aan de TU/e. Het plezier waarmee ik terugkijk op deze periode wordt bovenal bepaald door een aantal mensen die ik daarvoor wil bedanken.

Ten eerste wil ik Jan Kok en René van de Molengraft bedanken voor de mogelijkheid die zij mij gegeven hebben om dit project te starten. René, bedankt voor je enthousiaste manier van begeleiden en de stimulerende commentaren gedurende het project. Vooral denk ik met plezier terug aan de talloze college's, instructies en mondelingen die we samen verzorgd hebben. Deze waren een welkome afwisseling van het dagelijkse 'diepgraven'. Gedurende de tweede helft van mijn promotie heeft Maarten Steinbuch de fakkel als eerste promotor overgenomen van Jan Kok. Maarten, het was een waar genoegen om met je te hebben samengewerkt, vooral het tot leven brengen van het 'frequentie-domein' denken heeft voor veel input gezorgd. Dit werd nog eens versterkt door de praktijkstage uitgevoerd bij PHILIPS CFT onder begeleiding van Hub Vroomen, Johan Dries en Frank Sperling. Heren, bedankt voor een leerzame maar vooral ook plezierige tijd bij jullie club. Mijn tweede promotor, Henk Nijmeijer ben ik dankbaar voor het aanbrengen van de spreekwoordelijke 'puntjes op de i' van enkele wiskundige formuleringen en het nuanceren van enkele harde uitspraken.

Verder ben ik Georgo Angelis en Remco Leine dankbaar voor de talloze discussies die geleid hebben tot enkele mooie resultaten. Tevens hebben een aantal afstudeerders en stagiaires een waardevolle bijdrage geleverd aan dit proefschrift: Maarten Kuijpers, Rick Tebbens, Joost Nooijens en Bjorn Bukkems, allen bedankt! Ondanks de vele verhuizingen ben ik mijn (ex-)kamergenoten en collega's dankbaar voor een gezellige werksfeer, maar vooral het laatste jaar op vloer -1 met Rogier was een hele ervaring (Limburger ontmoet rasechte Amsterdammer). Tevens ligt deze kamer niet ver van mijn tweede 'thuis': het lab, waar ik naast mijn experimentele werk ook menig student begeleid heb. De echte bewoners van het lab, Karel Koekkoek, Harrie van de Loo en Niels Olthuis, wil ik hartelijk danken voor de plezierige tijden en de technische ondersteuning van mijn experimentele werk.

Buiten de TU/e wil ik alle (ex-)huisgenoten van Hemelrijken 153 bedanken voor een gezellige tijd waar altijd wat te beleven viel. Tevens wil ik mijn vrienden noemen waarmee ik vele steden en verre oorden heb mogen bezoeken: Rob, Jacco, Stefan, Ronald, Gwen en Emiel, bedankt voor de fantastische reizen! Tenslotte ben ik mijn broer en ouders dankbaar voor hun steun en interesse in mijn werk. Emiel, ondanks dat onze hereniging aan de TU/e maar van korte duur zal zijn denk ik met plezier terug aan de afgelopen 10 jaar waarin we



menig uurtje (lees tot in de kleine uurtjes) samen hebben doorgebracht zowel binnen als buiten de TU/e-grenzen. Wim, mogen er nog vele fietskilometers door het mooie limburgse land volgen en natuurlijk de mam, bedankt voor alles!

Ron

# Curriculum Vitae

- 1974** Born in Elsloo, the Netherlands.
- 1986-1992** Secondary School: Atheneum-B, Scholengemeenschap Sint Michiel, Geleen, The Netherlands.
- 1992-1997** Master student at Eindhoven University of Technology, Department of Mechanical Engineering, Systems and Control Group. The master project titled “Modelling and Control of Nonlinear Dynamic Systems” was carried out under supervision of Prof. Dr. Ir. J.J. Kok and Dr. Ir. M.J.G. v.d. Molengraft.
- 1998-2002** Ph.D. research at Eindhoven University of Technology, Department of Mechanical Engineering, Control Systems Technology Group. The Ph.D. project titled “Controlled Mechanical Systems with Friction” was carried out under supervision of Prof. Dr. Ir. M. Steinbuch, Prof. dr. H. Nijmeijer and Dr. Ir. M.J.G. v.d. Molengraft.
- 1999** Received the certificate of the “Dutch Institute of Systems and Control (DISC)” for successfully finishing the courses “System and Control Theory of Nonlinear Systems”, “Hybrid Systems”, “Object-oriented Modelling of Dynamic Systems”, “System Identification”, “Design Methods for Control” and “Adaptive Systems”. Attended the DISC summerschools titled “Identification for Control (1999)”, “Signal Processing for Control (2000)”, “The Impact of Optimization in Control (2001)”.
- 1999** An industrial traineeship at Philips Centre for Industrial Technology (CFT) for a duration of 3 month: “Controller Design and Performance Study of an Industrial Pick-and-Place Machine”.

# Stellingen

behorende bij het proefschrift

## Controlled Mechanical Systems with Friction

1. Hoewel de analyse van dynamische systemen in het frequentie-domein is voorbehouden aan lineaire dynamische systemen kan deze analyse techniek in combinatie met goed gekozen experimenten ook belangrijke informatie leveren over niet-lineaire aspecten van niet-lineaire dynamische systemen.
  - Deel 1 van dit proefschrift.
2. Ook dissipatieve elementen in een dynamisch systeem, zoals wrijving in mechanische systemen, kunnen bijdragen tot de destabilisatie van het systeem.
  - Deel 2 van dit proefschrift.
3. Bij de identificatie van een dynamisch systeem wordt de invloed van de gekozen modelstructuur op de keuze van het excitatiesignaal vaak onderbelicht.
4. De term ‘gain-scheduling’ is sterk aan inflatie onderhevig.
5. Om een 1-dimensionale mapping grafisch weer te geven zijn twee dimensies nodig.
6. De onderdrukking van informatieruis van de door zoekmachines gebruikte filters laat veel te wensen over.
7. Fysieke inspanning en mentale ontspanning gaan vaak hand in hand.
8. Zonder zowel linkse als rechtse opposenten kan er nooit sprake zijn van een gematigde politicus.
9. Het afbeelden van alle EU-landen op de euromunten is speculatief met betrekking tot het verwachte aantal eurolanden in de toekomst.
10. Het bij het grote publiek onbekende en door luchtvaartmaatschappijen verzwegen ‘Economy-class’ syndroom zou een belangrijkere beweegreden moeten zijn om het vliegtuig te mijden dan de kans op terroristische aanslagen.
11. Vrede is een werkwoord.
  - J.D. Tuinier en G. Visser, “Vredeseducatie: De praktijk van alledag.”, Baarn, Bekadidact cop., (2001).
12. Niet elke stelling is constructief.

Ron Hensen  
Eindhoven, januari 2002.